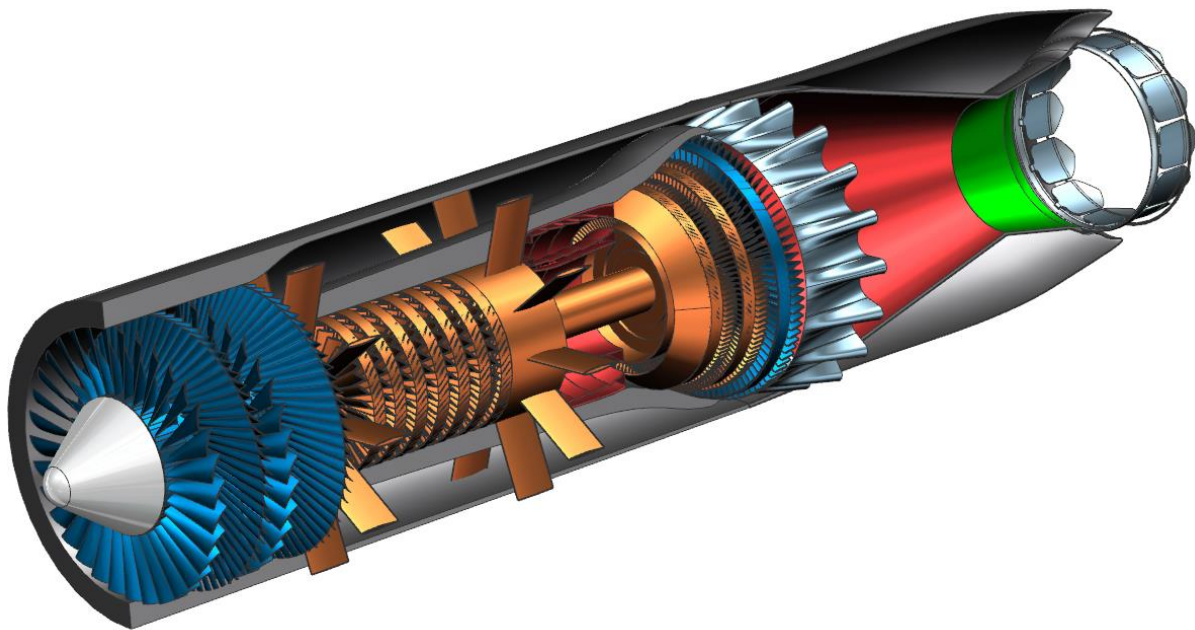


TF-CLAWS: Candidate Low-Bypass, Mixed-Flow Turbofan Engine for a Next Generation Trainer



Faculty Advisors:

Saeed Farokhi and Ray Taghvi

Team Lead:

Kyle P. Thompson

Team Members:

Daniel Fought

Charles Yeo

Timothy Luna

Weiting Liu

Zachary Smith



Department of Aerospace Engineering

May 16, 2016

TF-CLAWS: Candidate Low-Bypass, Mixed-Flow Turbofan Engine for a Next Generation Trainer

Design Team:

Daniel Fought
#555924



Timothy Luna
#665663



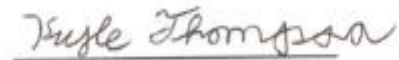
Weiting Liu
#578948



Zachary Smith
#665532



Kyle P. Thompson
#665630
Team Lead



Charles Yeo
#508019



Faculty Advisors:

Dr. Saeed Farokhi
#005092



Dr. Ray Taghavi
#024860



Abstract

The TF-CLAWS is a two-spool, mixed flow, low bypass ratio turbofan engine designed as a candidate for an advanced trainer capable of replacing the T-38. The performance of the TF-CLAWS is shown to be superior to the engine currently installed on the T-38, the J85-GE-5A afterburning turbojet engine.

The TF-CLAWS offers extreme performance gains over the baseline engine, providing a significantly lower TSFC for all major flight conditions, less overall engine weight, significantly lower fuel costs, and drastic increases to range and supersonic dash flight time duration. The improvements and technologies employed in the TF-CLAWS are presented as follows.

Engine Component	Improvements and Technology
Inlet System	<ul style="list-style-type: none"> • Diverterless Supersonic Inlet (DSI) • S-Duct Subsonic Diffuser • Honeycomb Aluminum Composite Acoustic Liner
Transonic Fan	<ul style="list-style-type: none"> • SiC/SiC CMC Fan Blades with Titanium Leading Edges
High-Pressure Compressor	<ul style="list-style-type: none"> • SiC/SiC CMC Compressor Blades
Combustion System	<ul style="list-style-type: none"> • Hybrid Diffuser (VCD and Conventional Post-Diffuser) • RQL Combustor Configuration • Convective Film Cooling via SiC/SiC CMC Tiles
High-Pressure Turbine	<ul style="list-style-type: none"> • SiC/SiC CMC Turbine Blades
Low-Pressure Turbine	<ul style="list-style-type: none"> • SiC/SiC CMC Turbine Blades
Mixer	<ul style="list-style-type: none"> • Forced Flow Lobe Mixer Design
Exhaust System	<ul style="list-style-type: none"> • Variable Area Ratio C-D Nozzle • Helmholtz Resonators and Chevron Vanes for Noise Mitigation • 2-D Thrust Vectoring Capabilities

TF-CLAWS

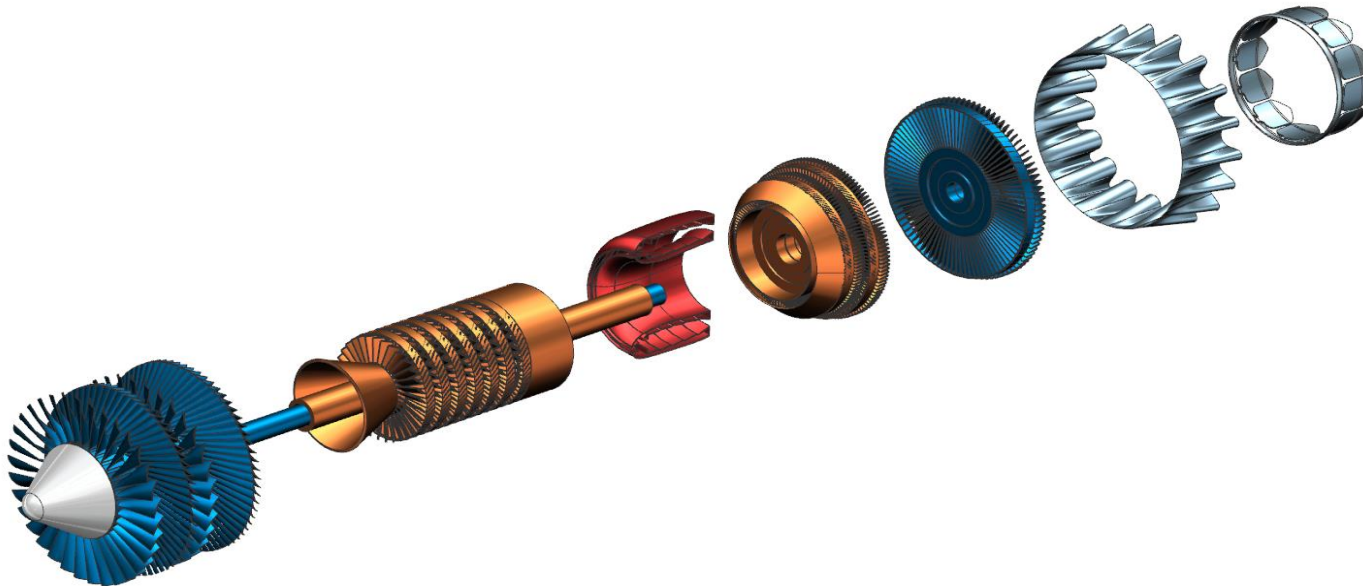
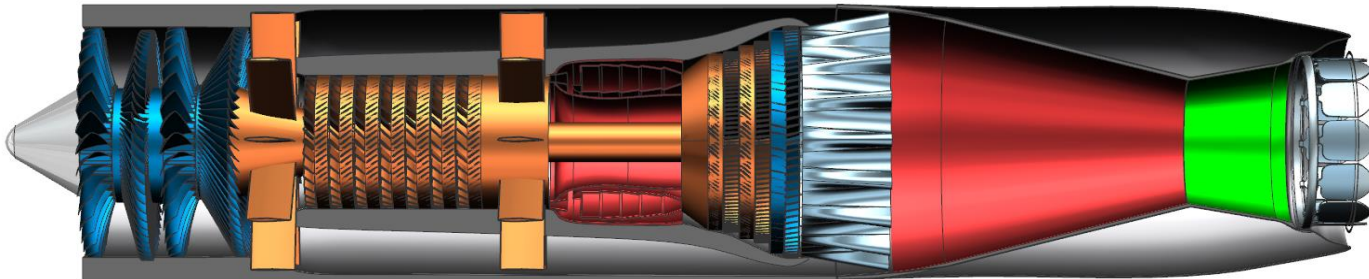
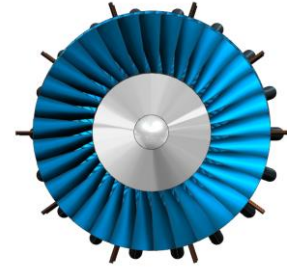


Table of Contents

	Page #
Abstract	ii
Table of Contents	iv
List of Figures	vii
List of Tables	ix
Nomenclature	xi
Acknowledgements	xvii
1 Introduction	1
2 Cycle Analysis	2
2.1 Advanced Engine Cycle Concepts for the TF-Claws	3
2.2 Engine Components and Diagrams	4
2.3 Baseline Engine Cycle Analysis and Validation	5
2.3.1 On-Design Analysis of Baseline Engine: Simulation Validation	5
2.3.2 Off-Design Analysis of Baseline Engine: Simulation Validation	6
2.4 TF-CLAWS Cycle Analysis: New Engine Optimization	7
2.4.1 On-Design Analysis of the TF-CLAWS: Exploring Parametric Space	7
2.4.2 Off-Design Analysis of the TF-CLAWS	10
2.5 Performance Comparison with the Baseline Engine Model	11
3 Mission Specification and Profile	12
3.1 Combat Patrol Mission	12
4 Engine Inlet Design	15
5 Compression System Design	19
5.1 Fan (LPC) Design	23
5.1.1 Rotor and Stator Flow Calculations	24
5.1.2 Fan Rotor and Stator Blade Design	25
5.1.3 Fan Stall Margin	26
5.1.4 Fan Blade Structural Analysis	27
5.2 High-Pressure Compressor (HPC) Design	28
5.2.1 HPC Rotor and Stator Flow Calculations	29
5.2.2 HPC Rotor and Stator Blade Design	30



5.2.3	HPC Stall Margin.....	31
5.2.4	HPC Blade Structural Analysis.....	31
6	Combustion System Design.....	32
6.1	Combustor Pre-Diffuser Configuration	32
6.2	RQL Combustor Configuration – Emissions Control.....	33
6.3	Liner Material Selection and Advanced Cooling Technique.....	34
6.4	Combustor Air Partitioning and Equivalence Ratios.....	35
6.5	Combustor Geometry.....	36
6.6	Combustor Efficiency	37
6.7	Combustor Fuel Injection	37
6.8	Combustor Ignition Source.....	38
6.9	Three-View of the Combustor of the TF-CLAWS.....	38
7	Turbine Design.....	39
7.1	High Pressure and Low Pressure Turbine.....	39
7.2	Pitchline Design Parameters	39
7.3	Turbine Flow Calculations.....	39
7.4	Material Selection	41
7.5	Turbine Aerothermodynamics	42
7.6	Turbine Blade Design and Annulus Sizing.....	43
7.7	Stress Considerations	44
7.8	Smith Chart	45
8	Mixer Design	45
9	Exhaust System Design.....	46
9.1	Introduction.....	46
9.2	Nozzle Sizing.....	47
9.3	Design Considerations	48
9.3.1	Selection of Cross-Sectional and Axial Geometry	48
9.3.2	Nozzle Scheduling Capability.....	49
9.3.3	Ejector Nozzle.....	50
9.3.4	Nozzle Cooling and Material Selection	51
9.3.5	Thrust Vectoring Capability	52
9.4	Incorporated Nozzle Concept	53



9.5 Exhaust System Geometry	53
10 Flow Path through the TF-CLAWS	54
11 Identification and Selection of Engine Subsystems	54
11.1 Starting	54
11.2 Bearings	55
11.3 Fuel System	55
11.4 Fire Suppression System	55
11.5 Anti-Icing System	56
11.6 Auxiliary Power Unit (APU)	56
11.7 Engine Control System	57
12 Engine Noise Attenuation	58
13 Fuel Cost Analysis	60
14 Mission Weight Sizing for the Next Generation Trainer	62
14.1 STAMPED Analysis and Database for Similar Airplanes	62
14.2 Determination of Mission Weights	63
15 Performance Constraint Analysis	64
15.1 Drag Polar Estimation	64
15.2 Takeoff Distance Constraints	64
15.3 Landing Distance Constraints	65
15.4 Climb Constraints	65
15.5 Dash Speed Constraints	66
15.6 Determination of Takeoff Wing Loading and Takeoff Thrust-to-Weight	66
16 TF-CLAWS Engine Integration on the Next Generation Trainer	68
17 Maintainability, Accessibility, and Serviceability	69
18 Recommendations	70
19 References	71



List of Figures

	Page #
Figure 1.1: T-38A Trainer Layout with Baseline Engine [1]	1
Figure 2.1: Mixed-Flow Turbofan Engine with a Fan Duct Burner and Ejector Nozzle [3].....	3
Figure 2.2: Novel Mixed-Flow Turbofan Engine with an Aft Fan (Direct Drive) [3]	3
Figure 2.3: Station Numbers for the TF-CLAWS – A Mixed-Flow Turbofan Engine [4].....	5
Figure 2.4: Parametric Studies of Cruise TET, BPR, FPR, OPR, and TSFC for the TF-CLAWS [4].....	8
Figure 2.5: Trade Studies Dictating Off-Design Cycle Parameters for the TF-CLAWS	10
Figure 3.1: Cruise Range and Dash Time Performance Gains Offered by the TF-CLAWS.....	15
Figure 4.1: Optimum Total Pressure Recovery of External Compression Inlets [8] / Diverterless Supersonic Inlet (DSI) [9].....	16
Figure 4.2: 3-D “Bump” Generated by MATLAB as an Integral Component to DSI [11].....	17
Figure 4.3: Definition Sketch of the TF-CLAWS Inlet [12]	19
Figure 4.4: Inlet System for the TF-CLAWS	19
Figure 5.1: Definition of Velocity Triangles for a Compressor Stage [8]	20
Figure 5.2: Definition Sketch of the Diffusion Passage of a Stage [8].....	22
Figure 5.3: Stall Margin Estimation Chart for a Compressor Stage [8]	23
Figure 5.4: Comparison of Fan Blade Profiles [8].....	25
Figure 6.1: Hybrid Diffuser Configuration [14]	32
Figure 6.2: Emissions Productions vs. Thrust [16].....	33
Figure 6.3: RQL Approach #1 [18].....	33
Figure 6.4: RQL Approach #2 [17].....	33
Figure 6.5: Tile Implementation on Liner Wall [27]	34
Figure 6.6: TBC Characteristics [22].....	35
Figure 6.7: Convection/Film Cooling Method [16].....	35
Figure 6.8: Example of RQL High-Load Operation [26]	36
Figure 6.9: Cooling Method, Effectiveness, & Cooling Air [8]	36
Figure 6.10: Combustion Efficiency & CLP Correlation [8]	37
Figure 6.11: Pre-Filming Airblast Atomizer [23]	38
Figure 6.12: Surface Discharge Igniter [27]	38
Figure 6.13: Side, Back, and Isometric Views of the Combustor of the TF-CLAWS	38
Figure 7.1: Representative Schematic of the Turbine of the TF-CLAWS	39
Figure 7.2: Definition Sketch for the Velocity Triangles of a Turbine Station [8]	40
Figure 7.3: GE F414 Turbofan Engine [5].....	41
Figure 7.4: Labyrinth Casing for a Turbine Nozzle [34]	43
Figure 7.5: Turbine Blade Definition Sketch [8]	43
Figure 7.6: Smith Chart for the Turbine of the TF-CLAWS at Takeoff [34].....	45
Figure 8.1: Mixer Flow [35]	46
Figure 8.2: Mixer Isometric View	46
Figure 9.1: Nozzle Definition Sketch and Station Numbers.....	47



Figure 9.2: ALMEC Ejector Testing [41].....	51
Figure 9.3: Side Section View of the Exhaust System of the TF-CLAWS	53
Figure 10.1: Flow Path through the TF-CLAWS	54
Figure 11.1: Typical Startup Sequence of the TF-CLAWS [49].....	54
Figure 11.2: Configuration of the Bearings [34]	55
Figure 11.3: Schematic Diagram of T-50 APS System [52]	56
Figure 11.4: Distributed Engine Control Employed on the TF-CLAWS [53]	57
Figure 12.1: EPNL Correlation with Perceived Noise [55].....	58
Figure 12.2: Helmholtz Resonator [55]	58
Figure 12.3: Acoustic Liner with Helmholtz Resonators [55].....	58
Figure 13.1: Forecasted Trend in Jet Fuel Prices [62].....	60
Figure 13.2: Fuel Costs over the Life of the Next Generation Trainer.....	61
Figure 15.1: Aircraft Constraint Diagram for the Next Generation Trainer.....	67
Figure 16.1: Front and Rear View of the TF-CLAWS on the Next Generation Trainer.....	68
Figure 16.2: Side View of the TF-CLAWS on the Next Generation Trainer.....	68
Figure 16.3: Bottom View of the TF-CLAWS on the Next Generation Trainer.....	68
Figure 16.4: Isometric View of the TF-CLAWS on the Next Generation Trainer.....	69

List of Tables

	Page #
Table 1.1: In-Flight Thrust Requirements for the Next Generation Trainer [1]	1
Table 1.2: General Characteristics of the Next Generation Trainer [1]	2
Table 1.3: Key Characteristics of Fifth Generation Fighters [2]	2
Table 2.1: Baseline Engine Performance at Takeoff	6
Table 2.2: Baseline Engine Performance at Off-Design Conditions	6
Table 2.3: Optimized Performance of the TF-CLAWS at Subsonic Cruise	9
Table 2.4: Comparison of Important Cycle Parameters at Subsonic Cruise	9
Table 2.5: Performance of the TF-CLAWS at Off-Design Conditions	11
Table 2.6: Comparison of Engine Performance between the Baseline Engine and the TF-CLAWS	11
Table 2.7: Comparison of Geometric Parameters between the Baseline Engine and the TF-CLAWS	12
Table 3.1: Combat Patrol Mission Fuel Weight for Baseline Engine	13
Table 3.2: Combat Patrol Mission Fuel Weight for TF-CLAWS	14
Table 3.3: Comparison of Combat Patrol Mission Fuel Weight	14
Table 4.1: Inlet Throat Sizing for all Flight Conditions	17
Table 4.2: Design Parameters of the Subsonic Diffuser of the Inlet of the TF-CLAWS	18
Table 5.1: Guidelines on the Range of Compressor Parameters [8]	21
Table 5.2: Design Parameters of the Fan of the TF-CLAWS at Takeoff	23
Table 5.3: Annulus Dimensions for the Fan of the TF-CLAWS	24
Table 5.4: Free-Vortex Design for the Fan and Stator of the TF-CLAWS at Takeoff	25
Table 5.5: Fan Blade Characteristics for the First Stage	26
Table 5.6: Fan Blade Structural Analysis	27
Table 5.7: Design Parameters of the HPC of the TF-CLAWS at Takeoff	28
Table 5.8: Annulus Dimensions for the HPC of the TF-CLAWS	28
Table 5.9: Free-Vortex Design for the First Stage of the HPC of the TF-CLAWS at Takeoff	29
Table 5.10: HPC Blade Characteristics for the First Stage	31
Table 5.11: HPC Blade Structural Analysis	31
Table 6.1: Summary of the Combustor Air Partitioning and Equivalence Ratios	35
Table 6.2: Selection and Results of the Cooling Methodology for the Combustor of the TF-CLAWS	36
Table 6.3: Dome and Liner Geometric Characteristics of the Combustor	36
Table 6.4: Combustor Zone Geometric Characteristics of the Combustor	36
Table 6.5: Combustion Efficiency for the TF-CLAWS at Subsonic Cruise and Takeoff	37
Table 6.6: Characteristics of the Combustor Fuel Injector	38
Table 7.1: Pitchline Design Parameters for the Turbine of the TF-CLAWS at Takeoff	39
Table 7.2: Detailed Stage Design for the HPT and LPT of the TF-CLAWS at Takeoff	40
Table 7.3: Material Properties of SiC/SiC Ceramic Matrix Composite	42

Table 7.4: Aerothermodynamic Analysis of Each Stage of the Turbine of the TF-CLAWS at Takeoff	42
Table 7.5: Turbine Entry Temperature Comparison between the Baseline Engine and the TF-CLAWS	42
Table 7.6: Summary of the Blade Design for the Turbine of the TF-CLAWS	43
Table 7.7: Summary of the Annulus Sizing for the Turbine of the TF-CLAWS	44
Table 7.8: Summary of Stress Calculations for the TF-CLAWS Turbine	44
Table 8.1: TF-CLAWS Mixer Parameters	45
Table 9.1: GasTurb 12 Flow Parameters and Sizing of the Nozzle	47
Table 12.1: Blade Passing Frequency of the TF-CLAWS	59
Table 13.1: Combat Patrol Mission Fuel Costs	61
Table 14.1: Database of Similar Aircraft to the Next Generation Trainer	63
Table 14.2: Combat Patrol Mission Weights for the Next Generation Trainer	63
Table 15.1: Drag Polar Estimations for the Next Generation Trainer	64

Nomenclature

<u>Symbol</u>	<u>Description</u>	<u>Units</u>
A.....	Cross-Sectional Area	ft ²
AR.....	Aspect Ratio	~
A _t /A _h	Blade Taper Ratio.....	~
A ₉ /A ₈	Exhaust Nozzle Area Ratio.....	~
b.....	Reaction Rate Parameter.....	~
BPR.....	Bypass Ratio.....	~
c.....	Blade Chord	ft
C.....	Absolute Flow Velocity	ft/s
C _D	Drag Coefficient	~
C _{D0}	Parasite Drag Coefficient	~
C _{D0,cr}	Parasite Drag Coefficient for Cruise.....	~
C _L	Lift Coefficient	~
C _{Lmax,L}	Maximum Lift Coefficient for Landing	~
C _{Lmax,TO}	Maximum Lift Coefficient for Takeoff.....	~
(C _h) _{ef}	Stalling Effective Pressure Rise Coefficient.....	~
c _p	Specific Heat at Constant Pressure	ft-lbf/slug-°R
c _v	Specific Heat at Constant Volume	ft-lbf/slug-°R
C _z	Absolute Axial Flow Velocity	ft/s
C _θ	Absolute Swirl Flow Velocity	ft/s
CGR	Climb Gradient	~
CLP	Combustor Loading Parameter	~
D.....	Diffusion Factor	~
e.....	Oswald Efficiency Factor	~
e.....	Polytropic Efficiency	~
F _n	Net Force.....	lbf
FN	Net Force.....	lbf
FPR	Fan Pressure Ratio	~
h.....	Channel Height.....	ft



H_L Combustor Liner Height	ft
H_r Combustor Dome Height	ft
i Blade Incidence Angle	deg
L Length	ft
L/D Lift-to-Drag Ratio	~
(L/g_2) Average Diffusion Length Ratio	~
\dot{m} Mass Flow Rate	lbm/s
\dot{m}_c Corrected Mass Flow Rate	lbm/s
M Mach Number	~
N Number of Engines	~
N_r Number of Rotor Blades	~
N_s Number of Stator Blades	~
o Throat Opening	ft
OPR Overall Pressure Ratio	~
p Pressure	lbf/in ²
p_t Total Pressure	lbf/in ²
\bar{q} Dynamic Pressure	lbf/ft ²
r Radius	in
R Gas Constant	ft-lbf/slug-°R
R Range	nmi
Re Reynolds Number	~
°R Degree of Reaction	~
s Blade Row Pitch	ft
S Wing Planform Area	ft ²
S' Swirl Number	~
s_{TOG} Ground Run Takeoff Distance	ft
t_{max}/c Maximum Thickness to Chord Ratio	~
T Temperature	°R
T_t Total Temperature	°R
TET Turbine Entry Temperature	°R



TSFC	Thrust Specific Fuel Consumption	lbm/hr/lbf
T/W	Thrust-to-Weight Ratio	~
U	Rotor Rotational Speed	ft/s
V	Velocity	ft/s
V_{sL}	Stall Velocity for Landing	ft/s
W	Flowrate	lbm/s
W	Relative Flow Velocity	ft/s
W	Weight	lbf
W_E	Aircraft Empty Weight	lbf
W_{TO}	Aircraft Takeoff Weight	lbf
W_z	Relative Axial Flow Velocity	ft/s
W_θ	Relative Swirl Flow Velocity	ft/s
WF	Fuel Flowrate	lbm/s
WRstd	Corrected Flowrate	lbm/s
W/S	Wing Loading	lbf/ft ²
W_E/W_{TO}	Empty Weight to Takeoff Weight Ratio	~
W_i/W_f	Weight Fraction	~

Greek Symbols

α	Absolute Flow Angle	deg
α	Bypass Ratio	~
α_{opt}	Optimal Ratio of Dome Height to Annulus Height	~
α_{sw}	Swirl Angle	deg
β	Relative Flow Angle	deg
γ	Specific Heat Ratio	~
γ°	Blade Stagger Angle	deg
δ^*	Blade Deviation Angle	deg
η	Isentropic Efficiency	~
θ	Combustor Loading Parameter	~
θ	Deflection Angle	deg



κ_1	Blade Leading-Edge Angle.....	deg
κ_2	Blade Trailing-Edge Angle.....	deg
λ	Engine Bypass Ratio.....	~
μ_g	Ground Friction Coefficient.....	~
π	Total Pressure Ratio.....	~
π_f	Fan Pressure Ratio.....	~
ρ	Density.....	slug/ft ³
ρ_{blade}	Blade Material Density.....	lbm/in ³
σ	Blade Row Solidity.....	~
σ_c	Blade Centrifugal Stress.....	lbf/in ²
σ_t	Blade Thermal Stress.....	lbf/in ²
τ	Total Temperature Ratio.....	~
φ	Flow Coefficient.....	~
ϕ	Equivalence Ratio.....	~
Φ	Cooling Effectiveness Parameter.....	~
ψ	Loading Coefficient.....	~
ω	Shaft Speed.....	rpm

Subscripts

DZ.....	Dilution Zone.....	---
f.....	Fan.....	---
h.....	Hub.....	---
HPC.....	High-Pressure Compressor.....	---
HPT.....	High-Pressure Turbine.....	---
LPT.....	Low-Pressure Turbine.....	---
m.....	Pitchline.....	---
PZ.....	Primary Zone.....	---
r.....	Relative Frame of Reference.....	---
SZ.....	Secondary Zone.....	---
t.....	Tip.....	---



th Throat
z Axial Direction
 θ Relative (Swirl) Direction.....

Acronyms

AIAA..... American Institute of Aeronautics and Astronautics
APU..... Auxiliary Power Unit
ATS Air Turbine Starter
BPF Blade Passing Frequency
CAD Computer-Aided Design
CD..... Convergent-Divergent.....
CDA Controlled Diffusion Airfoil.....
CMC..... Ceramic Matrix Composite.....
CO..... Carbon Monoxide.....
DCA Double Circular Arc
DoD..... Department of Defense.....
DSI Diverterless Supersonic Inlet
EPNL..... Effective Perceived Noise Level.....
FAA..... Federal Aviation Administration
FADEC Full Authority Digital Engine Control
FAR..... Federal Aviation Regulation.....
FOD..... Foreign Object Damage
FRP Fiber Reinforced Polymer.....
HPC..... High-Pressure Compressor
HPT High-Pressure Turbine
LCC..... Life Cycle Cost.....
LPC Low-Pressure Compressor
LPT Low-Pressure Turbine.....
MATLAB..... Matrix Laboratory.....
NASA..... National Aeronautics and Space Administration
NOx..... Nitric Oxides.....



OEI..... One Engine Inoperative---

O&S Operation and Support---

RFP. Request for Proposal.....---

RPM.....Rotations per Minute.....---

RQL..... Rich-Quench-Lean---

SiC..... Silicon Carbide---

STAMPED.... Statistical Time and Market Predictive Engineering Design.....---

TBC..... Thermal Barrier Coating.....---

TPR Total Pressure Recovery---

TRL..... Technology Readiness Level---

UHC Unburned Hydrocarbon---

VCD Vortex Controlled Diffuser.....---



Acknowledgements

The authors wish to thank the following individuals who were instrumental in the success of this engine design:

- Dr. Saeed Farokhi for his impeccable guidance and support;
- Dr. Ian Halliwell for his assistance in regards to any technical questions about the RFP;
- AE 524 students from previous years for making the authors' work significantly easier.

1 Introduction

This report presents the preliminary design of the mixed flow, two spool, low bypass ratio turbofan engine, designated the TF-CLAWS. The TF-CLAWS is a candidate engine for the proposed next generation trainer capable of replacing the T-38A as per the Request for Proposal (RFP). Currently, the T-38A is powered by two J85-GE-5A afterburning turbojet engines, which will serve as the baseline engine model for this report. The next generation trainer should allow for the advancements of 5th generation fighters for pilot training, and thus offer a lower cost-per-mile than the T-38A. The current T-38A and the baseline engine schematic are shown in Figure 1.1.

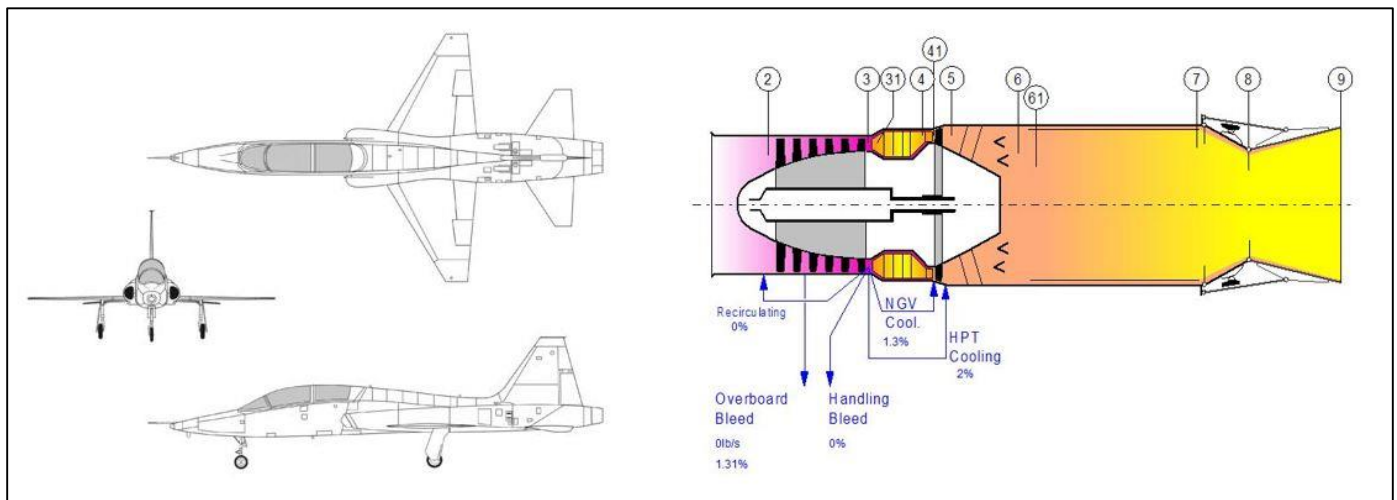


Figure 1.1: T-38A Trainer Layout with Baseline Engine [1]

The in-flight thrust requirements for the trainer (total of two engines) are shown in Table 1.1, the design requirements and characteristics for the next generation trainer in the RFP are shown in Table 1.2, and key fifth generation fighters characteristics are shown in Table 1.3.

Table 1.1: In-Flight Thrust Requirements for the Next Generation Trainer [1]

Flight Condition	Mach Number and Altitude	Thrust Requirement
Takeoff	Sea Level Static +27°F Std. Day	8,000 lbf
Cruise	Mach 0.85, 35,000 feet	1,270 lbf
Supersonic Flight	Mach 1.3, 40,000 feet	3,000 lbf
Loiter	Mach 0.5, 15,000 feet	2,460 lbf

Table 1.2: General Characteristics of the Next Generation Trainer [1]

RFP Design Requirements	Value
Crew	2
Length	46.0 ft
Wingspan	25.25 ft
Height	13.8 ft
Wing Area	170 ft ²
Maximum Fan Diameter	20 in
Maximum Takeoff Weight	12,000 lbm
Power Plant	2 x low bypass ratio turbofans; 4,000 lbf each @ SLS
Maximum Speed	Mach 1.3 at 40,000 feet
Cruise Speed	Mach 0.85 at 35,000 feet
Range	At Mach 0.85: 1,500 nmi
Loiter	Mach 0.5 @ 15,000 feet for 30 minutes
Service Ceiling	51,000 ft (16,000 m)

Table 1.3: Key Characteristics of Fifth Generation Fighters [2]

5th Generation Fighter Characteristics
Supersonic Cruise Capability
High Maneuverability: T/W > 1.0
Advanced Avionics
Multirole Capabilities
Networked Data Fusion from Sensors and Avionics

Subsequent sections demonstrate the cycle analysis and optimization of the TF-CLAWS at design and off-design conditions. A combat patrol mission is assumed for the TF-CLAWS and the new aircraft engine performance results are compared with the baseline engine. Furthermore, a detailed engine component design is also presented, which demonstrates and provides justification for the use of new materials and advanced technologies in the TF-CLAWS. Finally, this report presents a detailed CAD model of the next generation trainer, as well as a number of future promising areas and technological advances that will improve the TF-CLAWS in future design considerations.

2 Cycle Analysis

This chapter describes the basic structure of the TF-CLAWS engine and documents the cycle analysis program that was used to aid in the design of the low bypass ratio turbofan. The optimal cycle design is

presented in this chapter. The analysis code used to complete the cycle analysis was the gas turbine simulation software GasTurb 12, and the simulation of the TF-CLAWS is available from the authors upon request.

2.1 Advanced Engine Cycle Concepts for the TF-Claws

The first step in developing the optimal cycle for the TF-CLAWS is to consider a number of different, but promising cycle concepts and determine which cycle concept will provide the optimal combination of performance, complexity, technology readiness level (TRL), and cost. To this end, a number of different novel cycles were considered. The first of these novel concepts is a turbofan engine that incorporates a fan duct burner, in a mixed-flow turbofan configuration with an ejector nozzle, which is shown in Figure 2.1.

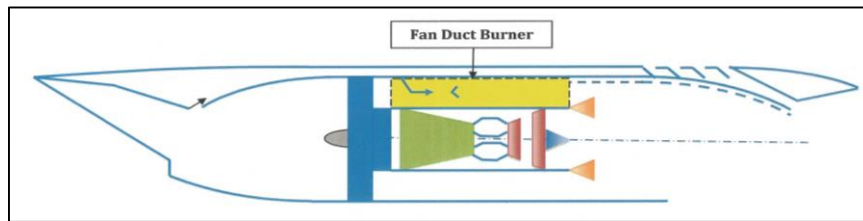


Figure 2.1: Mixed-Flow Turbofan Engine with a Fan Duct Burner and Ejector Nozzle [3]

This turbofan engine configuration would increase performance through the combustion and subsequent expansion of the bypass air, in addition to the core flow. However, this concept would increase fuel consumption, akin to an afterburner, to unacceptable levels, as the fan duct burner thermodynamically behaves as an afterburner, and afterburners are inherently inefficient, leading to lower cycle thermal efficiencies. In addition to the fan duct burner concept, another novel engine cycle considered was a mixed-flow turbofan engine with an aft fan (direct drive), again with an ejector nozzle configuration. This aft fan concept is shown in Figure 2.2.

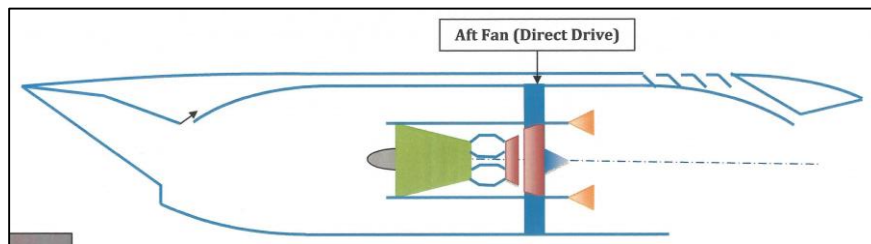


Figure 2.2: Novel Mixed-Flow Turbofan Engine with an Aft Fan (Direct Drive) [3]

This novel turbofan engine configuration would introduce significant weight savings compared to a traditional turbofan engine configuration, as the shaft connecting the low-pressure turbine to the low-pressure compressor would no longer be required. However, this concept would decrease the performance of the engine core, as the air flow entering the core would not be compressed by the fan and thus the overall pressure ratio of the engine would be decreased, thrust would be reduced, and fuel consumption would be increased. A second consideration against the use of this novel engine concept stemmed from development cost, as no fighter engine uses aft fan technology. Due to the inherent drawbacks of both the fan duct burner concept and the aft fan concept, the engine design team decided that a conventional mixed-flow turbofan engine would best suit the needs of the next generation trainer. While the fan duct burner concept would generate more thrust and the aft fan concept would reduce weight, a conventional mixed-flow turbofan engine design offers the lowest costs while still generating the required levels of thrust and offering low weight. Since the TF-CLAWS is being utilized on a military trainer aircraft, the most sensible option is to produce a conventional mixed-flow turbofan engine that is relatively inexpensive with emphasis on technological advances that will be proven ready by 2025. To this end, we have adopted promising technologies with $TRL > 9$.

2.2 Engine Components and Diagrams

The TF-CLAWS is a low bypass ratio, mixed flow, two-spool turbofan engine composed of the following eight main components:

- | | | |
|-----------------------------|-------------------------------------|-------------------|
| 1. Air Intake System | 4. Advanced Combustor & Fuel System | 7. Mixer |
| 2. Transonic Fan | 5. High-Pressure Turbine | 8. Exhaust System |
| 3. High-Pressure Compressor | 6. Low-Pressure Turbine | |

In addition to these eight main components, engine auxiliary systems (e.g., APU, FADEC, anti-icing) are fully designed and integrated in the aircraft. The location of these engine components is indicated in Figure 2.3 (from GasTurb 12 Analysis Code). As stated in the RFP, one of the major requirements for the TF-CLAWS is the ability to fit within the required engine envelope, which allows for a maximum fan diameter of less than 20”

and an overall nacelle length of 51” [1]. With this geometrical constraint in hand, then the engine components are designed and detailed flow through the TF-CLAWS determined. The TF-CLAWS performance superiority over the conventional low bypass ratio turbofan engine is that it has supercruise capabilities, and as such there is no afterburner installed in the TF-CLAWS, which drastically reduces fuel consumption and engine weight.

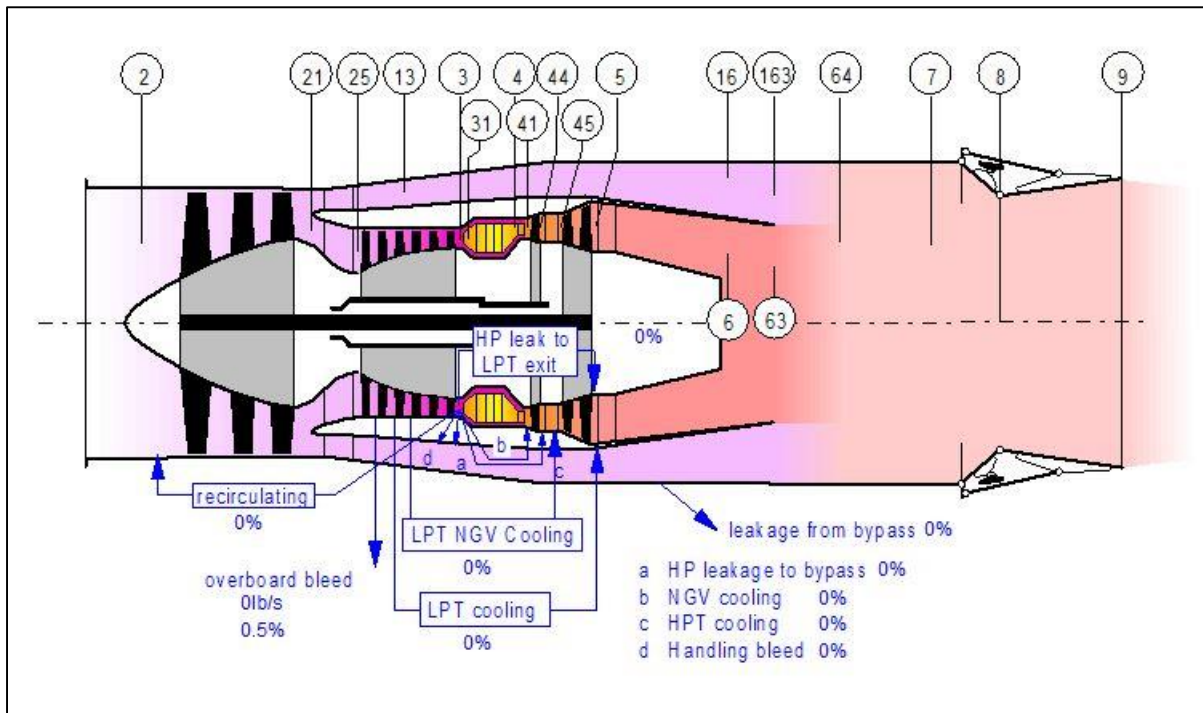


Figure 2.3: Station Numbers for the TF-CLAWS – A Mixed-Flow Turbofan Engine [4]

2.3 Baseline Engine Cycle Analysis and Validation

This section briefly describes the on-design and off-design cycle analysis and validation of the baseline engine in the selected analysis code, GasTurb 12 [4].

2.3.1 On-Design Analysis of Baseline Engine: Simulation Validation

As per the RFP, the design point for the baseline engine is a required takeoff thrust of 4,000 lbf at 27°F over the standard sea level static day. Table 2.1 presents the baseline engine characteristics at the takeoff condition. The exact cycle parameters for the takeoff condition are provided in the RFP, and are verified by the team through usage of the gas turbine engine simulation software GasTurb 12. GasTurb 12 will serve as the primary design code for the cycle analysis of the TF-CLAWS.

Table 2.1: Baseline Engine Performance at Takeoff

Station	W	T	P	WRstd	Reheat on	
amb	lb/s	R	psia	lb/s	FN	= 3855.79 lb
1	38.091	518.67	14.696		TSFC	= 2.2707 lb/(lb*h)
2	38.091	518.67	14.402	38.868	FN/w2	= 3256.84 ft/s
3	37.592	939.56	95.903	7.753	Prop Eff	= 0.0000
31	36.335	939.56	95.903		eta core	= 0.3103
4	36.916	2000.00	92.506	11.516	P5/P2	= 2.4601 EPR
41	37.411	1987.11	92.506	11.633	WF	= 0.58104 lb/s
49	37.411	1619.44	35.430	27.867	wFRH	= 1.85104 lb/s
5	38.173	1606.58	35.430	27.867	WF total	= 2.43208 lb/s
6	38.173	1606.58	34.013		A8	= 153.61 in ²
61	17.315	1606.58	34.013		XM8	= 1.00000
7	18.155	3829.29	32.425		P8/Pamb	= 2.2064
8	40.024	3829.29	32.425	22.357	wB1d/w2	= 0.01310
Bleed	0.499	518.67	14.402		Ang8	= 14.16 °
P2/P1 = 0.9800		P4/P3 = 0.9646	P6/P5 0.9600		CD8	= 0.9717
Efficiencies:	isent	polytr	RNI	P/P	wC1N/w2	= 0.01300
Compressor	0.8746	0.9026	0.980	6.659	wC1R/w2	= 0.02000
Burner	0.9950			0.965	Loading	= 100.00 %
Turbine	0.8811	0.8678	1.301	2.611	e45 th	= 0.87279
Reheat	0.8742			0.953	XM61	= 0.20000
					XM7	= 0.36971
					far7	= 0.06470
					PWX	= 0.00 hp
Spool mech Eff	0.9999	Speed	14000 rpm		A9/A8	= 1.03080
Con-Di Nozzle:					CFGid	= 0.99994
A9* (Ps9-Pamb)		-71.532				
hum [%]	war0	FHV	Fuel			
0.0	0.00000	18400.0	Generic			

2.3.2 Off-Design Analysis of Baseline Engine: Simulation Validation

As per the RFP, the aircraft must takeoff at 27°F over the standard sea level static day, cruise at Mach 0.85 at 35,000 feet, fly supersonically at Mach 1.3 at 40,000 feet, and loiter at Mach 0.5 at 15,000 feet. These become the off-design points for the cycle analysis of the baseline engine. Using GasTurb 12, an off-design analysis using a set of “Mission” points is carried out for the baseline engine. To generate the required thrust for each of the three off-design points, the turbine entry temperature is varied from the takeoff design point until the required thrust level is matched. For the subsonic cruise and loiter flight conditions, the afterburner is turned off. For the supersonic dash flight condition, the afterburner is engaged. The key parameters of the baseline engine off-design performance are summarized in Table 2.2. With the off-design performance of the baseline engine determined, the validation of the GasTurb 12 analysis code is now complete.

Table 2.2: Baseline Engine Performance at Off-Design Conditions

Mach Number	0.85	1.3	0.5
Altitude (ft)	35,000	40,000	15,000
F_n (lbf)	635	1500	1230
TSFC (lbm/hr/lbf)	1.066	1.936	1.025
T_{t4} (°R)	1714	1999	1843
T_{t7} (°R)	-	2739	-
OPR	6.136	6.268	6.262



2.4 TF-CLAWS Cycle Analysis: New Engine Optimization

Now that we have established parametric validation of the baseline engine using GasTurb 12, we proceed to develop a model for the TF-CLAWS. Rather than an afterburning turbojet engine that served as the baseline engine model, the TF-CLAWS is a mixed flow, two spool, low bypass ratio turbofan engine. The cycle analysis of the TF-CLAWS aims to reduce specific fuel consumption at all flight conditions, as well as to reduce the weight of the powerplant using advanced technology component design utilizing advanced materials and manufacturing techniques. To minimize the specific fuel consumption of the TF-CLAWS, we conduct trade studies to determine the optimal combination of bypass ratio, fan pressure ratio, turbine entry temperature, and overall pressure ratio. One of the most important design limits implemented in this cycle analysis is a maximum turbine entry temperature of 3300 °R. The basis for this design limit is that silicon carbide (SiC) ceramic-matrix-composite (CMC) material has been tested by GE Aviation to be able to withstand service temperatures upwards of 3300 °R without the need for traditional cooling techniques [5]. This represents a breakthrough technology in future gas turbine engine designs, in which turbines are uncooled. The prospect of using an uncooled turbine and the corresponding performance gains are validated at GE Aviation, and the design team has rated this technology with a TRL of 9 for the entry-into-service date of 2025 [5].

2.4.1 On-Design Analysis of the TF-CLAWS: Exploring Parametric Space

The on-design condition for the next generation trainer is defined as “top-of-climb,” which is at Mach 0.85 and 35,000 feet, the subsonic cruise condition. Generally speaking, engines with supersonic capabilities are normally sized at “top-of-climb” conditions, rather than at takeoff, and the TF-CLAWS follows this practice [1]. To begin this analysis, a few constraints and assumptions were made. First, the fan diameter of the new engine is limited to 20” by the existing engine envelope. This limits the cross-sectional area at the engine face (station 2), which thus limits the corrected mass flow rate at the engine face with a reasonable axial Mach number, i.e., ~0.5-0.6. For this reason, the corrected mass flow rate at all flight conditions (on-design and off-design points) was held below 50 lbm/s, to ensure that the fan diameter did not exceed the 20” limit. From here,

we then used the optimization program featured in GasTurb 12 to address the impact of bypass ratio, fan pressure ratio, HPC pressure ratio, and nozzle area ratio on TSFC. Some of the most critical trade studies to determine the optimal parameters for the on-design condition of the TF-CLAWS are shown in Figure 2.4. The black square shown in the carpet plots of Figure 2.4 represents the location of the overall optimization.

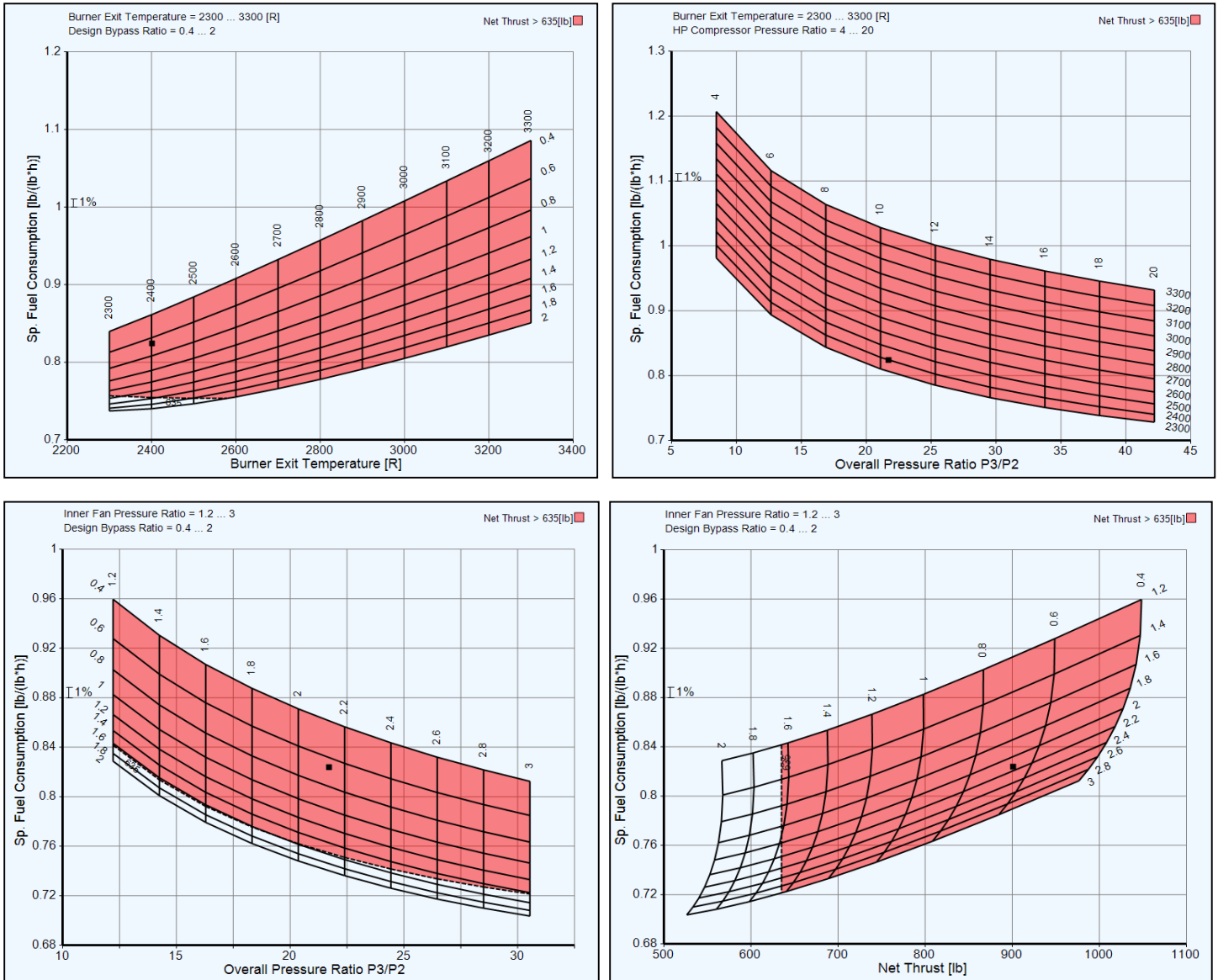


Figure 2.4: Parametric Studies of Cruise TET, BPR, FPR, OPR, and TSFC for the TF-CLAWS [4]

We note in Figure 2.4 that TSFC decreases as fan pressure ratio increases (and thus overall pressure ratio increases). Furthermore, as bypass ratio increases, TSFC decreases, and as turbine entry temperature decreases, TSFC decreases. Thus, for the design point of subsonic cruise a TSFC of 0.824 lbm/hr/lbf was selected, as well



as a bypass ratio of 0.659 and a turbine entry temperature of 2400 °R. The choice of design bypass ratio is a function of maximum turbine entry temperature and the variation of TSFC at all four of the main flight conditions, and will be explained in more depth in Section 2.4.2. The cycle parameters for the TF-CLAWS at subsonic cruise are described in Table 2.3, and Table 2.4 shows a comparison of important cycle parameters for both the TF-CLAWS and the baseline engine at subsonic cruise.

Table 2.3: Optimized Performance of the TF-CLAWS at Subsonic Cruise

Station	W	T	P	WRstd	FN	=	900.75	lb
amb								
1	18.038	393.85	5.458		TSFC	=	0.8241	lb/(lb*h)
2	18.038	450.89	5.492	45.000	WF Burner	=	0.20620	lb/s
13	7.165	670.38	19.368	6.190	S NOX	=	0.2820	
21	10.873	573.34	11.705	14.352	BPR	=	0.6590	
25	10.873	573.34	11.588	14.497	Core Eff	=	0.5213	
3	10.873	1182.53	119.151	2.025	Prop Eff	=	0.5103	
31	10.818	1182.53	119.151		P3/P2	=	21.694	
4	11.024	2400.02	113.193	3.079	P5/P2	=	3.5264	EPR
41	11.024	2400.02	113.193	3.079	P16/P6	=	1.00000	
43	11.024	1873.06	35.513		A63	=	112.61	in ²
44	11.024	1873.06	35.513		A163	=	46.73	in ²
45	11.024	1873.06	34.803	8.846	A64	=	159.35	in ²
49	11.024	1645.73	19.368		XM63	=	0.24412	
5	11.024	1645.73	19.368	14.901	XM163	=	0.23848	
6	11.024	1645.73	18.980		XM64	=	0.25000	
16	7.165	1672.38	18.980		P63/P6	=	0.99000	
64	18.189	1281.80	18.747		P163/P16	=	0.99000	
8	18.189	1182.53	119.150	22.416	A8	=	69.42	in ²
Bleed	0.054				CD8	=	0.95000	
					Ang8	=	251.00	°
Efficiencies:					P8/Pamb	=	5.42128	
Outer LPC	0.8811	0.9000	0.441	3.526	WLKB/W25	=	0.00000	
Inner LPC	0.8888	0.9000	0.441	2.131	WCHN/W25	=	0.00000	
HP Compressor	0.8647	0.9000	0.700	10.282	WCHR/W25	=	0.00000	
Burner	0.9995			0.950	Loading	=	100.00	%
HP Turbine	0.9120	0.9000	1.283	3.187	WCLN/W25	=	0.00000	
LP Turbine	0.9064	0.9000	0.524	1.797	WCLR/W25	=	0.00000	
Mixer	0.5000				WBHD/W21	=	0.00000	
HP Spool mech Eff	1.0000	Speed	14000 rpm		Far7	=	0.01147	
LP Spool mech Eff	1.0000	Speed	6500 rpm		WBLD/W25	=	0.00500	hp
P2/P1=	0.9900	P25/P21=	0.9900	P45/P44=	PWx	=	67.1	
Con-Di Nozzle:					P16/p13	=	0.9800	
A9*(Ps9-Pamb)	2.086				P6/P5	=	0.9800	
					A9/A8	=	1.40625	
					CFGtd	=	0.98673	

Table 2.4: Comparison of Important Cycle Parameters at Subsonic Cruise

Cycle Parameter	Baseline: Subsonic Cruise	TF-CLAWS: Subsonic Cruise	Percent Difference
F_n (lbf)	635	901	41.9%
TSFC (lbm/hr/lbf)	1.066	0.824	-22.7%
Overall Pressure Ratio	6.136	21.7	254%
T_{t4} (°R)	1714	2400	40.0%
Fan Pressure Ratio	-	2.131	-
Bypass Ratio	0	1.039	-

From this comparison of cycle parameters at subsonic cruise between the TF-CLAWS and the baseline engine, we note that the TF-CLAWS improves fuel efficiency by 22.7%, which is quite a remarkable result. The other most notable feature of the design for the TF-CLAWS is the notable rise in overall pressure ratio, which increases the thermal efficiency of the engine significantly. Finally, the TF-CLAWS produces an excess thrust at cruise that positively impacts the new trainer aircraft performance. This and other performance gains are discussed in Section 3.1.

2.4.2 Off-Design Analysis of the TF-CLAWS

With the cycle parameters at the on-design point of subsonic cruise determined, it is necessary to assess the performance of the TF-CLAWS at major off-design conditions as well. The RFP states that the next generation trainer must takeoff at 27°F over the standard sea level static day (i.e., hot day), fly supersonically at Mach 1.3 and 40,000 feet, and loiter at Mach 0.5 and 15,000 feet. To conduct the off-design analysis, a series of mission points were defined in GasTurb 12, corresponding to the three above listed flight conditions. For the TF-CLAWS at off-design conditions, the goal was to obtain the required thrusts while achieving improved fuel efficiency from the baseline engine model. Figure 2.5 presents two critical trade studies that dictate the off-design cycle parameters for the TF-CLAWS: one showing the relationship between cruise bypass ratio and the turbine entry temperature required at takeoff to generate 4,000 lbf of thrust, and the other showing the relationship between cruise bypass ratio and TSFC at each of the four main flight conditions.

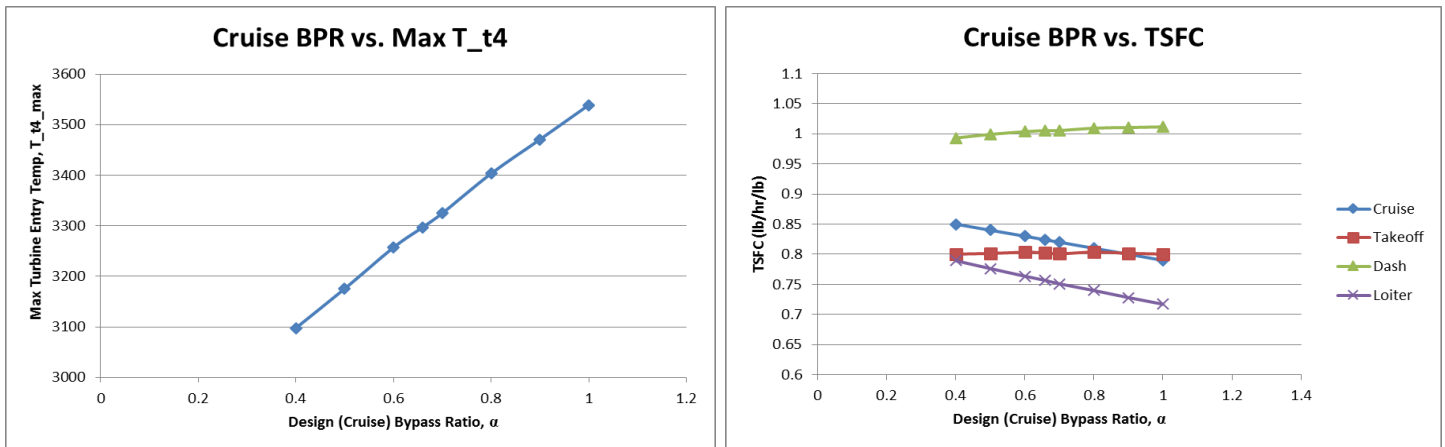


Figure 2.5: Trade Studies Dictating Off-Design Cycle Parameters for the TF-CLAWS

From Figure 2.5, we note that as on-design bypass ratio increases, the TSFC at cruise and loiter decreases, while the TSFC at takeoff and supersonic dash increases. The final on-design bypass ratio chosen was 0.659, as this value was the largest cruise bypass ratio in which the maximum turbine entry temperature across all flight conditions was held at 3300 °R or below. From this iterative cycle analysis relating on-design parameters to off-design performance, it was possible to generate the final cycle characteristics for each off-design condition. The key parameters of the TF-CLAWS off-design performance are summarized in Table 2.5.

Table 2.5: Performance of the TF-CLAWS at Off-Design Conditions

Mach Number	0	1.3	0.5
Altitude (ft)	0	40,000	15,000
F_n (lbf)	4000	1500	1230
TSFC (lbm/hr/lbf)	0.802	1.005	0.757
T_{t4} ($^{\circ}$R)	3296	3102	2262
A_9/A_8	1.248	1.99	1.124
OPR	27.2	26.1	16.8
π_f	2.411	2.359	1.832
α	0.54	0.564	0.726

2.5 Performance Comparison with the Baseline Engine Model

Upon comparison of the on-design performance (subsonic cruise) of the baseline engine and the TF-CLAWS as shown in Table 2.4, we note that the TSFC is reduced by 22.7%, a remarkable increase in engine fuel efficiency. Table 2.6 shows a comparison of the most important cycle parameters at takeoff, supersonic dash, and loiter for both the baseline engine and the TF-CLAWS.

Table 2.6: Comparison of Engine Performance between the Baseline Engine and the TF-CLAWS

Flight Condition	Cycle Parameter	Baseline Engine	TF-CLAWS	Percent Difference
Takeoff	F_n (lbf)	3856	4000	3.73%
	TSFC (lbm/hr/lbf)	2.271	0.802	-64.7%
Supersonic Dash	F_n (lbf)	1500	1500	Match
	TSFC (lbm/hr/lbf)	1.936	1.005	-48.1%
Loiter	F_n (lbf)	1230	1230	Match
	TSFC (lbm/hr/lbf)	1.025	0.757	-26.1%

From Table 2.6, we note that fuel efficiency of the TF-CLAWS completely dominates the baseline engine at every operating point. For takeoff, the TF-CLAWS decreases fuel consumption by nearly two-thirds of the baseline engine! This is a phenomenal performance gain and is one of the major selection criteria of this engine design. For supersonic dash, the TF-CLAWS cuts fuel consumption nearly in half compared to the baseline engine! This drastic fuel reduction for dash grants the next generation trainer the ability to supercruise very efficiently. These impressive performance gains are functions of the major design selections of the TF-CLAWS, namely the lack of an afterburner (which enables supercruise) and SiC/SiC CMC turbine blades (which eliminate cooling of the turbine blades). In addition to the gains in fuel efficiency of the TF-CLAWS

over the baseline engine, the total weight of the TF-CLAWS is also significantly less than that of the baseline engine. Table 2.7 presents a comparison of major geometric parameters between the two engines.

Table 2.7: Comparison of Geometric Parameters between the Baseline Engine and the TF-CLAWS

Geometric Parameter	Baseline Engine	TF-CLAWS	Percent Difference
Max. Engine Diameter (in)	22	17.6	-20%
Length (in)	108.1	70	-35.2
Weight (lbf)	584	459	-21.4%

Based on these considerations, the TF-CLAWS absolutely dominates the baseline engine in terms of both fuel efficiency and operational limits, while also drastically reducing the overall weight.

3 Mission Specification and Profile

This chapter describes the assumed mission for the next generation trainer to approximate the total fuel required for the mission. The main mission assumed for the next generation trainer is a combat patrol mission.

3.1 Combat Patrol Mission

Through utilization of GasTurb 12, it is possible to generate a multi-segment mission for any aircraft/engine. The combat patrol mission that the next generation trainer equipped with two TF-CLAWS will fly is summarized as follows:

1. Warm-up and taxi for 15 minutes
2. Takeoff and ascent to cruise at 35,000 ft
3. Cruise for 1500 nmi at Mach 0.85, 35,000 feet
4. Dash for 60 seconds at Mach 1.3, 40,000 ft
5. Loiter at Mach 0.5, 15,000 ft for 30 minutes
6. Descend and Landing (7.5 minute duration)

From this combat patrol mission profile, as well as the cycle parameters for each of the operational points documented in Section 2, then it is possible to determine the fuel consumption over the course of the entire mission for both the TF-CLAWS and the baseline engine and to compare the results. To determine the fuel consumed for each portion of the mission, it is prudent to translate both range and flight time duration into overall fuel consumption. The weight of fuel for each leg of the mission that is controlled by flight time duration can be calculated through Equation 3.1. To determine the fuel consumed for legs of the mission that are controlled by range, the Breguet range equation must be utilized (Equation 3.2). This equation alone gives

the weight fraction of that leg of the mission. From that weight fraction, the fuel consumption can then be calculated (see Equation 3.3). As part of the Breguet range equation, the lift-to-drag ratio for the aircraft must be known. For a military trainer, a reasonable value of lift-to-drag ratio can be assumed to be 10, a value taken from Table 2.2 of Jan Roskam’s “Airplane Design, Part I: Preliminary Sizing of Airplanes” [6].

$$\text{Fuel Weight} = F_n * \text{TSFC} * \text{Duration of Leg} \quad (3.1)$$

$$R = (V/\text{TSFC}) * (L/D) * \ln(W_i/W_f) \quad (3.2)$$

$$\text{Fuel Weight} = W_i(1 - W_f/W_i) \quad (3.3)$$

The additional parameters and assumptions are listed as follows:

1. The next generation trainer will have a takeoff weight of 10,486 lbm (see Section 14.2 for preliminary weight estimations for the next generation trainer);
2. Fuel consumption resulting from the climb from subsonic cruise to supersonic dash is considered negligible;
3. Fuel consumption resulting from the descent from supersonic dash altitude to loiter altitude is negligible;
4. The TSFC for the landing condition is the same as for warm-up and taxi conditions, which is a conservative estimate.

From these parameters, assumptions, and the equations listed previously, the fuel consumption for the combat patrol mission of the next generation trainer may be calculated. The fuel consumption of the next generation trainer using two baseline engines is shown in Table 3.1, and the fuel consumption of the next generation trainer using two TF-CLAWS engines is shown in Table 3.2. The baseline engine and TF-CLAWS are compared in Table 3.3.

Table 3.1: Combat Patrol Mission Fuel Weight for Baseline Engine

Phase	TSFC (lbm/hr/lbf)	Time (hr)	Range (nmi)	Total Thrust (lbf)	Fuel Weight (lbm)
Warm-up and Taxi	1.03	0.25	-	5360	1380
Max Power TO and Climb	2.271	0.0833	-	7712	1459
Cruise at M = 0.85	1.066	-	1500	1270	2129
Dash at M = 1.3	1.936	0.0167	-	3000	96.8
Loiter at M = 0.5	1.025	0.5	-	2460	1261
Landing	1.03	0.125	-	5360	690
Total	-	-	-	-	7016

Table 3.2: Combat Patrol Mission Fuel Weight for TF-CLAWS

Phase	TSFC (lbm/hr/lbf)	Time (hr)	Range (nmi)	Total Thrust (lbf)	Fuel Weight (lbm)
Warm-up and Taxi	0.648	0.25	-	5360	868
Max Power TO and Climb	0.802	0.0833	-	8000	535
Cruise at M = 0.85	0.824	-	1500	1802	2025
Dash at M = 1.3	1.005	0.0167	-	3000	50.3
Loiter at M = 0.5	0.757	0.5	-	2460	931
Landing	0.648	0.125	-	5360	434
Total	-	-	-	-	4843

Table 3.3: Comparison of Combat Patrol Mission Fuel Weight

Engine	Total Fuel Weight (lbm)
Baseline Engine	7016
TF-CLAWS	4843
Percent Difference	-32%

The performance results are very impressive. A reduction in total fuel weight of 32% is extremely promising and lends validity to the cycle analysis and design. The superiority of the TF-CLAWS over the baseline engine can also be demonstrated in terms of performance gains in lieu of raw fuel weight savings. If the TF-CLAWS were to use the same amount of fuel as the baseline engine (i.e. an increase in fuel consumption of 2173 lbf), then either the subsonic cruise range can be increased *or* the flight time spent in supersonic dash can be increased. Figure 3.1 presents the performance gains that the TF-CLAWS offers over the baseline engine. From Figure 3.1, we note that the next generation trainer, when equipped with the TF-CLAWS, can either increase cruise range by 2,188 nautical miles *or* increase supersonic dash flight time by 44 minutes (which represent major improvements in training missions)! Figure 3.1 serves to demonstrate the extreme favorability of the TF-CLAWS over the baseline engine.

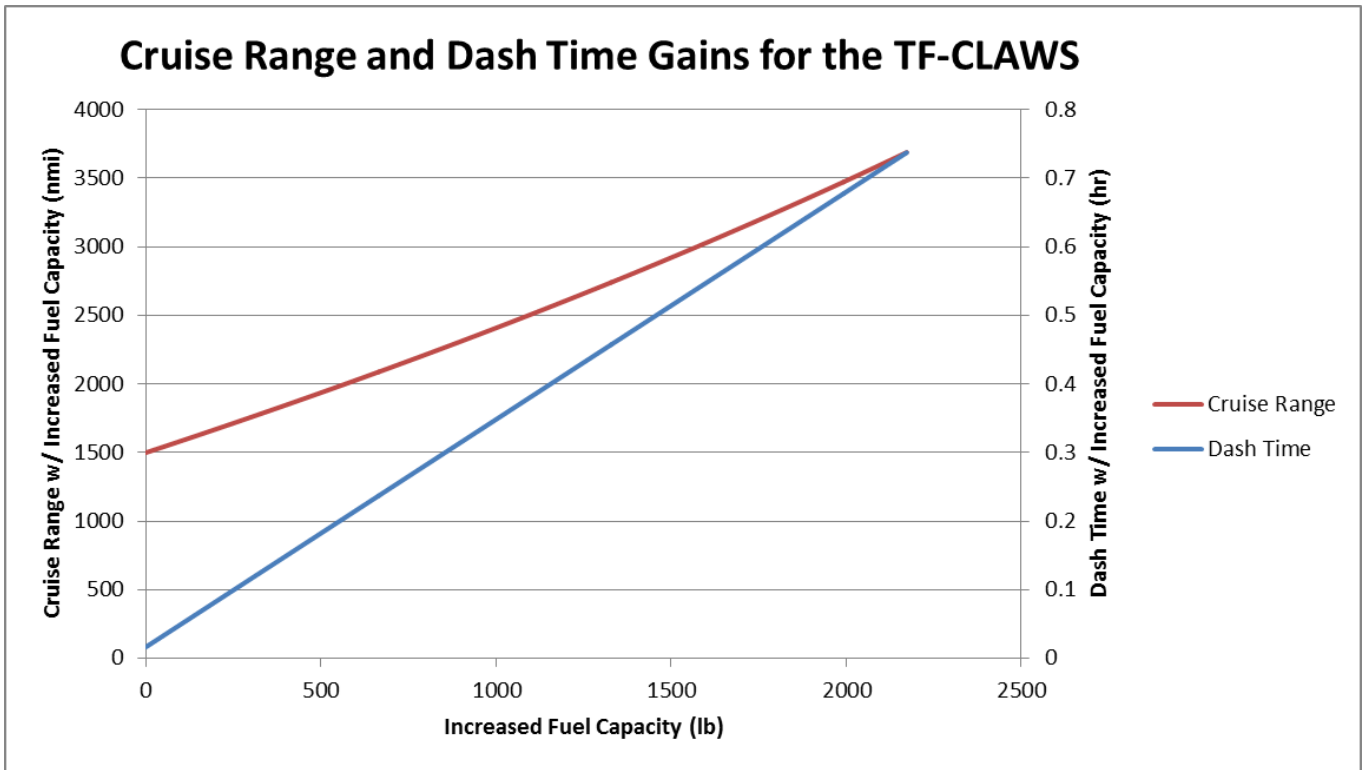


Figure 3.1: Cruise Range and Dash Time Performance Gains Offered by the TF-CLAWS

4 Engine Inlet Design

The inlet for the TF-CLAWS is an external-compression supersonic inlet, and it is more advanced than the inlet from the baseline engine outlined in the RFP. The engine inlet has twin side-mounted external compressor apertures with a diverterless supersonic inlet (DSI). A two-ramp full external-compression inlet is selected and integrated into the DSI. The inlet configuration selection is based on the supersonic Mach range in the flight envelope as specified by the RFP. The external compression inlet is the best option to enable a higher total pressure recovery (TPR), as supersonic flow deceleration over multiple shocks is more efficient than deceleration through a normal shock. The RFP suggests two types of inlet cross-sections: axisymmetric and two-dimensional. The two-dimensional supersonic diffuser can provide larger variations in inlet integration. By comparing those two inlet cross-sections, the supersonic diffuser is selected to be two-dimensional [7].

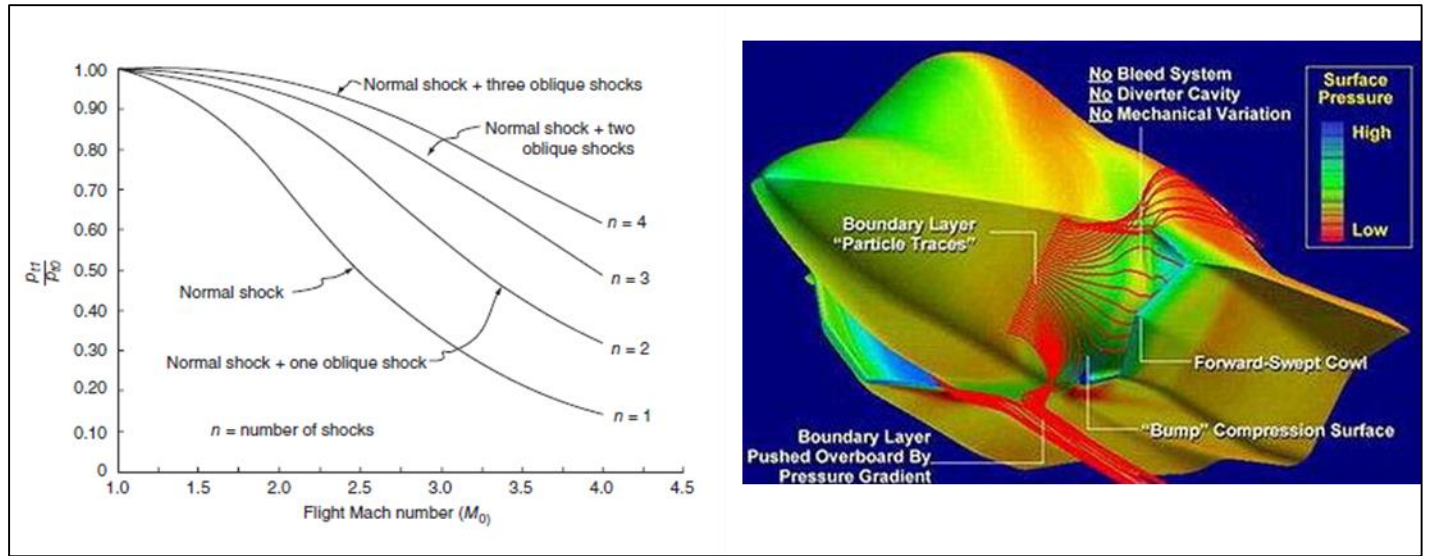


Figure 4.1: Optimum Total Pressure Recovery of External Compression Inlets [8] / Diverterless Supersonic Inlet (DSI) [9]

The DSI uses a highly three-dimensional “bump” compression surface and forward-swept inlet cowl to redirect the boundary layer around the engine intake. It also compresses the air to lower airspeeds for the supersonic flight regime. Compared to older fighter aircraft, such as the F-16, F-22 and Su-27, the DSI reduces external installation drag, weight, manufacturing complexity, and costs [10]. The 3-D bump-type inlet improves total pressure recovery as well.

A two-ramp, full external compression inlet is first designed, then integrated into a “bump.” The ramp angles are calculated using the Oswatitsch optimization technique to maximize the shock pressure recovery. Oswatitsch optimization states that all shocks should have equal strengths to optimize pressure recovery [8]. The inlet is designed for the supersonic dash condition of Mach 1.3 at an altitude of 40,000 feet. By using the following Oswatitsch optimization expression:

$$M_1 \sin \theta_1 = M_2 \sin \theta_2 = \dots = M_{n-1} \sin \theta_{n-1} \quad (4.1)$$

The ramp angles are determined to be $\theta_1 = 2^\circ$ and $\theta_2 = 1.87^\circ$. From these ramp angles, the total pressure recovery is calculated to be 0.9967. A three-dimensional bump compression surface is generated based on the

double ramp system by MATLAB. For the subsonic flight condition, the inlet total pressure recovery is assumed by the military specification MIL-E-5008B to be 1, i.e., $\eta_{R_{spec}} = 1$ for $M_0 \leq 1$.

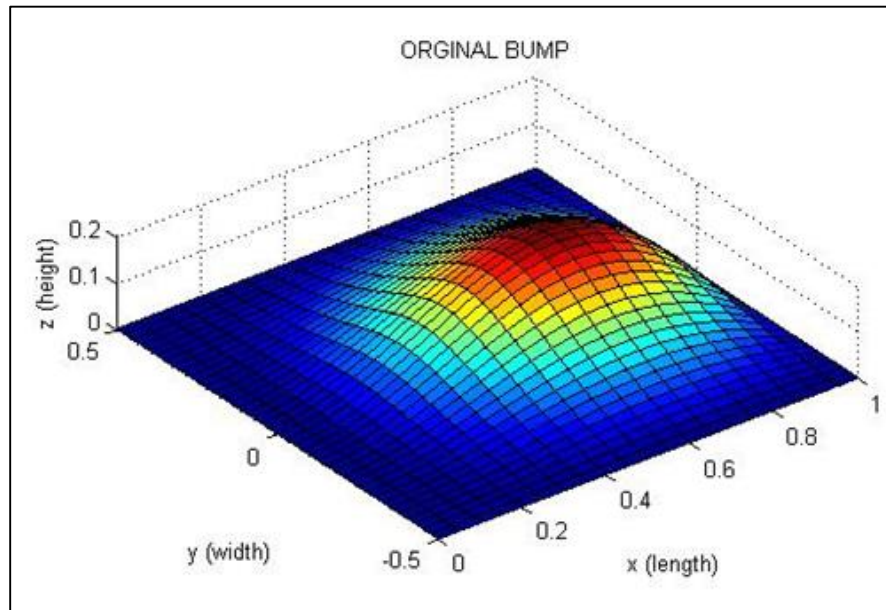


Figure 4.2: 3-D “Bump” Generated by MATLAB as an Integral Component to DSI [11]

An additional consideration in the design of the inlet is that the engine mass flow rate demands are different at the various Mach numbers and altitudes within the flight envelope. Therefore, the inlet throat must be able to satisfy all requirements for each flight condition. Table 4.1 presents the results of the inlet throat sizing for all flight conditions.

Table 4.1: Inlet Throat Sizing for all Flight Conditions

Flight Condition	Throat Area, $A_{th}(ft^2)$	Throat Mach Number, M_{th}	Mass Flow Rate, \dot{m} (lbm/s)
Takeoff	1	0.863	46.89
Subsonic Cruise	1	0.688	17.95
Supersonic Dash	1	0.536	26.43
Loiter	1	0.809	24.18

In order to position the normal shock at the ideal location, the mass flow which reaches the engine face must be carefully controlled. Thus, an air bleed valve at the throat is used to remove excess mass flow.

The subsonic diffuser of the TF-CLAWS serves two functions. First, it transitions the inlet duct cross-section from rectangular at the entrance to circular at the exit, and then decelerates the flow velocity and

delivers uniform flow to the engine face while maintaining minimal total pressure loss. The serpentine inlet duct (S-duct) was chosen for the subsonic diffuser. It reduces the radar cross section (RCS), while also mitigating fan noise. With the throat area, area at the engine face, and the flight conditions known, then the subsonic diffuser is sized and the key results of the design are shown in Table 4.2.

Table 4.2: Design Parameters of the Subsonic Diffuser of the Inlet of the TF-CLAWS

Design Parameter	Value
Diffuser Wall Angle	2.4°
L_d/H_t	8.4
Diffuser Length	120 in
S-Duct Bend Angle	25°

The structure of the inlet is viewed as a means of achieving minimal weight and noise. Inlet weight is driven by cross-sectional size, length, mechanical complexity, and structural loads. Main structural loads for the inlet are pressure, aircraft maneuvers, and “hammershock” load. The “hammershock” load from engine stall is the primary design load. The highest possible “hammershock” loads usually occur during stall at high dynamic pressures, supersonic speeds, and low altitude. However, findings from modern research, as well as historical data, denote that the possibility of stall at those conditions are very low. Therefore, the primary design load is reduced from 70 psi to 44 psi, which reduces the inlet duct weight by 40% [10]. The inlet of the TF-CLAWS employs 3D Fiber Reinforced Polymer (FRP) composites in the inlet duct to reduce weight and fabrication costs, as well as to improve the impact damage tolerance.

The fan noise from the supersonic fan blade tips is one of the major issues addressed in the inlet design. A 28-inch acoustic liner is designed and installed on the inner cowling of the inlet forward of the fan booster to reduce the blade-passing frequency (BPF) noise. The inlet acoustic liner will be a honeycomb aluminum composite in order to reduce weight and increase structural stiffness. With all of the major components of the inlet system of the TF-CLAWS designed, then a definition sketch of the inlet system is shown in Figure 4.3 and a 3-D representation of the inlet is shown in Figure 4.4.

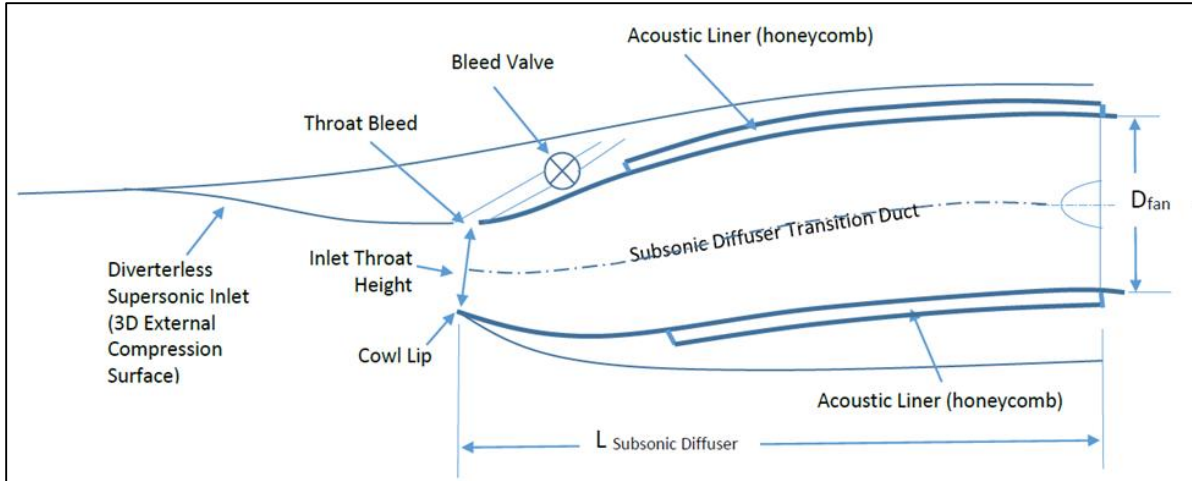


Figure 4.3: Definition Sketch of the TF-CLAWS Inlet [12]

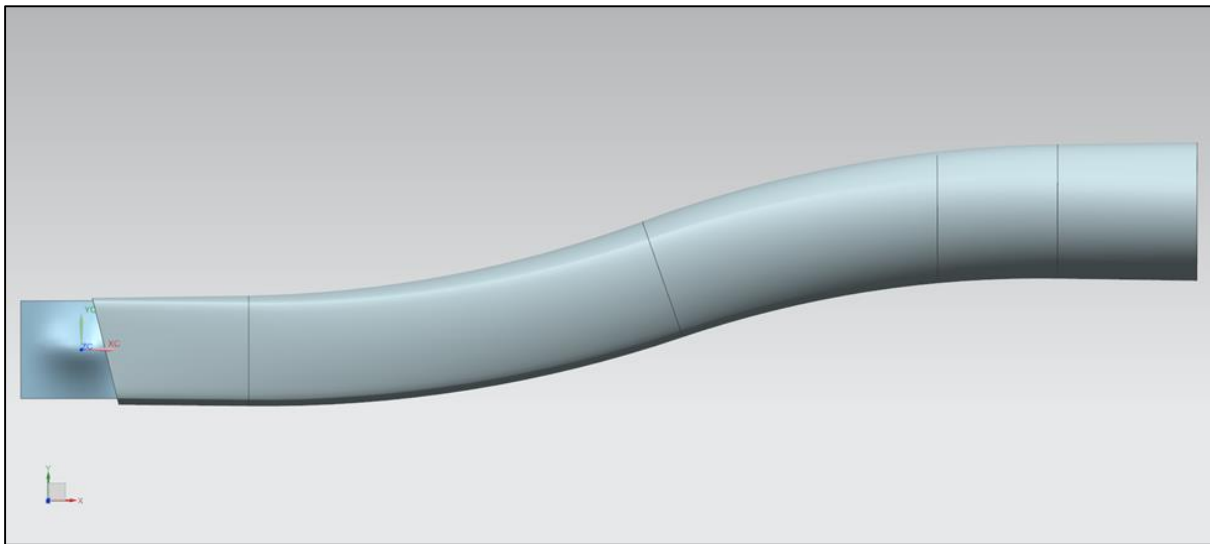


Figure 4.4: Inlet System for the TF-CLAWS

5 Compression System Design

This section documents the detailed design of the compression system for the TF-CLAWS. Included within this section are the design guidelines, assumptions, preliminary design properties, and structural/material analysis for each component of the compression system. The compression system of the TF-CLAWS is a two-spool concept, with a transonic fan and low-pressure compressor (LPC) operating on the low-speed spool and a high-pressure compressor (HPC) operating on the high-speed spool. To begin the design process for both the transonic fan and the HPC, the tip relative Mach number for the rotor of the first stage must be selected [8].

From this design selection of tip relative Mach number, it is pertinent to perform a detailed stage-by-stage design of the each component of the compression system at the hub, pitchline, and tip stream surfaces. To perform a detailed compression system stage design, we use the principles of blade vortex design, which describes the swirl velocity profile in the radial direction downstream of the rotor that is anchored at the pitchline radius [8]. For the purposes of the design of the stages of the compression system, a “free-vortex” design is applied to determine flow characteristics of the hub, pitchline, and tip stream surfaces [8]. The hub, pitchline, and tip stream surfaces may be described using the principle of “velocity triangles,” a concept which is shown in Figure 5.1.

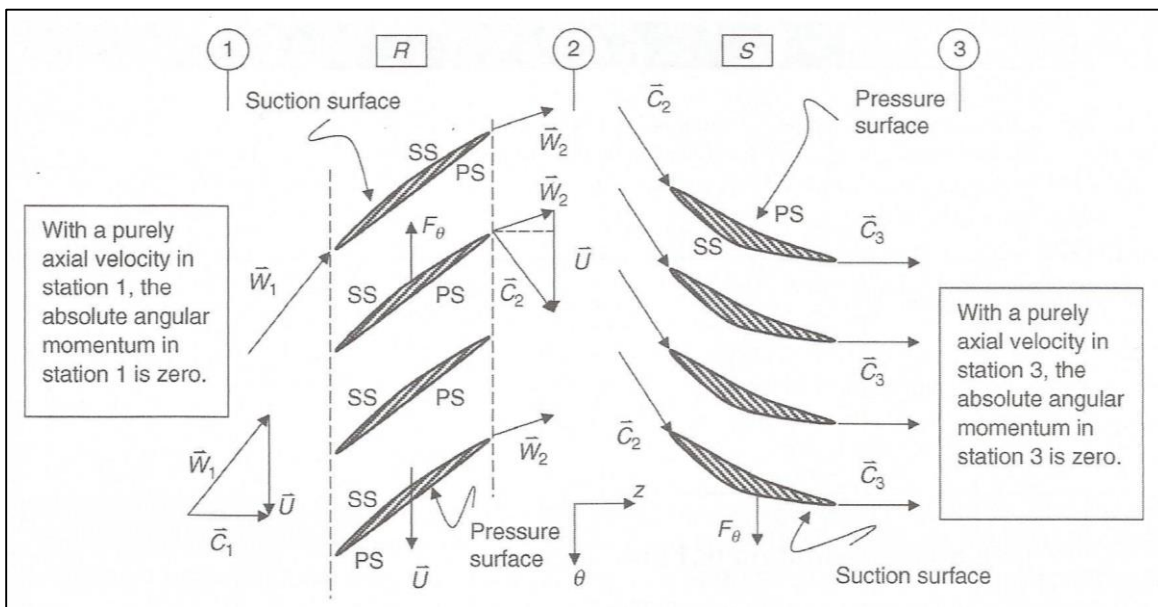


Figure 5.1: Definition of Velocity Triangles for a Compressor Stage [8]

Once the flow profile at the three stream surfaces is known for each stage of the compression system, then the geometry of the rotor and stator blades is selected (e.g., cross-sectional shape, aspect ratio, solidity, etc.). The material for the blades is then selected, and stress analyses are conducted to determine the margin of safety for the blade material selection. With the design process of the compression system in mind, then the guiding criteria in the design of any compression system are tabulated in Table 5.1, which includes nominal ranges and typical values for each criterion [8].

Table 5.1: Guidelines on the Range of Compressor Parameters [8]

Parameter	Range of Values	Typical Value
Flow Coefficient, ϕ	$0.3 \leq \phi \leq 0.9$	0.6
D-Factor	$D \leq 0.6$	0.45
Axial Mach Number, M_z	$0.3 \leq M_z \leq 0.6$	0.55
Tip Tangential Mach Number, M_T	$1.0 \leq M_T \leq 1.5$	1.3
Degree of Reaction, ${}^\circ R$	$0.1 \leq {}^\circ R \leq 0.9$	0.5 (for $M < 1$)
Reynolds Number Based on Chord	$300,000 \leq Re_c$	$> 500,000$
Tip Relative Mach Number (1 st Stage)	$(M_{1r})_{tip} \leq 1.7$	1.3-1.5
Stage Average Solidity	$1.0 \leq \sigma \leq 2.0$	1.4
Stage Average Aspect Ratio	$1.0 \leq AR \leq 4.0$	< 2.0
Polytropic Efficiency, e_c	$0.85 \leq e_c \leq 0.92$	0.9
Loading Coefficient, ψ	$0.2 \leq \psi \leq 0.5$	0.35
DCA Blade (Range)	$0.8 \leq M \leq 1.2$	Same
NACA-65 Series (Range)	$M \leq 0.8$	Same
De Haller Criterion	$W_2/W_1 \geq 0.72$	0.75
Blade Leading-Edge Radius	$r_{L.E.} \sim 5-10\%$ of t_{max}	5% t_{max}
Compressor Pressure Ratio per Spool	$\pi_c \leq 20$	Up to 20
Axial Gap Between Blade Rows	$0.23c_z$ to $0.25c_z$	$0.25c_z$
Aspect Ratio, Fan	$\sim 2-5$	< 1.5
Aspect Ratio, Compressor	$\sim 1-4$	~ 2

To arrive at a successful compressor design, a few of the design parameters listed in Table 5.1 are of special significance and dictate the selection of the other design parameters. These special design parameters are degree of reaction, blade row solidity, diffusion factor (D-Factor), and the De Haller criterion. In a successful compressor design, these four design parameters are iterated until they reach compliance with the range of values described in Table 5.1. Degree of reaction, blade row solidity, diffusion factor, and De Haller criterion are expressed in Equations 5.1 to 5.4, respectively.

$${}^\circ R = 1 - \frac{c_{\theta 2} + c_{\theta 1}}{2U} \quad (5.1) \qquad \sigma = \frac{c}{s} \quad (5.2)$$

$$D = 1 - \frac{W_2}{W_1} + \frac{|W_{\theta 2} - W_{\theta 1}|}{2\sigma W_1} \quad (5.3) \qquad \frac{W_2}{W_1} \geq 0.72 \quad (5.4)$$

In addition to the importance of the four previously-described parameters, perhaps the other single-most important consideration for any compressor is stall margin. One effective methodology to assessing the stall margin of a compressor is to use a stage-by-stage approach, in which each compressor stage is evaluated on the

basis of stalling effective static-pressure rise coefficient to ensure that stall margin requirements are met. This stage-by-stage evaluation of the stall margin for a compressor was developed by Koch, in which he developed an analogy between the stalling pressure rise capability of an axial-flow compressor stage and two-dimensional diffusers [8]. The stall margin for a compressor stage is described by both the stalling effective static-pressure rise coefficient, $(C_h)_{ef}$, and the average diffusion length ratio of the stage, L/g_2 . These two critical parameters are calculated by Equations 5.5 and 5.6, respectively.

$$(C_h)_{ef} = (C_h)_{adj} \left[\frac{(V_1'^2)_{rotor} + (V_1^2)_{stator}}{(V_1'^2)_{rotor} + F_{ef}(V_1^2)_{stator}} \right] \quad (5.5)$$

$$\left(\frac{L}{g_2}\right)_{stage} = \left[\frac{(L/g_2)_{rotor} \cdot q_1' + (L/g_2)_{stator} \cdot q_1}{q_1' + q_1} \right] \quad (5.6)$$

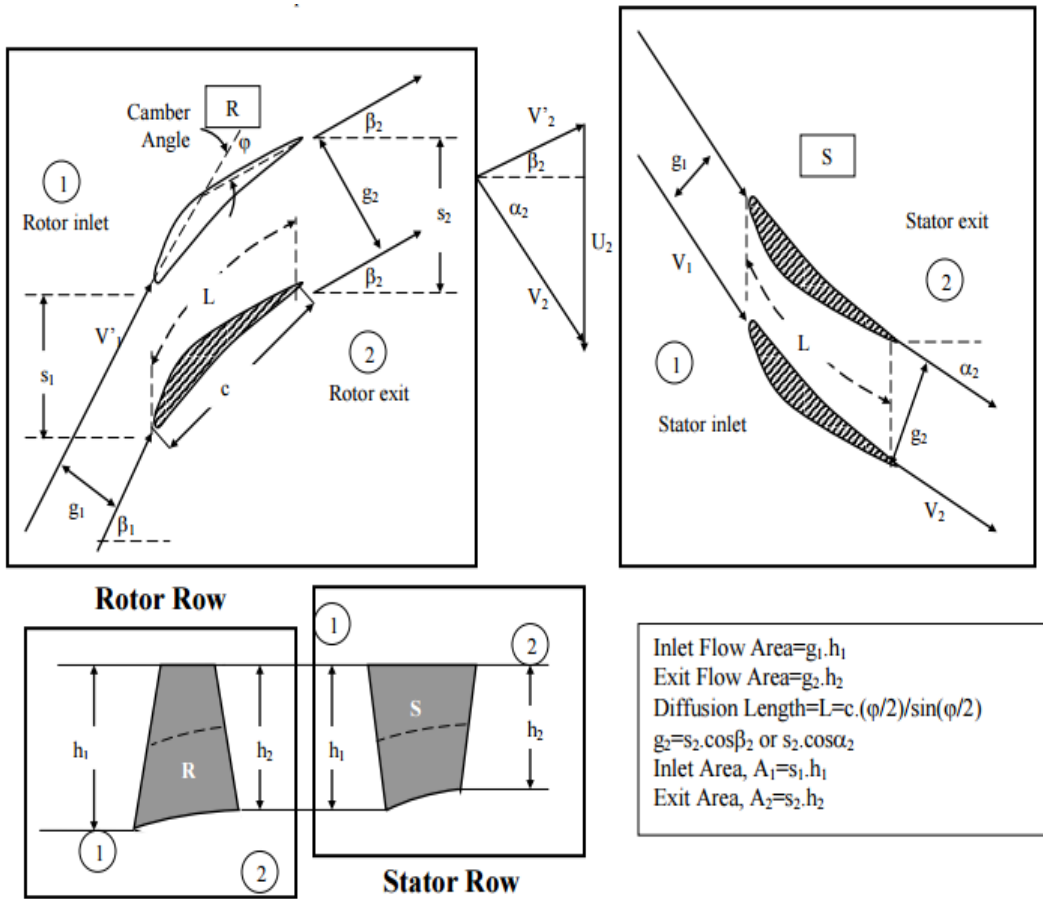


Figure 5.2 shows a definition sketch which explains the geometric parameters required to calculate the average diffusion length of the stage, L/g_2 . These geometric parameters, in addition to the velocity vectors obtained from free vortex design, are then used to calculate the stalling effective static-pressure rise coefficient,

$(C_h)_{ef}$. The average diffusion length of the stage and the stalling effective static-pressure rise coefficient are then plotted on Figure 5.3, a chart which relates the two parameters to the stall margin of a given compressor

stage. In Figure 5.3, the 0-10% stall margin range is considered the “critical” range, and as such it is a design intent to exceed this critical range of stall margin.

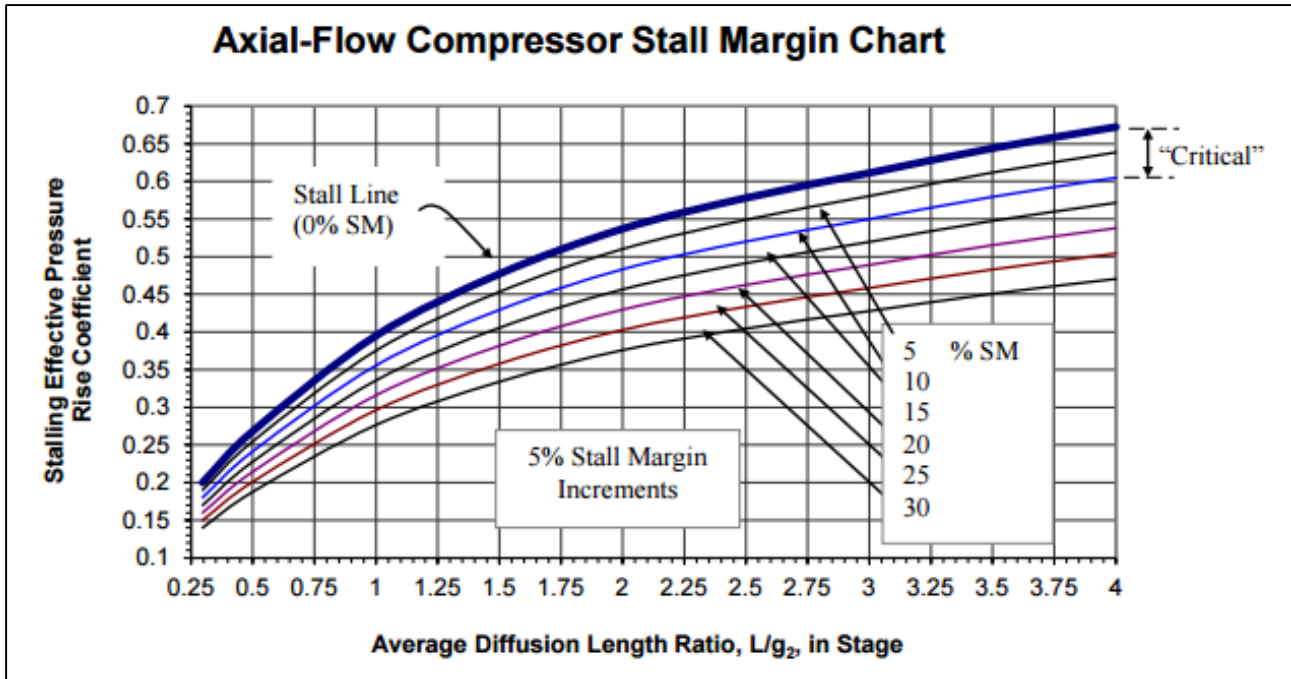


Figure 5.3: Stall Margin Estimation Chart for a Compressor Stage [8]

5.1 Fan (LPC) Design

Unlike the baseline engine, the TF-CLAWS is a low bypass, mixed flow turbofan engine, rather than a turbojet engine. Thus, the addition of a fan introduces both increased thrust potential as well as increased fuel efficiency. The fan of the TF-CLAWS is of transonic design, consisting of two stages with a pressure ratio of 2.411 at takeoff. The fan of the TF-CLAWS has a hub-to-tip radius ratio of 0.5 at the fan entrance and operates at a shaft speed of 19,271 RPM at takeoff. Table 5.2 summarizes the main global design parameters of the fan of the TF-CLAWS at takeoff.

Table 5.2: Design Parameters of the Fan of the TF-CLAWS at Takeoff

Design Parameter	Value
π_f	2.411
e_f	0.9
p_{t2}	14.55 psi
T_{t2}	545.7 °R
ω	19,271 RPM

Design Parameter	Value
τ_f	1.379
η_f	0.754
p_{t21}	35.08 psi
T_{t21}	752.4 °R
Number of Stages	2

From the data shown in Table 5.2, the fan of the TF-CLAWS must be designed on the basis of the total temperature rise required per stage, which is calculated to be 105.1 °R per stage. With the thermodynamic characteristics of the fan in hand, then the geometric properties of the fan are readily determined. From design iterations performed in GasTurb 12, the major fan annulus dimensions are known and are presented in Table 5.3.

Table 5.3: Annulus Dimensions for the Fan of the TF-CLAWS

Flow Station	Hub Radius (in)	Tip Radius (in)	Area (in ²)
Fan Inlet (Station 2)	4.29	8.58	173.3
Fan Exit (Station 21)	7.46	8.58	56.05

Furthermore, GasTurb 12 simulations include calculations of the axial chord lengths for each rotor and stator blade row of the HPC. The TF-CLAWS design has resulted in a fan length of 7.89 inches, an acceptable length for a two-stage low-bypass fan.

5.1.1 Rotor and Stator Flow Calculations

In addition to the global design parameters of the fan, it is pertinent to perform a detailed stage-by-stage design of the fan at the hub, pitchline, and tip stream surfaces. To perform a detailed fan stage design, we use the principles of blade vortex design, which describes the swirl velocity profile in the radial direction downstream of the rotor that is anchored at the pitchline radius [8]. For the purposes of the design of the stages of the fan, a “free-vortex” design is applied to determine flow characteristics of the hub, pitchline, and tip stream surfaces [8]. Table 5.4 summarizes the three-stream analysis of the first stage of the fan (subscripts 1 and 2 denotes inlet and exit of the blade row, respectively).

Table 5.4: Free-Vortex Design for the Fan and Stator of the TF-CLAWS at Takeoff

Parameter	First Rotor			First Stator		
	Hub	Pitchline	Tip	Hub	Pitchline	Tip
U (ft/s)	721.1	1082	1442	953.8	1198	1442
r (in)	4.29	6.43	8.58	5.67	7.12	8.58
$M_{1,abs}$	0.574	0.574	0.574	0.939	0.726	0.643
$M_{1,rel}$	0.867	1.131	1.421	0.568	0.679	0.989
C_z (ft/s)	636.5	636.5	636.5	636.5	636.5	636.5
W_1 (ft/s)	961.8	1255	1576	655.1	807.9	1189
$C_{\theta 1}$ (ft/s)	0	0	0	876.1	584.1	438.1
$C_{\theta 2}$ (ft/s)	876.1	584.1	438.1	0	0	0
C_2 (ft/s)	1083	863.9	772.7	636.5	636.5	636.5
W_2 (ft/s)	655.1	807.9	1189	1147	1357	1576
T_{t2} (°R)	650.8	650.8	650.8	650.8	650.8	650.8
p_{t2} (psi)	25.34	25.34	25.34	25.34	25.34	25.34
T_2 (°R)	553.2	588.7	601.1	617.1	617.1	617.1
p_2 (psi)	14.35	17.84	19.19	21.04	21.04	21.04
$M_{2,abs}$	0.939	0.726	0.643	0.523	0.523	0.523
$M_{2,rel}$	0.568	0.679	0.989	0.941	1.114	1.294
α_1 (deg)	0	0	0	54	42.5	34.5
α_2 (deg)	54	42.5	34.5	0	0	0
β_1 (deg)	-48.6	-59.5	-66.2	13.7	-38	-57.6
β_2 (deg)	13.7	-38	-57.6	-56.3	-62	-66.2
°R	0.393	0.73	0.848	0.541	0.756	0.848
σ	1.65	1.1	0.825	2.26	1.8	1.495
De Haller	0.681	0.644	0.754	0.588	0.737	0.824
D-Factor	0.595	0.568	0.414	0.591	0.451	0.366
φ	0.883	0.588	0.441	-	-	-
ψ	1.215	0.54	0	-	-	-

5.1.2 Fan Rotor and Stator Blade Design

As the Mach number varies significantly from the hub-to-tip in the fan stages, it is pertinent to effectively split the blades into three unique sections: the subsonic stream surface at the hub, the transonic stream surface at pitchline, and the supersonic stream surface at the tip. Stated differently, the rotor blades in the fan will have a variable cross-section along the span of the blade.

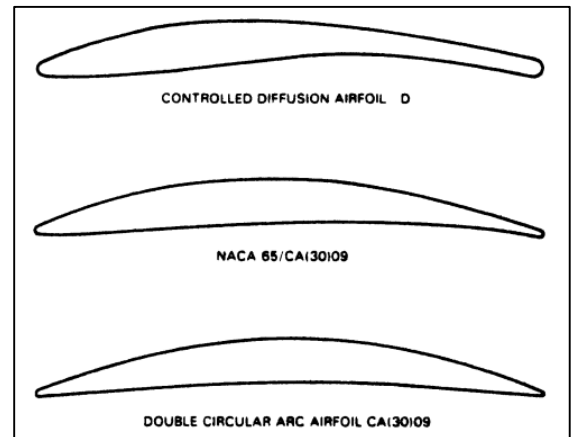


Figure 5.4: Comparison of Fan Blade Profiles [8]

This discretization of the fan rotor blades necessitates the selection of a cross-section at the hub, pitchline, and tip on the basis of Mach number. Therefore, for the subsonic regime of the hub, the fan rotor blades are best served with a NACA-65-(21)10 airfoil [8]. For the transonic regime at pitchline, the fan rotor blades are best served using a controlled diffusion airfoil (CDA) [8]. For the supersonic regime at the tip, the fan rotor blades are best served using a double circular arc (DCA) profile [8]. Figure 5.4 demonstrates the differences between a NACA-65 series airfoil, a CDA, and a DCA profile. Finally, the stator blades of the fan will employ a DCA profile along the entire length of the blade for the sake of simplicity.

In addition to the calculation of the blade angles, then the blade height, aspect ratio, mean chord, and number of blades for the first stage of the fan are also determined from free-vortex stage design. In particular, the total number of blades needed for each stage are calculated via Equations 5.7 and 5.8. The selection of the number of stator blades is made to eliminate any resonance modes in the stage [8]. Table 5.5 summarizes the blade profile design selections for the first stage of the fan of the TF-CLAWS.

$$N_r = \frac{2\pi r_m}{s_m} \quad (5.7)$$

$$N_s = 2N_r \pm 1 \quad (5.8)$$

Table 5.5: Fan Blade Characteristics for the First Stage

Design Parameter	Rotor	Stator
Blade Height (in)	4.29	2.90
AR	2	2
Mean Chord (in)	2.144	1.452
Axial Chord (in)	1.346	1.006
Pitch (in)	2.02	1.09
Number of Blades	20	41
Taper Ratio	0.8	0.8

5.1.3 Fan Stall Margin

Stall margin estimation for the first stage of the fan is performed using the procedures outlined in Section 5. Via Equations 5.5 and 5.6, the first stage of the fan has a stalling effective static-pressure rise coefficient of 0.381 and an average diffusion length of 1.201. Plotting these values in Figure 5.3 yields a stall margin of 13% for the first stage of the fan at takeoff, which is well within acceptable values.

5.1.4 Fan Blade Structural Analysis

The blades of the fan of the TF-CLAWS will make usage of the silicon carbide CMC described in Section 2. This usage of SiC/SiC CMC for the blades of the fan will reduce weight and increase the strength of the blades. To protect the composite from foreign object damage (FOD), a sheath of Ti-6Al-4V is added to the leading edge of the fan blades. The usage of this kind of titanium on the leading edge of the fan blades has been shown to be effective; in the GE90 high-bypass turbofan engine, the fan blades equipped with Ti-6Al-4V on the leading-edge were able to block two eight pound birds without blade separation or catastrophic failure [13]. In addition to the aerodynamic criteria discussed in the previous sections, the rotor blades at each stage of the fan must withstand a variety of stresses: centrifugal, bending, vibrational, and thermal stresses. The dominant stress in the rotor design, however, is centrifugal stress [8]; consequently, if the rotors have a positive margin of safety under centrifugal loading, then the rotor blades can be assumed safe in other stress modes. Equation 5.9 expresses the centrifugal stress on a compressor blade. In this expression, ρ_{blade} is the blade material density (0.0723 lbm/in³ for SiC/SiC CMC) [5], ω is the angular speed of the compressor (in rad/s), A is the flow area at the blade row, and A_t/A_h is the blade taper ratio (previously selected as 0.8). With an allowable centrifugal stress of 40,000 psi for SiC/SiC CMC, then the centrifugal stress analysis of the fan blades is summarized in Table 5.6.

$$\sigma_c = \rho_{\text{blade}} \frac{\omega^2 A}{4\pi} (1 + A_t/A_h) \quad (5.9)$$

Table 5.6: Fan Blade Structural Analysis

Design Parameter – Rotor, 1 st Stage of Fan	Value
Allowable Centrifugal Stress, σ_{all}	40,000 psi
Material Density, ρ_{blade}	0.0723 lbm/in ³
Blade Taper Ratio, A_t/A_h	0.8
Flow Area, A	173.3 in ²
HPC Angular Speed, ω	19,271 RPM
Design Centrifugal Stress, σ_c	18,914 psi
Margin of Safety	1.115

5.2 High-Pressure Compressor (HPC) Design

The high-pressure compressor (HPC) of the TF-CLAWS consists of seven stages with a pressure ratio of 11.4 at takeoff. The HPC of the TF-CLAWS has a hub-to-tip radius ratio of 0.5 at the compressor entrance and operates at a shaft speed of 39,577 RPM at takeoff. Table 5.7 summarizes the main global design parameters of the HPC of the TF-CLAWS at takeoff.

Table 5.7: Design Parameters of the HPC of the TF-CLAWS at Takeoff

Design Parameter	Value	Design Parameter	Value
π_{HPC}	11.4	τ_{HPC}	2.127
e_{HPC}	0.9	η_{HPC}	0.892
p_{t25}	34.67 psi	p_{t3}	395.8 psi
T_{t25}	752.4 °R	T_{t3}	1600 °R
ω	39,577 RPM	Number of Stages	7

From the data shown in Table 5.7, the HPC of the TF-CLAWS must be designed on the basis of the total temperature rise required per stage, which is calculated to be 132.7 °R per stage. With seven stages in total, the total temperature requirement at the HPC exit, T_{t3} , is actually exceeded. The final stage is required, however, to ensure that the pressure ratio for the HPC is satisfied, which is indeed the case. With the thermodynamic characteristics of the HPC in hand, then the geometric properties of the compressor are readily determined. From design iterations performed in GasTurb 12, the major HPC annulus dimensions are known and are presented in Table 5.8.

Table 5.8: Annulus Dimensions for the HPC of the TF-CLAWS

Flow Station	Hub Radius (in)	Tip Radius (in)	Area (in ²)
HPC Inlet (Station 25)	2.45	4.90	56.6
HPC Exit (Station 3)	4.29	4.90	17.7

Furthermore, GasTurb 12 simulations include calculations of the axial chord lengths for each rotor and stator blade row of the HPC. The TF-CLAWS design has resulted in a HPC length of 13.33 inches – a significant reduction in length. This reduction in length, coupled with the use of SiC/SiC CMCs and fewer stages than the baseline engine has significantly decreased the weight of the HPC.

5.2.1 HPC Rotor and Stator Flow Calculations

In addition to the global design parameters of the HPC, it is pertinent to perform a detailed stage-by-stage design of the compressor at the hub, pitchline, and tip stream surfaces. To perform a detailed compressor stage design, we use the principles of blade vortex design, which describes the swirl velocity profile in the radial direction downstream of the rotor that is anchored at the pitchline radius [8]. For the purposes of the design of the stages of the HPC, a “free-vortex” design is applied to determine flow characteristics of the hub, pitchline, and tip stream surfaces [8]. Table 5.9 summarizes the three-stream analysis of the first stage of the HPC (subscripts 1 and 2 denotes inlet and exit of the blade row, respectively).

Table 5.9: Free-Vortex Design for the First Stage of the HPC of the TF-CLAWS at Takeoff

Parameter	First Rotor			First Stator		
	Hub	Pitchline	Tip	Hub	Pitchline	Tip
U (ft/s)	846.8	1270	1694	1112	1403	1694
r (in)	2.45	3.68	4.90	3.22	4.06	4.90
$M_{1,abs}$	0.556	0.556	0.556	0.883	0.693	0.618
$M_{1,rel}$	0.855	1.122	1.414	0.54	0.693	1.009
C_z (ft/s)	724.5	724.5	724.5	724.5	724.5	724.5
W_1 (ft/s)	1114	1462	1842	732.2	963.5	1417
$C_{\theta 1}$ (ft/s)	0	0	0	952.7	635.1	476.3
$C_{\theta 2}$ (ft/s)	952.7	635.1	476.3	0	0	0
C_2 (ft/s)	1197	963.5	867	724.5	724.5	724.5
W_2 (ft/s)	732.2	963.5	1417	1327	1579	1842
T_{t2} (°R)	885.1	885.1	885.1	885.1	885.1	885.1
p_{t2} (psi)	51.18	51.18	51.18	51.18	51.18	51.18
T_2 (°R)	767.3	808.8	823.3	842	842	842
p_2 (psi)	35.09	42.27	45.02	48.74	48.74	48.74
$M_{2,abs}$	0.883	0.693	0.618	0.51	0.51	0.51
$M_{2,rel}$	0.54	0.693	1.009	0.935	1.112	1.298
α_1 (deg)	0	0	0	52.7	41.2	33.3
α_2 (deg)	52.7	41.2	33.3	0	0	0
β_1 (deg)	-49.5	-60.3	-66.8	8.3	-41.2	-59.2
β_2 (deg)	8.3	-41.2	-59.2	-56.9	-62.7	-66.8
°R	0.4375	0.75	0.859	0.572	0.774	0.859
σ	1.8	1.2	0.9	2.02	1.6	1.33
De Haller	0.657	0.659	0.769	0.605	0.752	0.836
D-Factor	0.58	0.522	0.375	0.592	0.454	0.372
φ	0.856	0.57	0.428	-	-	-
ψ	1.125	0.5	0	-	-	-

5.2.2 HPC Rotor and Stator Blade Design

As the relative Mach number at the inlet of the first rotor of the HPC is transonic at the hub stream surface and supersonic at the pitchline and tip stream surfaces, then a controlled diffusion airfoil (CDA) profile is selected for the hub and a double circular arc (DCA) profile is selected for pitchline and tip, as these geometric profiles offer the most favorable pressure distribution for each respective stream surface [8]. For a HPC blade profile, it is recommended to select a thickness to chord ratio of 9% at the hub, which is assumed to taper linearly to the tip, where the thickness to chord ratio is 3% [8]. Furthermore, the optimum incidence angle for the blade is selected on the basis of cascade loss “bucket curves,” and for a DCA blade with a solidity of 1.33 and a stagger of 42.5° the optimum incidence angle is 3° [8].

With the incidence angle determined, we proceed to the determination of the deviation angle of the blade. The deviation angle of the blade can be calculated through use of Carter’s rule [8]. With the deviation angle, incidence angle, and the relative flow angles determined from free-vortex stage design, the leading-edge and trailing-edge blade angles are calculated. Equations 5.10 through 5.12 describe the calculation process of all the necessary blades angles, namely deviation angle (δ^*), blade leading-edge angle (κ_1), and blade trailing-edge angle (κ_2).

$$\delta^* = \frac{\Delta\beta}{4\sqrt{\sigma}} \quad (5.10)$$

$$\kappa_1 = \beta_1 - i \quad (5.11)$$

$$\kappa_2 = \beta_2 - \delta^* \quad (5.12)$$

In addition to the calculation of the blade angles, the blade height, aspect ratio, mean chord, and number of blades for the first stage of the HPC are determined from free-vortex stage design. In particular, the total number of blades needed for each stage can be calculated through use of Equations 5.7 and 5.8 in Section 5.1.2. The selection of the number of stator blades is made to eliminate any resonance modes in the stage [8]. Table 5.10 summarizes the blade profile design selections for the first stage of the HPC of the TF-CLAWS.

Table 5.10: HPC Blade Characteristics for the First Stage

Design Parameter	Rotor	Stator
Blade Height (in)	2.45	1.68
AR	2	2
Mean Chord (in)	1.226	0.842
Axial Chord (in)	0.742	0.563
Pitch (in)	0.77	0.42
Number of Blades	22	45
Taper Ratio	0.8	0.8

5.2.3 HPC Stall Margin

Stall margin estimation for the first stage of the HPC is performed using the procedures outlined in Section 5. Via Equations 5.5 and 5.6, the first stage of the HPC has a stalling effective static-pressure rise coefficient of 0.36 and an average diffusion length of 1.359. Plotting these values in Figure 5.3 yields a stall margin of 21% for the first stage of the HPC at takeoff, which is well within acceptable values.

5.2.4 HPC Blade Structural Analysis

The blades of the HPC of the TF-CLAWS will make usage of the silicon carbide CMC described in Section 2, which will reduce weight and increase the strength of the blades. In addition to the aerodynamic criteria discussed in the previous sections, the rotor blades at each stage of the HPC must withstand a variety of stresses: centrifugal, bending, vibrational, and thermal stresses. The dominant stress in the rotor design, however, is centrifugal stress [8]; consequently, if the rotors have a positive margin of safety under centrifugal loading, then the rotor blades can be assumed safe in other stress modes. Following the same procedure outlined in Section 5.1.4, then the centrifugal stress analysis of the HPC blades is summarized in Table 5.11.

Table 5.11: HPC Blade Structural Analysis

Design Parameter – Rotor, 1st Stage of HPC	Value
Allowable Centrifugal Stress, σ_{all}	40,000 psi
Material Density, ρ_{blade}	0.0723 lbm/in ³
Blade Taper Ratio, A_t/A_h	0.8
Flow Area, A	56.7 in ²
HPC Angular Speed, ω	39,577 RPM
Design Centrifugal Stress, σ_c	26,083 psi
Margin of Safety	0.534

6 Combustion System Design

The TF-CLAWS utilizes an annular combustion chamber, following the practices of commercial and 5th generation fighter aircraft engines such as the F-119, F-135, Pratt & Whitney 1000GTF and CFM International LEAP family series.

In addition to annular design, the TF-CLAWS will use the Rich Burn-Quick Quench-Lean Burn (RQL) combustion system configuration to address the issue of emissions. The RQL concept is a reliable, low cost approach with many advantages in meeting the full range of combustion system requirements. The performance advantages of this concept will be discussed at length in Section 6.2.

The TF-CLAWS combustor was designed over a wide operating range, from on-design and off-design flight conditions. Perhaps most importantly, the combustor must conform to the maximum turbine entry temperature of 3300 °R, which occurs at the off-design takeoff condition, as stipulated by the optimized engine cycle.

6.1 Combustor Pre-Diffuser Configuration

Compressor outlet axial flow velocity of as high as 370 ft/s ($M = 0.5$) must be ideally reduced within a short axial distance before combustion commences. This flow deceleration is accomplished by employing a diffuser between the compressor exit and burner entrance.

The TF-CLAWS combustor will use a hybrid diffuser that combines a vortex controlled diffuser (VCD) with a conventional wide-angled post-diffuser located at the exit. The hybrid diffuser boasts superior performance as it can achieve a static pressure recovery at least 25% higher than conventional diffusers of the same length [14].

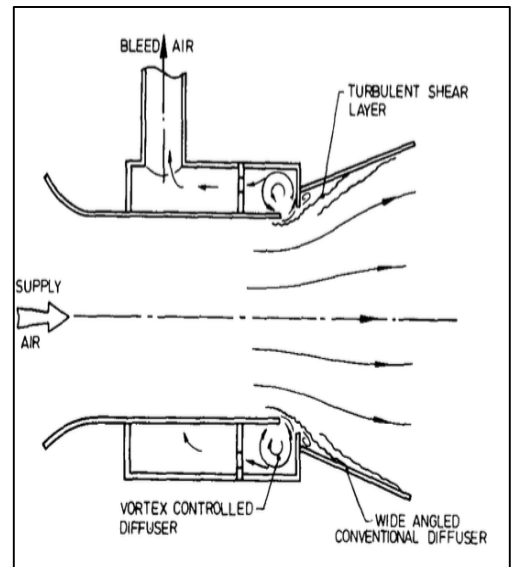


Figure 6.1: Hybrid Diffuser Configuration [14]

According to Adkins, Motharu and Yost [14], even without bleed, the hybrid diffuser can match the static pressure recovery of a conventional diffuser with only half the diffusion length.

6.2 RQL Combustor Configuration – Emissions Control

Although U.S military aircraft are exempt from EPA emissions standards governing commercial aircraft, federal law provides states with an important measure of control over the emissions of military aircraft through the general conformity rule of the 1970 Clean Air Act (CAA) [15]. The pollutants emitted by engines that are of most interest are carbon monoxide (CO), unburned hydrocarbons (UHC), nitric oxides (NOx) and particulate matter (Smoke & Soot). The amount and type of pollutants emitted are dependent on engine power conditions.

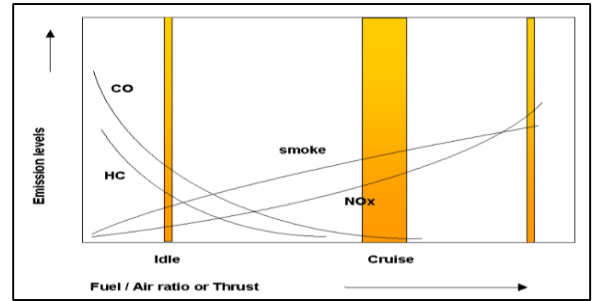


Figure 6.2: Emissions Productions vs. Thrust [16]

The RQL (Rich Burn-Quick Quench-Lean Burn) is a combustion technique used to lower the local flame temperature and reduce NOx emissions by performing combustion in fuel-rich state, and a fuel-lean state. NOx emissions are significantly reduced during high power conditions by carrying out combustion in fuel-rich state, $\phi_{PZ} > 1$ in the primary zone. Afterwards, at the end of primary zone, an instantaneous shift occurs from fuel-rich burn to fuel-lean burn by introducing an excessive blast of dilution air, hence the term quick quench [17]. Due to short residence from high mixing rates, NOx formation is inhibited.

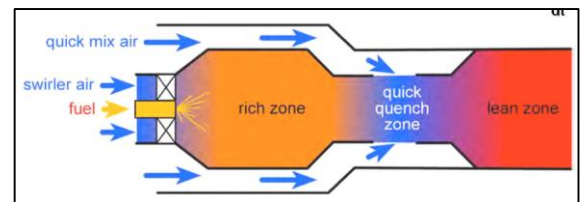


Figure 6.3: RQL Approach #1 [18]

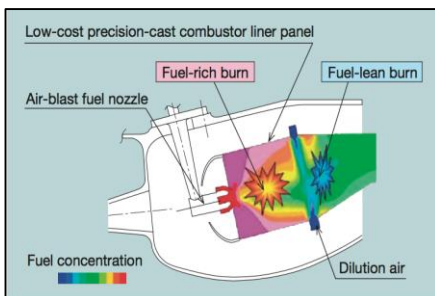


Figure 6.4: RQL Approach #2 [17]

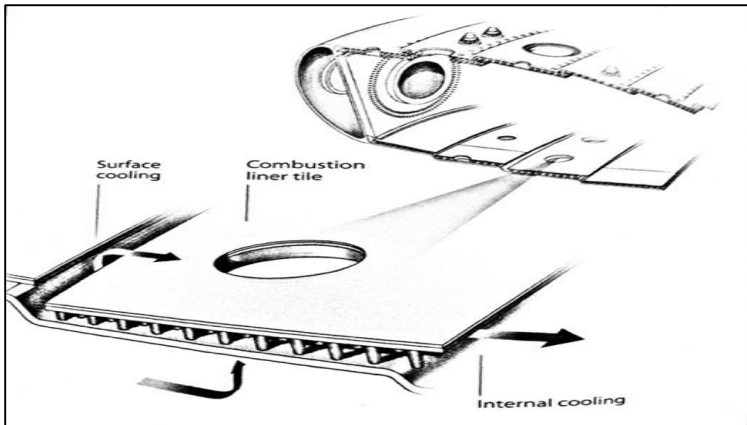
At low power conditions, combustion efficiency is high due to near-stoichiometric ($\phi_{PZ} \approx 1$) fuel-air ratio which minimizes unburned hydrocarbon and CO emissions. NOx formation rates are low due to the combined effects of low temperatures and oxygen depletion compared to high load conditions [19].

The RQL concept was chosen over the fuel-staged combustor for several reasons. These lean-stage systems, however, have the disadvantages of increased cost, weight and complexity along with the potential for

combustion instabilities and higher CO and UHC emissions due to quenching [20]. The RQL approach to combustor design is a traditional one, but years of development have optimized the key characteristics of RQL to meet increasingly stringent combustor requirements. The RQL combustor configuration is backed by industry, as it has been employed on the TALON X in the new Pratt & Whitney PW1000 series geared turbofan engine [20].

6.3 Liner Material Selection and Advanced Cooling Technique

Nickel-based super alloys like Hastelloy X, Nimonic 75 and 263 have been the standard choice of combustor liner material for decades. As demand for higher overall engine performance warrants higher combustor operating temperatures, the TF-CLAWS combustor will utilize the more superior HA188 cobalt-based super alloy, which has excellent high temperature strength and good oxidation resistance up to 2460 °R. It is also readily fabricated and formed by conventional techniques. The combustor of the Pratt & Whitney F100 engine used on the F-15 fighter jet is constructed using HA 188 super alloy [21].



The highest turbine entry temperature of 3300 °R at takeoff, however, exceeds the maximum service temperature of the burner liner by 840 °R. To protect the burner liner during takeoff, the liner hot side is fitted with ultra-lightweight ceramic matrix composites, CMC (SiC/SiC) tiles. Thermal

barrier coating (TBC) is also applied to provide an insulating layer that reduces base material temperature and mitigate the effects of hot streaking [22].

Together with CMC tiles, the convective film cooling method is employed whereby air enters through holes in the combustor walls and impinges on the tiles. The air then moves through a series of pedestals designed to improve the convective heat transfer, before exiting the front and rear of the tiles to form an insulating film.

The tiles are specifically designed to be removable for maintenance. Maintenance time and cost is reduced because changing the tile is simpler than repairing the liner [23]. The industry confidence of utilizing the tiled combustor cooling method and CMC material is increasing. The tile cooling method has been employed on Pratt & Whitney V2500, PW4000 and Rolls Royce Trent 1000 engines [23,16]. GE Aviation has begun ground testing their latest GE-9X engine which incorporates CMC material in the combustor liner in April this year [24].

CHARACTERISTICS	
•	15–25 Mil (380–640 Micron) Thickness
•	Insulating – Porous
•	Plasma Sprayed in Air
•	Two Layers
–	Bond Coat – NiCrAlY
–	Top Coat – YTTRIA Stabilized Zirconia
ADVANTAGE	
•	Reduced Metal Temperature of Cooled Components
•	8–16°F (4–9°C) Reduction Per Mil (25.4 Micron) of Coating

Figure 6.6: TBC Characteristics [22]



Figure 6.7: Convection/Film Cooling Method [16]

6.4 Combustor Air Partitioning and Equivalence Ratios

The analytical methods used to estimate combustor air partitioning was derived from Mattingly, Heiser & Pratt Aircraft Engine Design [25]. The air partitioning was analyzed at cruise and at takeoff, the most stringent flight condition.

The tailoring between fuel-rich or fuel-lean equivalence ratios in the primary zone is a critical factor in RQL combustor system design. Consequently, the air partitioning is also dependent on equivalence ratios values. For the RQL combustor, the typical equivalence ratio of lean-burn combustion is between 0.5 to 0.8 and fuel rich primary zone is between 1.2 to 1.6 [18].

A near-stoichiometric equivalence ratio of 0.8 was selected for the low-load subsonic cruise condition. A fuel-rich equivalence ratio of 1.2 was selected for the high-load takeoff condition.

Table 6.1: Summary of the Combustor Air Partitioning and Equivalence Ratios

Flight Cond.	Fuel Proportion	Φ_{PZ}	Φ_{SZ}	Φ_{exit}	\dot{m}_{PZ} (lb/s)	\dot{m}_{SZ+DZ} (lb/s)	\dot{m}_{total} (lb/s)	Φ
Cruise	Near-Stoichiometric	0.8	0.46	0.28	3.79	7.08	10.87	0.24
Takeoff	Rich	1.2	0.48	0.28	7.07	23.43	30.5	0.71

The cooling air requirement corresponding to different types of cooling methods is determined using Figure 6.9 [8]. As previously explained, the convective film cooling method was selected to cool the TF-CLAWS combustor liner. Transpiration cooling was not chosen due to problem of pore clogging.

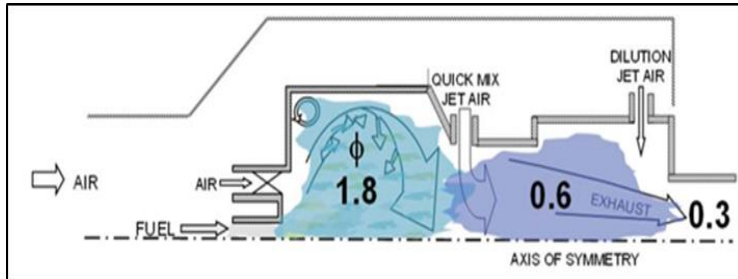


Figure 6.8: Example of RQL High-Load Operation [26]

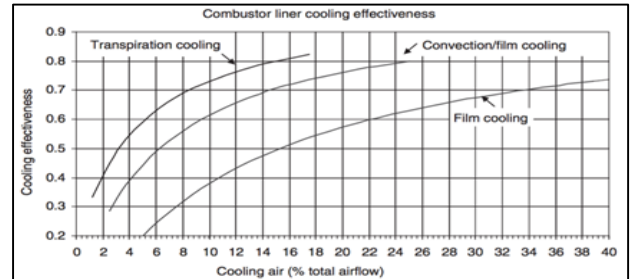


Figure 6.9: Cooling Method, Effectiveness, & Cooling Air [8]

Table 6.2: Selection and Results of the Cooling Methodology for the Combustor of the TF-CLAWS

Cooling Method	Flight Condition	Cooling Air (% Total Airflow)	$\dot{m}_{cooling}$ (lb/s)
Convection/Film	Cruise	2	0.22
Convection/Film	Takeoff	14	4.39

6.5 Combustor Geometry

The methods used for combustor geometry determination follow the techniques of Mattingly, Heiser & Pratt Aircraft Engine Design [25]. The combustor geometry was compared at both subsonic cruise and at takeoff, which is the most stringent flight condition.

Table 6.3: Dome and Liner Geometric Characteristics of the Combustor

Dome and Liner	Subsonic Cruise	Takeoff
Optimum Ratio, α_{OPT}	0.7	0.87
Dome Height, H_r (in.)	2.36	2.36
Liner Height, H_L (in.)	1.65	2.05

Table 6.4: Combustor Zone Geometric Characteristics of the Combustor

Combustor Zone	Subsonic Cruise	Takeoff
L_{PZ} , (in.)	1.10	0.86
$L_{SZ} + L_{DZ}$, (in.)	5.80	7.16
Total Length (in.)	6.90	8.00

6.6 Combustor Efficiency

Lefebvre in his publication on gas turbine combustion introduced a combustor loading parameter (CLP) which correlates well with combustor efficiency and is expressed via:

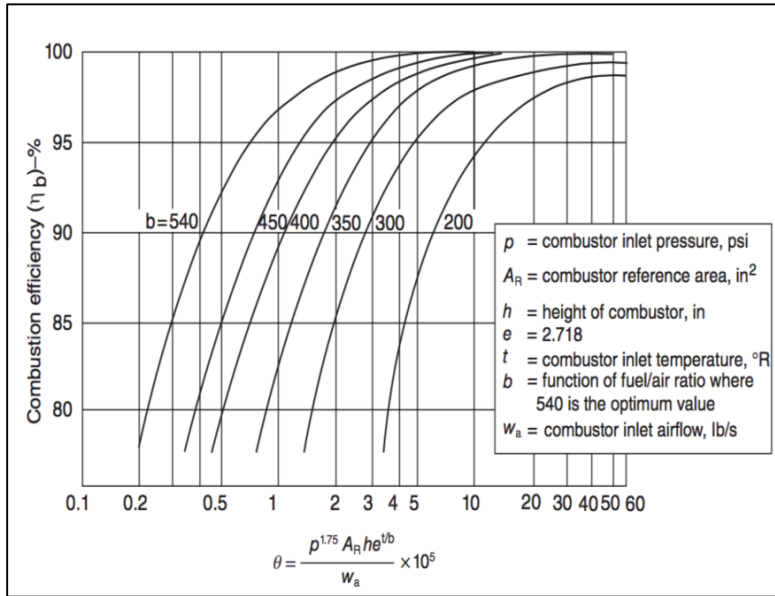


Figure 6.10: Combustion Efficiency & CLP Correlation [8]

$$CLP = \theta = \frac{p_{t3}^{1.75} \cdot A_{ref} \cdot H \cdot e^{\frac{T_{t3}}{b}}}{\dot{m}_3} \quad (6.1)$$

The reaction rate parameter, b , depends on the primary zone equivalence ratio, ϕ_{PZ} , and is expressed via the following equation by Herbert (1957):

$$b = 382 \left[\sqrt{2} \pm \ln \frac{\phi_{PZ}}{1.03} \right] \quad (6.2)$$

where (+) for $\phi_{PZ} < 1.03$, (-) for $\phi_{PZ} > 1.03$

Table 6.5: Combustion Efficiency for the TF-CLAWS at Subsonic Cruise and Takeoff

Design Parameter	Subsonic Cruise	Takeoff
ϕ_{PZ}	0.8	1.2
CLP	9.5×10^5	26.8×10^5
b	444	598
Combustion Efficiency	98%	100%

6.7 Combustor Fuel Injection

The TF-CLAWS will utilize pre-filming type air blast atomizers in which fuel is first spread out into a thin continuous sheet and is then subjected to the atomizing action of high velocity air [23]. Air blast atomizers are advantageous over pressure atomizers as they require lower fuel pump pressures and produce a finer spray. The thorough mixture of fuel and air from air blast atomization also results in low soot formation and smoke. The methods used for quick combustor swirler-injector design was derived from Mattingly, Heiser & Pratt Aircraft Engine Design [25].

Table 6.6: Characteristics of the Combustor Fuel Injector

Injection System	Subsonic Cruise	Takeoff
Number of Fuel Injectors	13	13
Swirler Tip Radius, r_t (in.)	0.67	0.47
Swirler Hub Radius, r_h (in.)	0.39	0.39
Swirler Area, A_{SW} (in ²)	0.91	0.37
Swirl Blade Angle, α_{SW}	45°	45°
Swirl Number, S'	0.81	0.94

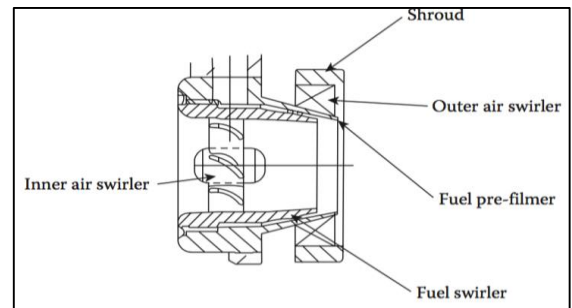


Figure 6.11: Pre-Filming Airblast Atomizer [23]

6.8 Combustor Ignition Source

The TF-CLAWS will utilize a surface discharge type igniter that consists of a central iridium electrode and outer electrode. This type is the most widely used and reliable form

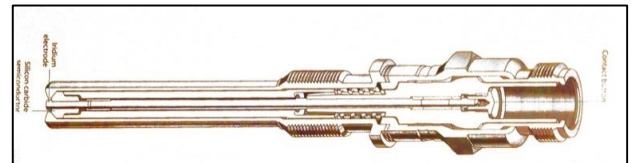


Figure 6.12: Surface Discharge Igniter [27]

of ignition for gas turbine engines. The spark igniter is located within the primary zone near the location where fuel-air mixtures pass over the electrodes. To preserve the life of the igniter, it is located away from the hottest part of the primary zone [25]. Due to the rather small overall combustor size, only two igniters will be required and will be placed on opposite sides of the annulus.

6.9 Three-View of the Combustor of the TF-CLAWS

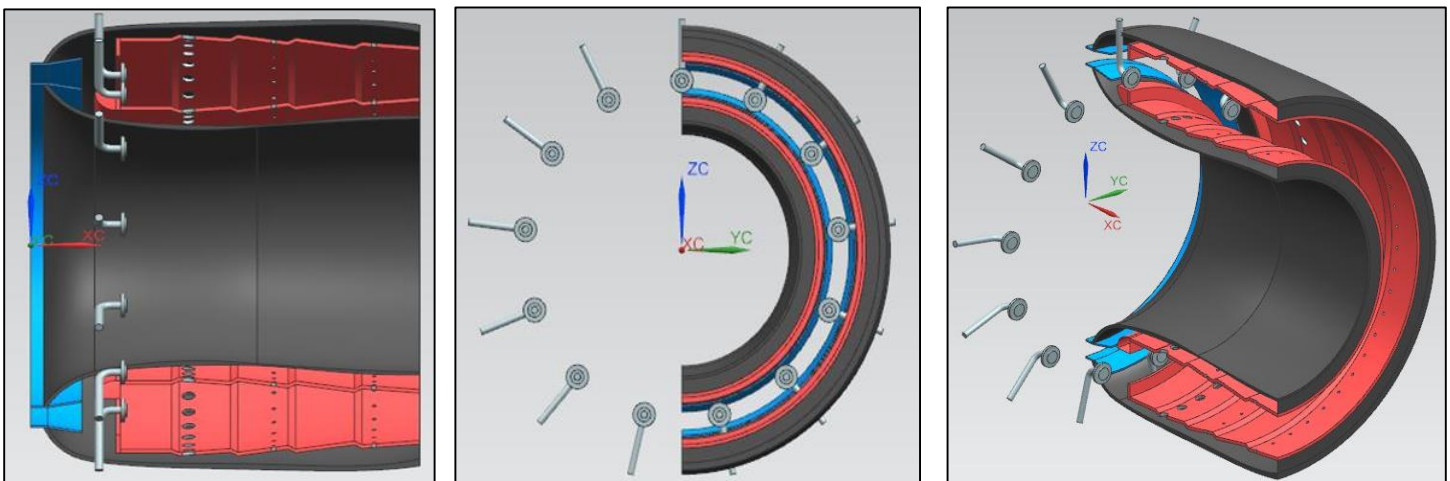


Figure 6.13: Side, Back, and Isometric Views of the Combustor of the TF-CLAWS

7 Turbine Design

7.1 High Pressure and Low Pressure Turbine

This candidate engine for a next generation trainer contains a high-pressure (HPT) and low-pressure (LPT) turbine. The HPT supplies power to the high-pressure compressor and the LPT provides power to the fan in a two-spool system. Primary considerations for designing a turbine include cycle analysis, material selection, manufacturing, blade and disk design, cooling, life, stress, and bearings.

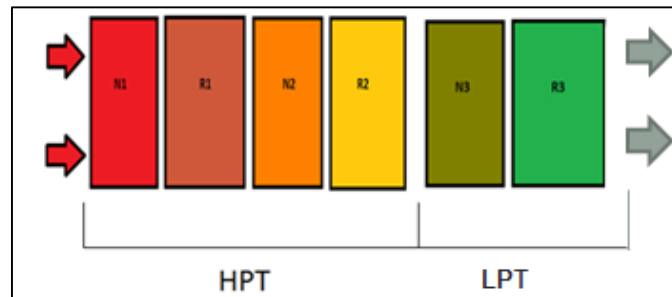


Figure 7.1: Representative Schematic of the Turbine of the TF-CLAWS

7.2 Pitchline Design Parameters

The turbine is designed for constant axial velocity ($C_z = \text{constant}$) and adiabatic flow through all turbine nozzles. All design choices and parameters are shown in Table 7.1. The angular speed of the HPT and LPT are determined by the HPC and transonic fan.

Table 7.1: Pitchline Design Parameters for the Turbine of the TF-CLAWS at Takeoff

Design Parameter	Value
\dot{m}_1 (lb _m /s)	31.23
T_{t1} (°R)	3296
p_{t1} (psi)	376.7
M_2	1.03
α_1 (deg)	0
α_2 (deg)	67.5
ω_{HPT} (rpm)	39,577
ω_{LPT} (rpm)	19,271

7.3 Turbine Flow Calculations

This section describes the absolute and relative flow paths in the HPT and LPT. Beginning with design choices and parameters outlined in “GasTurb 12”, a step-by-step process was followed to calculate the velocity

triangles at every point in between the stators and rotors [8]. The turbine was designed to have zero pitchline swirl at the turbine exit. Figure 7.2 shows an example of the velocity triangles in a turbine. Table 7.2 presents the detailed stage design for the HPT and LPT, with Stations 41-44 corresponding to the HPT and Stations 45-47 corresponding to the LPT.

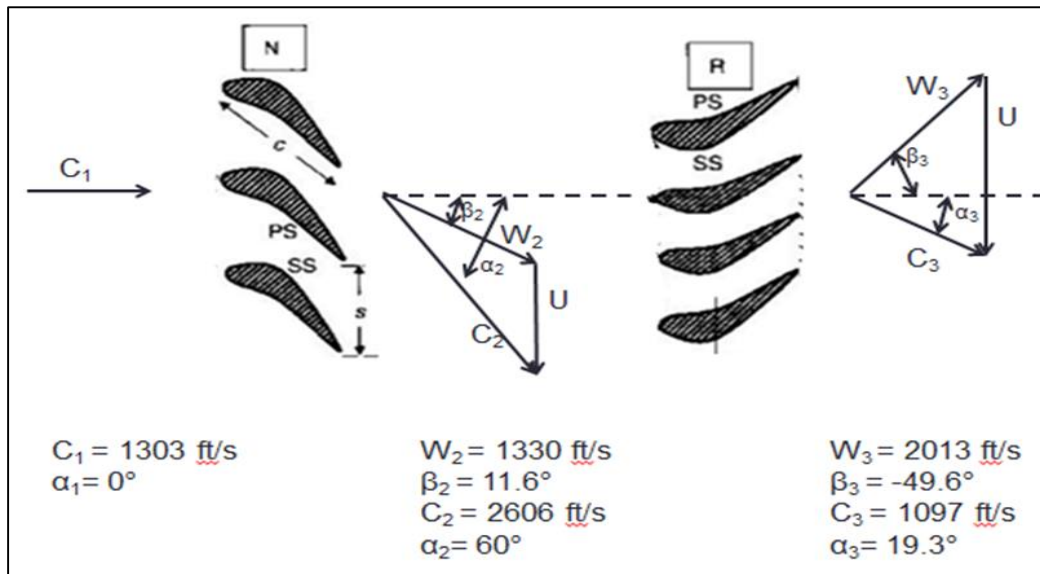


Figure 7.2: Definition Sketch for the Velocity Triangles of a Turbine Station [8]

Table 7.2: Detailed Stage Design for the HPT and LPT of the TF-CLAWS at Takeoff

Station No.	C (ft/s), Absolute Velocity			W (ft/s), Relative Velocity			U (ft/s), Rotational Speed		
	Hub	Pitchline	Tip	Hub	Pitchline	Tip	Hub	Pitchline	Tip
41	1303	1303	1303	--	--	--	--	--	--
42	2606	2606	2606	1433	1330	1304	--	--	--
43	1304	1380	1494	2064	2012	2055	1659	1990	2321
44	2027	2027	2027	1303	1381	1606	--	--	--
45	1303	1396	1716	1955	2026	1985	1528	2011	2614
46	2027	2272	2271	1557	1535	1408	--	--	--
47	1313	1303	1376	1589	1710	1613	699	1049	1326

Station No.	α (deg), Absolute Flow Angle			β (deg), Relative Flow Angle			Relative:Absolute Mach Number		
	Hub	Pitchline	Tip	Hub	Pitchline	Tip	Hub	Pitchline	Tip
41	0	0	0	0	0	0	0.48:0.48	0.48:0.48	0.48:0.48
42	60	60	60	24.6	11.5	-2.79	0.56:1.03	0.53:1.03	0.52:1.03
43	2.54	19.2	29.3	-50.8	-49.6	-50.6	0.84:0.53	0.82:0.56	0.84:0.61
44	50	50	50	1.05	-19.35	-35.8	0.55:0.85	0.58:0.85	0.67:0.85
45	1.48	21.1	40.6	-48.2	-49.9	-48.9	0.85:0.56	0.86:0.61	0.86:0.73
46	55	55	55	33.2	31.9	22.3	0.70:0.90	0.70:0.94	0.61:0.97
47	-7.13	0	18.75	-34.9	-40.3	-36.2	0.72:0.59	0.79:0.60	0.72:0.61

7.4 Material Selection

Material advancement has led gas turbine engines to become more powerful and efficient. Materials with high performance levels are highly sought after and are the primary focus of continuing research and development

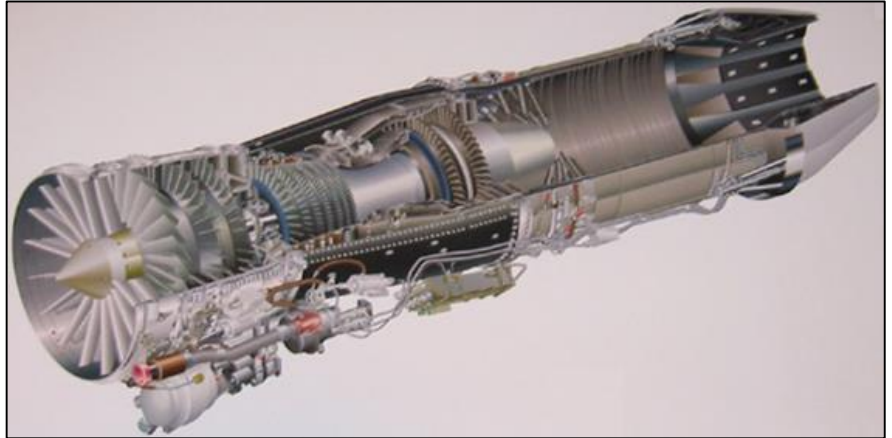


Figure 7.3: GE F414 Turbofan Engine [5]

[28]. The ability of a material to

withstand high temperatures and high stresses in service is important to a turbine material. Traditionally, nickel-based super-alloys are used in gas turbine blades and disks. However, as gas turbine technology advanced, these super-alloys became inadequate, and different coatings and cooling techniques became necessary to operate at the higher temperatures and stresses seen in service [29]. The new type of material being developed for use in gas turbine engines is ceramic matrix composites (CMCs) [30]. These materials consist of fibers cured in a matrix, usually carbon or silicon carbide.

Silicon carbide fibers and silicon carbide matrix CMCs (SiC/SiC) are attractive because they have favorable thermal properties, will require no cooling, and are 67% lighter than the lightest nickel-base superalloy (which is similar to Inconel) [31]. The silicon fibers can withstand higher temperatures if they are heat treated during manufacturing [32]. The ceramic matrix composite SiC/SiC was chosen to be the material for the turbine blades. This decision is justified as General Electric tested SiC/SiC turbine blades in 2015 in a GE F414 turbofan engine [5], seen in Figure 7.3. The CMC went through 500 “grueling” cycles in the LPT of the GE F414, generating confidence that it will be available in 2025, with a Technology Ready Level (TRL) of 9. Table 7.3 displays material properties of the SiC/SiC CMC [33].

Table 7.3: Material Properties of SiC/SiC Ceramic Matrix Composite

Material Property	Value
Max Service Temperature (°R)	3,370
Density (lbm/in ³)	0.0723
Tensile Strength (ksi)	435
Young's Modulus (Msi)	43

7.5 Turbine Aerothermodynamics

The same process used to solve the turbine velocity triangles was used for the turbine aerothermodynamics [8]. The turbine entry temperature and pressure derived from “GasTurb 12” are used to march through each stage of the turbine. The total temperature, total pressure, and degree of reaction at pitchline for each stage of the turbine can be seen in Table 7.4.

Table 7.4: Aerothermodynamic Analysis of Each Stage of the Turbine of the TF-CLAWS at Takeoff

Station Number	Total Temperature (R)	Total Pressure (psi)	Degree of Reaction
41	3296	376.7	-
42	3296	373.4	-
43	2777	184.9	0.318
44	2777	182.9	-
45	2466	113.1	0.499
46	2466	111.7	-
47	2167	65.8	0.161

Overall cycle analysis and turbine material selection determined that the turbine blades do not need to be cooled. With a pattern factor of 0.11, and a ZrO₂ thermal barrier coating that increases the allowable service temperature by 150 °R, cooling is not necessary. Thus, the mass flow rate will remain constant throughout the turbine.

Table 7.5: Turbine Entry Temperature Comparison between the Baseline Engine and the TF-CLAWS

Design Parameter	Baseline Engine	TF-CLAWS
Max Turbine Entry Temperature (°R)	2100	3296
Percent Cooling	0	0

7.6 Turbine Blade Design and Annulus Sizing

Blade design and turbine stresses will be the focus as the design of the turbine progresses. The blade design consists of blade chord (c), throat opening (o), blade spacing (s), and stagger angle (γ°). Throat opening and stagger angle are calculated using the following equations [8]:

$$o = s * \cos\alpha \quad (7.1)$$

$$\gamma^\circ(\text{Nozzle}) = \arctan\left(\frac{C_{\theta m}}{2C_z}\right) \quad (7.2)$$

$$\gamma^\circ(\text{Rotor}) = \arctan\left(\frac{W_{\theta m}}{2C_z}\right) \quad (7.3)$$

Assuming a Zweifel Coefficient of 1, the blade design characteristics are shown in Table 7.6, along with a definition sketch of the blade characteristics in Figure 7.4.

Table 7.6: Summary of the Blade Design for the Turbine of the TF-CLAWS

Turbine Stage	s (in)	c _z (in)	γ (deg)	c (in)	o (in ²)	No. of Blades
N1	0.22	0.26	40.89	0.35	0.11	124
R1	0.25	0.33	-25.92	0.36	0.24	119
N2	0.27	0.38	37.62	0.48	0.17	102
R2	0.29	0.43	-37.63	0.54	0.27	94
N3	0.30	0.48	42.19	0.65	0.17	92
R3	0.32	0.54	-6.49	0.55	0.32	91

As stated earlier, the turbine configuration is of variable pitchline radius and variable hub radius design. The annulus sizing is crucial to efficiency as tip clearance and flow losses can wreak havoc on a gas turbine engine performance. The turbine makes use of a labyrinth seal, shown in Figure 7.5. The casing significantly decreases flow losses before and after stators. Labyrinth seals are also integrated in the rotating blade rows.

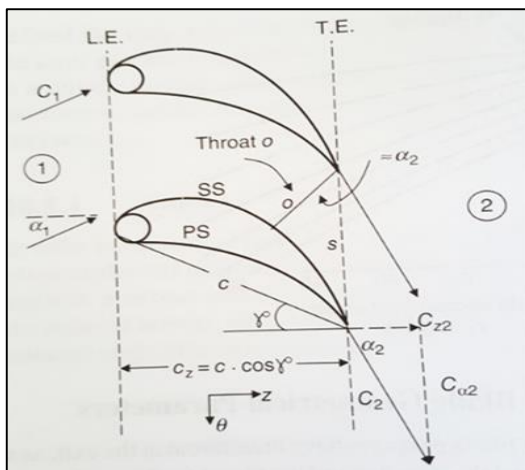


Figure 7.5: Turbine Blade Definition Sketch [8]

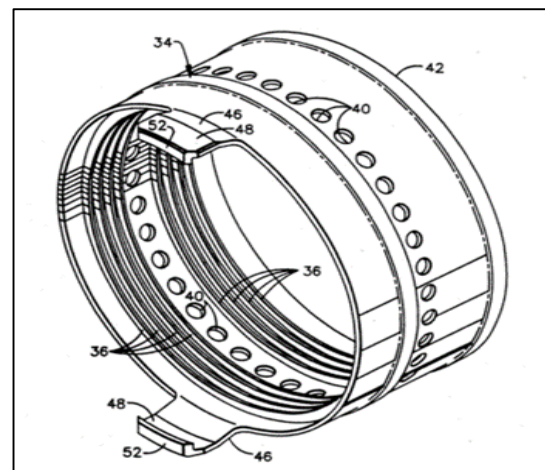


Figure 7.4: Labyrinth Casing for a Turbine Nozzle [34]

The annulus sizing makes use of the continuity equation, which can be used to solve for the flow areas through the stators and rotors.

$$\dot{m} = \frac{\sqrt{\gamma} P_t}{R T_t} A M \left(1 + \frac{\gamma-1}{2} M^2 \right)^{-\frac{\gamma-1}{2(\gamma-1)}} \quad (7.4)$$

Using Equation 7.4, and the design choice of the pitchline radius, the annulus was sized and is shown in Table 7.7.

Table 7.7: Summary of the Annulus Sizing for the Turbine of the TF-CLAWS

Design Parameter	HPT				LPT	
	N1	R1	N2	R2	N3	R3
Pitchline Radius (ft)	0.45	0.475	0.48	0.49	0.52	0.55
Hub Radius (ft)	0.363	0.396	0.365	0.356	0.359	0.384
Tip Radius (ft)	0.537	0.554	0.595	0.624	0.681	0.716
Area (ft ²)	0.495	0.470	0.692	0.826	1.053	1.146

7.7 Stress Considerations

The turbine blades will be made from SiC/SiC CMC. Stresses in turbine blades are a major concern due to the high rotational speeds, corrosive environment, and high temperatures. These are the primary aspects to consider when choosing blade material. The equation for centrifugal stress in turbine blades is based on rotational speed, material density, and blade design; shown in Equation 7.5. Stresses in turbines include centrifugal, thermal, bending, and vibrational stresses. Along with stress analysis, it is crucial when designing a turbine to avoid resonance via vibration. Campbell diagrams are used to analyze the shaft speed in RPM and determine vibration frequencies. For the centrifugal stress calculation, the area ratio was assumed to be in the range of 0.8-0.9. The centrifugal stresses for the turbine are shown in Table 7.8.

$$\sigma_c = \left(\frac{\rho A \omega^2}{4\pi} \right) \left(1 + \frac{A_t}{A_h} \right) \quad (7.5)$$

Table 7.8: Summary of Stress Calculations for the TF-CLAWS Turbine

Stresses	R1	R2	R3
AN ² (ft ³ /s)	9.18E+08	1.55E+09	5.83E+08
σ _c (psi)	47,700	103,700	38,700
σ _t (psi)	6000	5239	2169

7.8 Smith Chart

A Smith Chart consists of the flow coefficients and stage loading parameters for each stage of the turbine. These values determine the efficiency of the turbine at each stage. The Smith Chart for the TF-CLAWS turbine yielded satisfactory results for the efficiency of the turbine at each stage, and is shown in Figure 7.6.

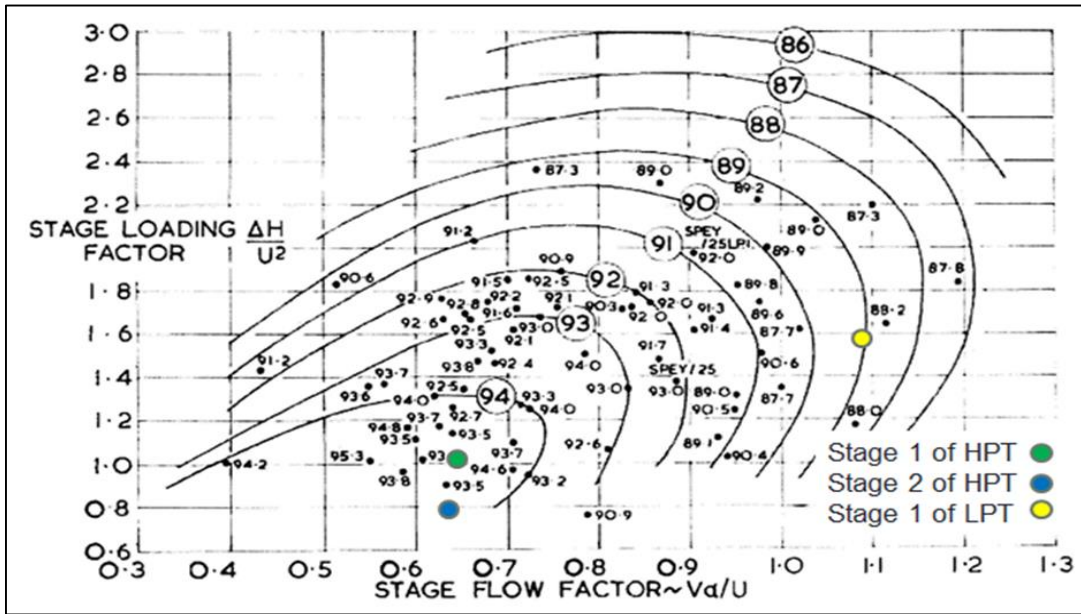


Figure 7.6: Smith Chart for the Turbine of the TF-CLAWS at Takeoff [34]

8 Mixer Design

The core flow is mixed with the fan flow from the bypass duct using a forced flow lobed mixer. This mixer has splitter guides with trailing edges. In order to ensure good vortex flow through the mixer, the peak regions of the large sinusoidal trailing edge should have a large slope. Also, a short lobed forced mixer induces minimal drag and has less weight [35]. The flow through the mixer is demonstrated in Figure 8.1.

The mixer designed for the TF-CLAWS engine has the following dimensions summarized in Table 8.1, and an isometric view of the mixer is shown in Figure 8.2.

Table 8.1: TF-CLAWS Mixer Parameters

Design Parameter	Value
Length (in)	6
Diameter (in)	17.2
Number of Lobes	18



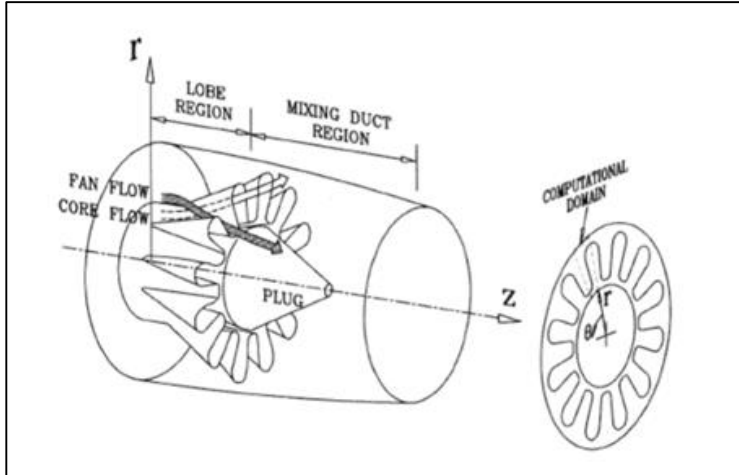


Figure 8.1: Mixer Flow [35]

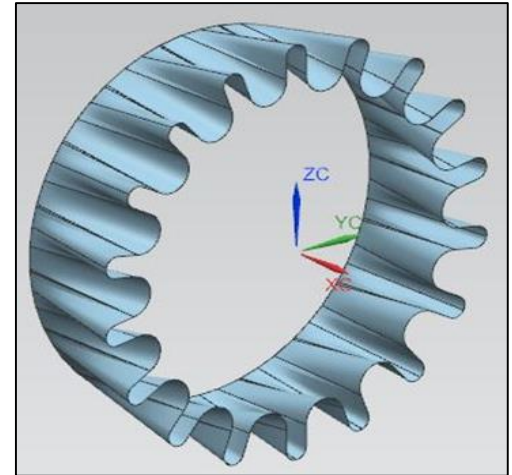


Figure 8.2: Mixer Isometric View

9 Exhaust System Design

9.1 Introduction

The requirements for the nozzle of the TF-CLAWS are as follows: the nozzle must fit within the footprint generally specified, approximately 20 inches or less in diameter; the nozzle must be convergent-divergent; the nozzle must feature noise attenuation; the nozzle should assist in emulating the flight characteristics of fifth generation fighter craft, within reason; the nozzle must be designed with cost of purchase and maintenance as a primary consideration; and the nozzle must be designed to operate without afterburning.

The requirements for the nozzle of the TF-CLAWS are as follows: accelerates flow with minimum total pressure loss; matches flow and atmospheric pressures at the exit as closely as desired; permits reheat operation without affecting primary operation; allows for nozzle wall cooling; mixes the core and bypass air; allows for thrust reversal; provides low observable characteristics; provides thrust vectoring capabilities; and provides all prior points with the minimum cost, weight, and boattail drag while meeting life and reliability goals.

The TF-CLAWS nozzle is divided into three sections: the subsonic convergent section, the throat, and the divergent section, as seen in Figure 9.1. The convergent section, shaded in red, is accepting air from the mixer.

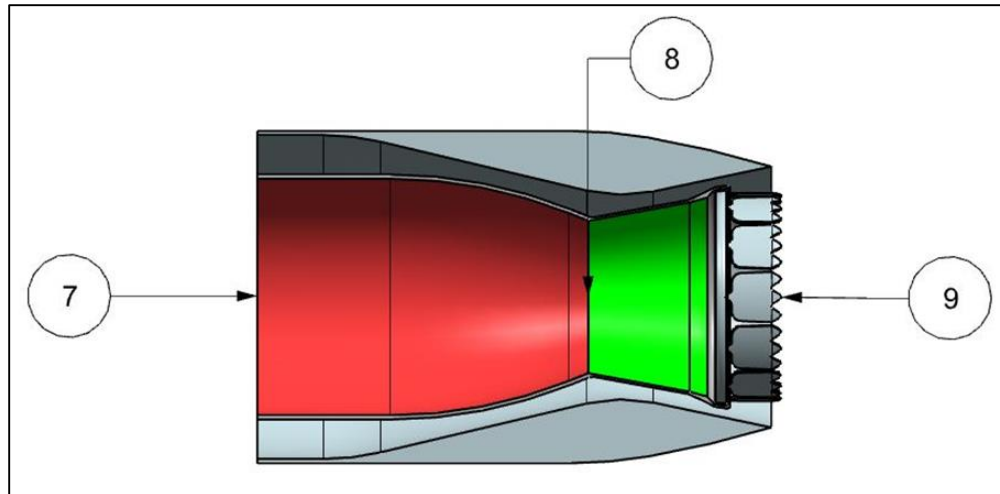


Figure 9.1: Nozzle Definition Sketch and Station Numbers

9.2 Nozzle Sizing

Using the continuity equation for a sonic throat, we can size the throat area according to:

$$A_8 = \left(\frac{\dot{m}_8}{P_{t8}} \right) \sqrt{\frac{RT_{t8}}{\gamma}} \left(\frac{2}{\gamma+1} \right)^{-\left(\frac{\gamma+1}{2(\gamma+1)} \right)} \quad (9.1)$$

The area expansion ratio also follows the continuity equation according to:

$$A_9 = A_8 \left\{ \left[1 + \frac{\gamma-1}{2} M_9^2 \right]^{\frac{\gamma+1}{2(\gamma-1)}} \right\} \left\{ \left[\frac{\gamma+1}{2} \right]^{-\frac{\gamma+1}{2(\gamma-1)}} \right\} M_9^{-1} \quad (9.2)$$

The nozzle throat is sized initially to the subsonic cruise flight condition using Equation 9.1 assuming a gas constant for air of $1716 \left(\frac{\text{ft-lb}}{\text{slug-}^\circ\text{R}} \right)$ and an average ratio of specific heats in the exhaust section of 1.3. The nozzle exit is then sized via Equation 9.2. The throat size is fixed at this size and this is carried forward into all other flight conditions. The exit area at other flight conditions is then tuned using Equation 9.2 to produce choked flow in the throat at flight conditions while minimizing the static pressure difference between the exhaust flow and the freestream.

Table 9.1: GasTurb 12 Flow Parameters and Sizing of the Nozzle

Flight Condition	\dot{m}_8 (lb/s)	p_{t8} (lb/ft ²)	T_{t8} (°R)	M_8	M_9	A_8 (ft ²)	A_9 (in ²)
Takeoff	47.72	4630.8	1301.9	1.0	1.578	0.46	0.58
Subsonic Cruise	18.19	501.2	812.4	1.0	1.758	0.46	0.67
Dash	26.61	424.3	946.1	1.0	2.151	0.46	0.95
Loiter	26.70	1192.3	876.7	1.0	1.411	0.46	0.53

9.3 Design Considerations

The design process for the TF-CLAWS trainer engine follows the general outline described by Gamble, Terrell, and DeFrancesco of SPIRITECH [36]: the exhaust system geometry is selected, the method for nozzle scheduling is selected, methods for noise attenuation are selected, and thrust vectoring capability is selected. Additionally, the decision to discard an ejector nozzle and a thrust reversal system is made.

The design philosophy for the TF-CLAWS exhaust system is to design a lightweight, relatively inexpensive system that is capable of fifth generation flight characteristics.

9.3.1 Selection of Cross-Sectional and Axial Geometry

Selection of the geometry is heavily driven by the form factor of the baseline engine. The original engine houses an axisymmetric nozzle of less than twenty inches in diameter; strongly implying that the replacement engine nozzle should fit within the form factor of the original. Primary candidate geometries include axisymmetric, 2D, and plug.

Considerations:

Axisymmetric nozzles are found in most modern combat aircraft, such as the F-18 and F-35; although not inherently stealthy [37] these nozzles are the simplest to manufacture and design. An axisymmetric nozzle is ideal for containing a pressurized gas and produces a lighter weight and cheaper nozzle than equivalent 2D and plug designs.

Testing has shown that 2D nozzles suffer little in regards to performance [38] and the 2D nozzle, housed on aircraft such as the F-22, YF-23, and B-2 aircraft, provides major advantages in stealth capability and airframe integration [39]. 2D nozzles, however, are associated with weight penalties; the structure must be designed to resist bending loading across the nozzle caused by internal pressure. Also, large design cost penalties arise during airframe integration [40]. These nozzles can, as in the F-22, be used to produce two dimensional thrust vectoring across a large domain, but generally do not produce 3D thrust vectoring easily or relatively cheaply as a result of the complexity associated with maneuvering a non-symmetric shape.

Plug nozzles possess the advantages of noise control and relatively mechanically simple area scheduling [39]. Plug nozzles generally weigh more than their axisymmetric counterparts as a result of added material and often suffer from an inherent lack of cooling in the plug itself.

Result:

Out of all three primary candidate geometries this team selected the axisymmetric nozzle after careful consideration. The 2D nozzle would introduce relatively inexpensive thrust vectoring capability but, when compared with the axisymmetric, falls far outside the selection criteria due to expense of purchase and maintenance. The plug nozzle was discarded due to its weight and ultimate expense; the increasing amount of expensive heat resistant material contributes directly to weight and cost and makes effective and cheap thrust vectoring a difficult proposition.

9.3.2 Nozzle Scheduling Capability

Considerations:

For aircraft operations beyond sonic conditions, the area ratio of the exit to the throat is of great interest and is a primary method of controlling the pressure match between exhaust and ambient conditions. The mission requirements of the TF-CLAWS are not singular and therefore require a method of nozzle scheduling. Common methods of area control include: geometrically scheduling, passive control, and fully variable.

Geometric scheduling, such as on F-14 and F-18 nozzles, links exit area mechanically to throat area, reducing weight and complexity, but optimizes only for a few design points. Additionally, both the F-14 and F-18 possess afterburning capability, which is not included in the TF-CLAWS engine. Passive control, used on the original F-15 and F-16 nozzles, uses internal pressure to arrange linked divergent flaps in an ideal manner; the light weight, simplicity, and large optimized flight envelope are all advantages of a passive control system. A fully variable system, such as the F-22 uses, has the advantage of ideal performance across nearly the full range of a flight envelope but suffers from weight, complexity, and cost issues [36].

Additionally, as will be mentioned further, ejector nozzle and thrust vectoring concepts allow for effective nozzle scheduling.

Result:

The fully variable and fixed concepts were discarded out of hand; the variable due to cost and weight and the fixed due to its inability to optimize performance through more than one flight condition.

Both the geometrically scheduled and passively controlled methods show promise for integration in an inexpensive trainer engine, but ultimately a modified passive control method edges out geometric scheduling methods; the advantage of optimized flight through multiple flight conditions most closely matches the flight characteristics of fifth generation fighters while remaining relatively inexpensive.

9.3.3 Ejector Nozzle

Considerations:

An ejector nozzle entrains high pressure air by introducing a pressure differential between low pressure core and high pressure ambient fluid streams which entrains ambient air into the ejector inlet, through a channel, and into the outlet [41]. When the two streams intermingle they are initially forced to remain separate due to the shear layer between the streams [39]. The intermixing increases with the axial distance along the divergent portion of the nozzle and the two streams are partially or fully mixed by the time they exit the nozzle, thereby reducing jet exit velocity and increasing mass flow through the nozzle [42]. The incoming high velocity core stream transfers kinetic energy of the exhaust stream into the large mass of entrained ambient air.

The performance augmentation associated with increased mass flow rate peaks at very low M and drops with airspeed [41][43]. Ejectors have been successfully tested by GE as early as 1992 [44]. This also has, as seen on the F-111 engine, the capability to aerodynamically alter the area ratio in the nozzle [40] in addition to the added benefits of nozzle cooling [45] and increased propulsive efficiency [43].

Control volume theory can reasonably predict ideal values for the thrust augmentation generated by an ejector nozzle. Defining α as the ratio of secondary to primary mass flow rates (\dot{m}_s/\dot{m}_p), β as the ratio of secondary to primary ejector areas (A_s/A_p), and δ as the ratio of forward airspeed to primary jet velocity (V_A/V_P), Equation 9.3 may be solved for an upper limit of ideal thrust gains.

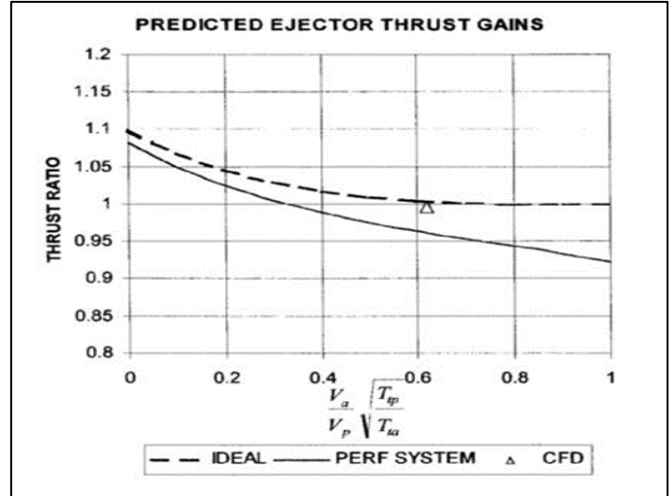


Figure 9.2: ALMEC Ejector Testing [41]

$$\Phi = \frac{(\alpha+1)^2 - (\beta+1)(\alpha+1)\delta}{(\beta+1) \left[\left(1 - \left(\frac{\alpha}{\beta} \right)^2 + \delta \right)^{\frac{1}{2}} - \delta \right]} \quad (9.3)$$

A joint NASA Langley, Western New England College, and Stage III Technologies study in 2002 modeled non-ideal effects on the Alternating Lobed Mixer Ejector Concept nozzle on the Gulfstream GII, GIIB, and GIII [41], as seen in Figure 9.2.

Result:

Ultimately, although an ejector nozzle promises moderate performance gains and noise reduction (as seen in the following section) at takeoff conditions, the increase in weight and complexity coupled with minor performance gains resulted in the exclusion of an ejector from the final nozzle concept. This concept could possibly be included in a future version of the TF-CLAWS engine if the monetary and weight costs associated with increased mechanical complexity can be reduced.

9.3.4 Nozzle Cooling and Material Selection

Considerations:

The nozzle experiences a wide range of temperatures throughout the flight regime and across the length of the nozzle. The maximum expected temperature in the nozzle, barring the presence of shock, is found at the throat; temperatures in excess of 1300°R are expected during takeoff conditions. SiC CMC’s, mentioned



previously, are being actively studied as nozzle material by Boeing, Rolls-Royce, and Snecma, in conjunction with NASA as part of NASA's ERA program [46]. These materials offer operating temperatures 200° to 300°F higher than conventional superalloys [46], have been tested at temperatures up to 700°F for long dwell periods [47], and do not require an oxidation resistant coating due to material composition [46]. Snecma, in separate testing of a CMC mixer nozzle, achieved a 45 lb reduction in weight from a comparable conventional metal mixer nozzle [46]. SiC/SiC CMC technology is nearly as ideal in a Nozzle environment as oxide/oxide CMC technology; GE is heavily invested in SiC/SiC CMC technology, has tested CMC technology extensively, and anticipates certification and flight by 2018 for a SiC/SiC CMC equipped GE-9X engine [48].

Result:

The capability of SiC/SiC CMC material to provide increased strength capability, elevated operating temperatures, and significantly reduced weight results in this material selected to line the nozzle. The likelihood this technology will be at a TRL of 9 by 2025 is good and the inclusion of this material removes the necessity to cool the nozzle.

9.3.5 Thrust Vectoring Capability

Considerations:

One of the primary characteristics of nearly all fifth generation fighter craft is the inclusion of thrust vectoring. Thrust vectoring grants an airframe a series of flight advantages such as extended conventional flight endurance through stationary flight trimming, a widened flight envelope, possible avenues of nozzle scheduling, transient flight maneuvering, increased safety, and a commensurate reduction in necessary flight controls, while reducing noise at takeoff. These advantages translate directly and indirectly to cost savings through the lifecycle of the fighter craft.

The F119 engines contained on the F-22 contain 2D thrust vectoring capability in a 20° arc on the pitch axis, while the Sukhoi PAKFA has the capability to vector in a cone about the nominal thrust axis, though the current state of its thrust vectoring capability is unknown. Additionally, the Chengdu J-20, powered by the WS-

10G engine, is supposedly capable of thrust vectoring, though, again, the current state of this engine is not public knowledge.

Producing effective thrust vectoring for an inexpensive trainer engine is a challenge, though a possibility. Industria de Turbo Propulsores S.A. (ITP) produced a series of thrust vectoring nozzles in the early 2000's in an effort to improve on the EJ2000 engine. The nozzles produced ranged from full 3D thrust vectoring capability to a relatively simple two-ring 'pitch only' nozzle, capable of 2D vectoring, and were studied in deflection modes of up to 30°.

Result:

The current state of fifth generation fighters indicates that thrust vectoring is an integral characteristic; a feasible method of incorporating this into a low cost trainer is the two ring pitch only concept modeled by ITP. This is carried forward into final design.

9.4 Incorporated Nozzle Concept

The ultimate down selection process resulted in a nozzle concept with the following characteristics: axisymmetric nozzle; modified passive area scheduling, with additional effective area control provided by thrust vectoring capability; acoustic liners with Helmholtz resonators; rounded chevron vanes; pitch-only thrust vectoring provided by a two ring concept.

9.5 Exhaust System Geometry

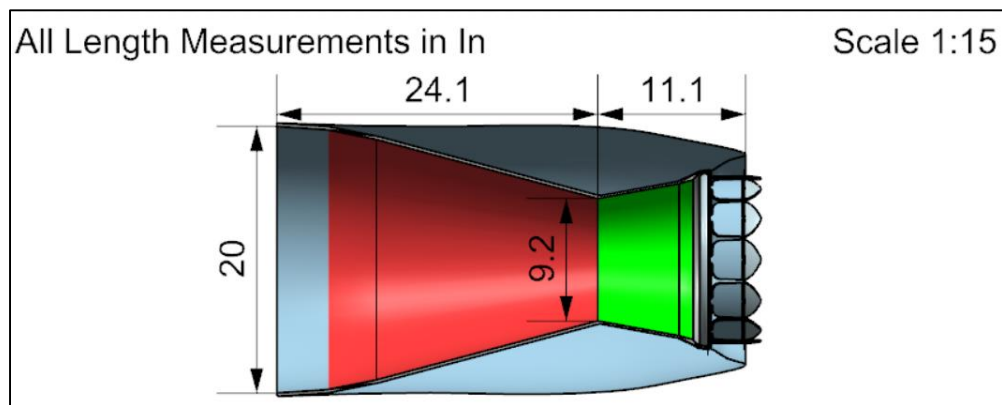


Figure 9.3: Side Section View of the Exhaust System of the TF-CLAWS

10 Flow Path through the TF-CLAWS

With the major components of the TF-CLAWS designed, then the flow path through the engine may be presented. Figure 10.1 presents the flow path through the TF-CLAWS. Note that the “blue” components correspond to the transonic fan and low-pressure compressor, the “orange” components correspond to the high-pressure compressor and high-pressure turbine, and the “red” component corresponds to the combustion system.

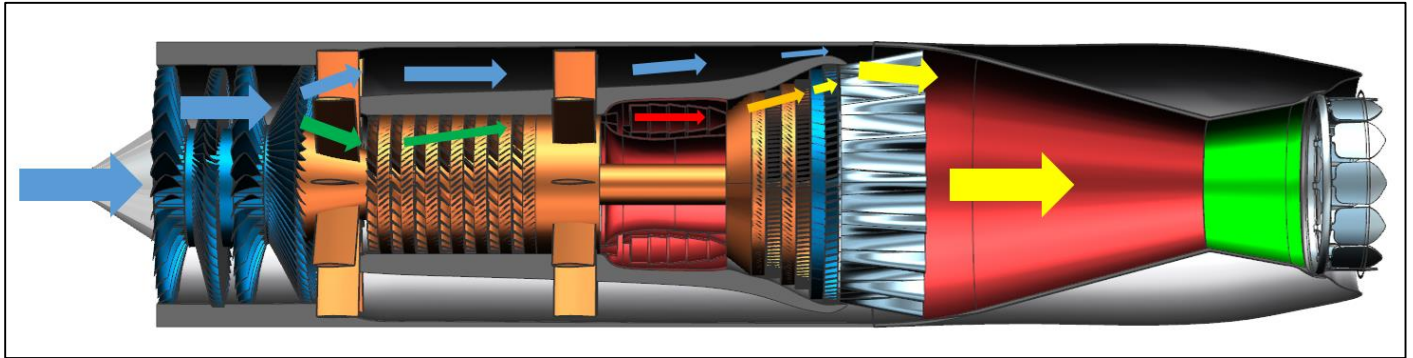


Figure 10.1: Flow Path through the TF-CLAWS

11 Identification and Selection of Engine Subsystems

This chapter describes the subsystems that are used on the TF-CLAWS. These subsystems provide important features that are critical for the successful design of any aircraft engine.

11.1 Starting

As with any engine, the TF-CLAWS requires a startup sequence. The compressor must rotate fast enough to supply enough air to the combustor for combustion to occur. A starter rotates the compressor until a sustained combustion occurs and the engine can operate on its own. The starter is pneumatically powered and only sends air first to ensure the air is flowing in the right direction before fuel is added. A diagram of a typical startup sequence can be seen in Figure 11.1.

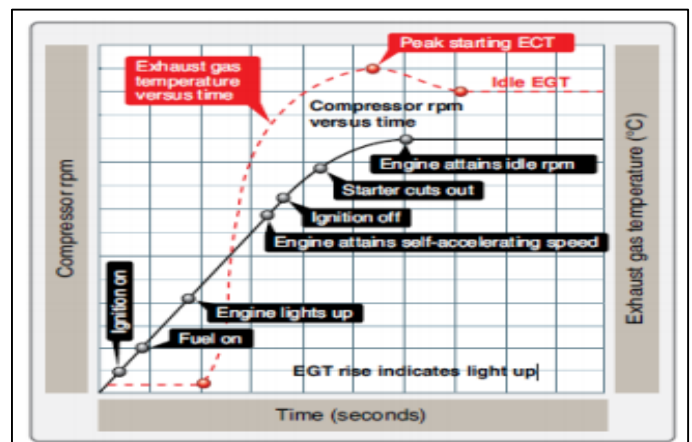


Figure 11.1: Typical Startup Sequence of the TF-CLAWS [49]

11.2 Bearings

The stability of rotating machinery relies on the type, quality, and placements of its bearings. Bearings also allow for very small tip clearances, an important design factor in gas turbine engines. Two types of bearings were investigated for this engine: classic ball/roller bearings

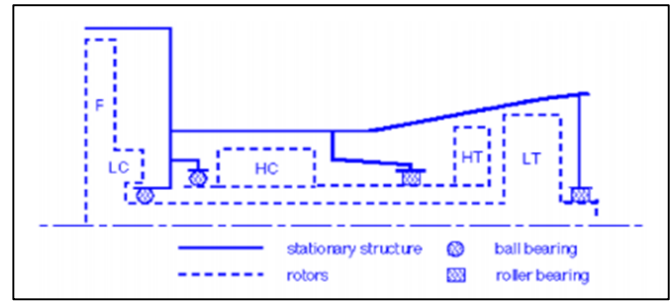


Figure 11.2: Configuration of the Bearings [34]

and magnetic bearings. Classic bearings are known to be effective and work well. The main drawbacks of classic bearings are that they are heavy, take up space, and require an additional lubrication system to function. The location of the bearings is shown in Figure 11.2, to minimize bending stresses, as detailed by Kerrebrock.

Magnetic bearings were also investigated for possible use in the TF-CLAWS. They have been tested theoretically and experimentally, but it is uncertain if the technology will be ready by 2025 [50]. The classic bearings are proven to be reliable by the aircraft propulsion industry, and will be used in this engine. The material for the bearings will be M50NiL steel due to its fracture toughness, fatigue life, and ability to withstand high temperature environments [51].

11.3 Fuel System

The TF-CLAWS utilizes an electronically controlled fuel system with signals from FADEC. The fuel is pumped from the aircraft fuel tanks to a low pressure system. It is then transferred to a high pressure system to pressurize the fuel and inject it into the combustor. Both systems contain filters to ensure high quality fuel. These filters help the engine run efficiently and increase the life of the system. The fuel flow can be run manually and separate from FADEC in case of an emergency.

11.4 Fire Suppression System

Fire suppression is crucial in engine design because the engine requires combustion to operate and operates at very high temperatures. The first step in fire suppression is detection. Gas-filled detectors will be placed at

different locations in the engine. These detectors release gas into a tube and can sense temperature. A switch is released alarming the crew whenever dangerously high temperatures are detected. A fire in the engine requires an in-air restart or an emergency landing. These emergency procedures will not be necessary if fires are prevented. Fires will be prevented by routing all lines containing flammable fluid away from hot spots and designing the lines to have extra layers of flame retardant materials. Fluid line connections and condition should be inspected routinely to prevent a flammable line breaking and causing a fire.

11.5 Anti-Icing System

The ice protection system prevents ice formation in the engine and leading edges of the inlet duct. One of the major consequences of ice formation in the engine is that there will be inadequate airflow going through the engine, which will shorten the lifespan of the engine while also decreasing performance. There are two systems working in tandem to prevent ice formation and buildup: the electrical system and hot air supply system. The electrical system, specifically the heating pads bonded to the outer skin of the cowls on the engine, aid in the prevention of ice buildup on the engine. For deicing, the hot air supply system is used. The hot air is taken from the HPC stages and is dispersed through regulatory valves to the engine components. Finally, the DSI has a smaller inlet area which means less surface area for ice crystals to form.

11.6 Auxiliary Power Unit (APU)

The TF-CLAWS engine is started using an auxiliary power system (APS) which is a pneumatic link system that consists of an auxiliary power unit (APU), air turbine starter (ATS), flow control valve and airframe mounted accessory drive. The APU is a small gas turbine engine that provides pneumatic and shaft power. The compressed air from the APU is

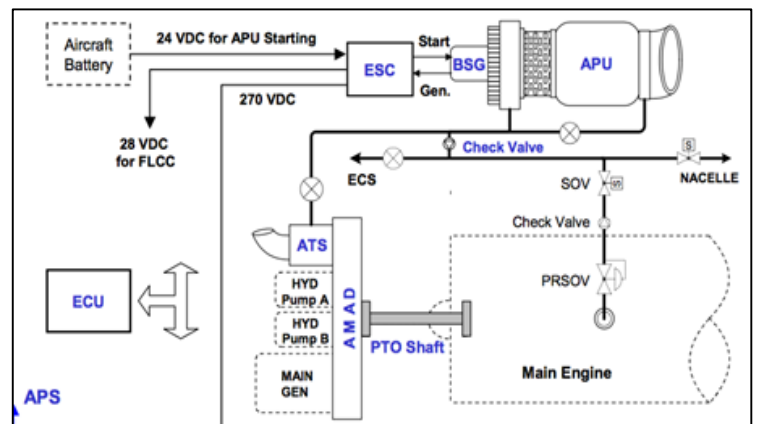


Figure 11.3: Schematic Diagram of T-50 APS System [52]

delivered via airframe ducting to the ATS, which converts pneumatic power to shaft power that starts the main engine and main aircraft accessories [52]. This system is currently being used in the Korea Aerospace Industries (KAI) T-50 Golden Eagle which is a current candidate of the T-X program to replace the aged T-38 trainer.

11.7 Engine Control System

The distributed engine control currently under development is more of an advanced and evolutionary version of centralized energy control that works more efficiently and accurately compared to traditional centralized control. By converting the distributed engine control to a Full Authority Digital Engine Control (FADEC) system, numerous operating factors

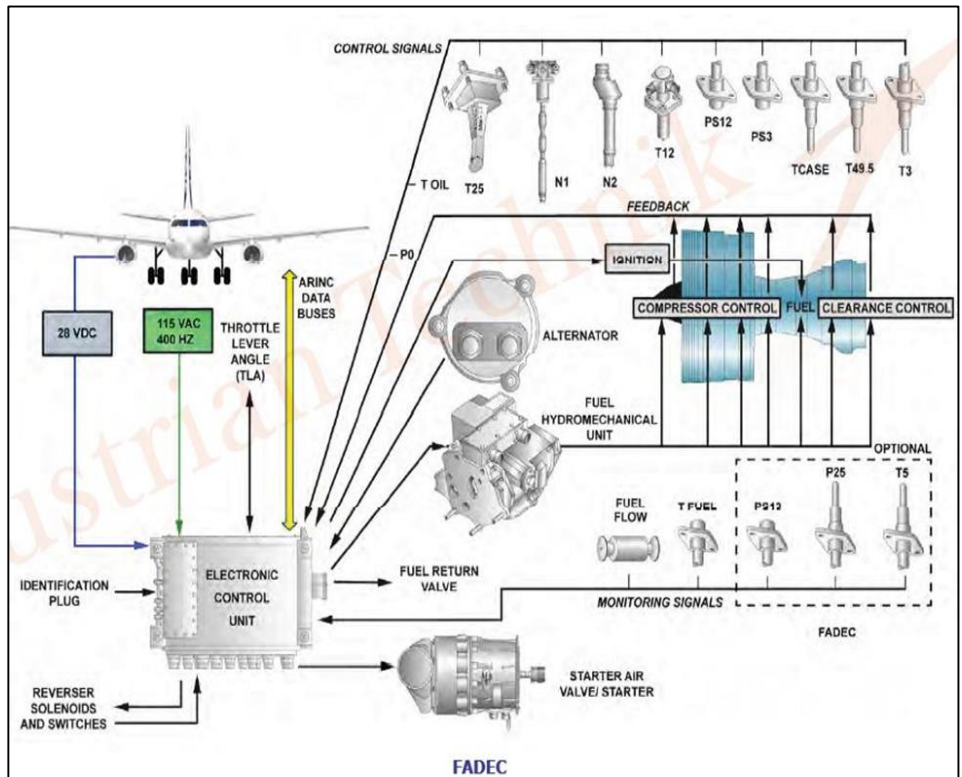


Figure 11.4: Distributed Engine Control Employed on the TF-CLAWS [53]

or elements are taken into consideration when evaluating the efficiency of the engine, such as engine temperature, pressure ratio, fluid flow, etc. The mechanism of FADEC is to run various inputs/factors simultaneously and generate a high degree of optimization and reduce the number of operating errors. Additionally, a second FADEC system can be implemented to ensure the performance of engine control to be consistent and continuous.

12 Engine Noise Attenuation

Noise at takeoff is a serious issue for military craft (due to community noise); on the military side noise-induced hearing loss was, as of 2015, the Navy fleet's number one occupational health expense [54]. The primary source of noise from gas turbine engines is the jet exhaust and turbomachinery noise.

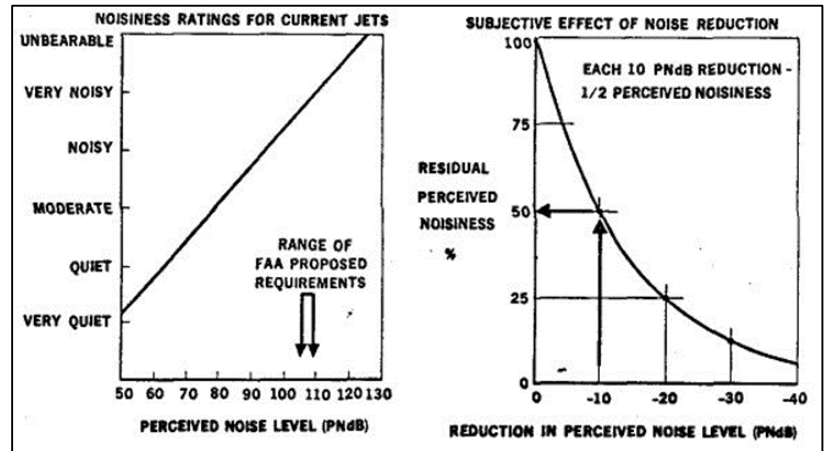


Figure 12.1: EPNL Correlation with Perceived Noise [55]

Initially, the TF-CLAWS engine reaps a significant advantage from the decision to exclude an afterburner. A 2009 study found that usage of an afterburner increased effective perceived noise level (EPNL) by 5 to 10 dB above the levels found at military power [55], implying that perceived noise at takeoff could be halved if afterburner usage was removed.

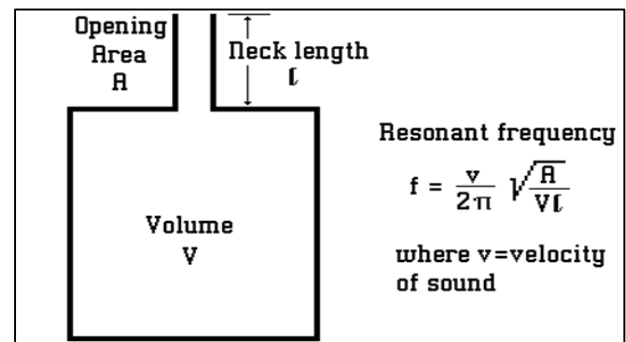


Figure 12.2: Helmholtz Resonator [55]

A series of noise mitigation strategies are used in TF-CLAWS to reduce noise: a diverterless supersonic inlet (DSI), Helmholtz resonators in acoustic liners, an S-duct subsonic diffuser for the inlet system, blade sweep in the fan, use of sweep and lean in the fan stator blades, use of wide-chord, low-aspect ratio blades, and chevron vanes.

Helmholtz resonators target specific frequencies by using a trapped volume to absorb acoustic energy through harmonic oscillation of a mass slug in the neck [56]. These resonators are a function of speed of sound in the fluid medium coupled with the cavity volume.

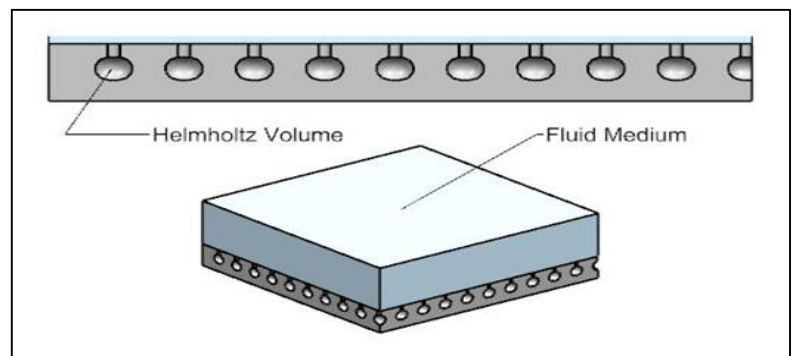


Figure 12.3: Acoustic Liner with Helmholtz Resonators [55]

The blade passing frequency of the fan and turbines provides a target frequency to design against.

$$\text{BPF} = \frac{nt}{60} \quad (12.1)$$

In Equation 12.1, n is the angular speed of the turbine in RPM, t is the number of blades on the turbine rotor, and BPF is measured in Hz.

Table 12.1: Blade Passing Frequency of the TF-CLAWS

Turbine Component	n	t	BPF
HPT Rotor 1	40000	132	88000
HPT Rotor 2	40000	112	74700
LPT Rotor	18600	98	3040

Testing indicates that slight performance degradation, in the neighborhood of 1%, does occur when using an acoustic liner, primarily due to the drag characteristics of the liner [37].

Chevron noise reduction works by protruding the tips of chevron vanes into the exhaust stream. These protruding tips generate streamwise vorticity and promote mixing, thereby reducing noise. Noise reduction of chevron vanes is a strong function of shape; in a numeric study rounded vanes were predicted to reduce EPNL by 6 dB over sharp and flat vanes [57].

A study conducted by NASA and Learjet indicates that installing sharp chevrons into the core air reduces EPNL by 2.5 dB and reduces generated thrust by approximately 0.5% [58] and that even a very minor intrusion into the core can have drastic effects on EPNL [54] with minor performance impact. A 2012 study [41] investigating chevrons also found that chevrons assisted with total pressure recovery in a nozzle system, increasing total pressure recovery by more than 8%.

A difficulty found when designing a nozzle with chevrons is that the chevrons are most useful during takeoff, when the jet plume is normally overexpanded [59]. The overexpanded gas requires that chevrons be of sufficient length to intrude into the shear layer at takeoff, but this length is such that when the gas is fully expanded during nominal flight conditions performance penalties are found.

Finally, thrust vectoring, according to an analysis conducted in 2008, promises to reduce peak noise at takeoff by more than 7 dB [60].

Ultimately the engine will be designed using a passive acoustic liner in the turbine section with included Helmholtz resonators, coupled with rounded chevron vanes. The acoustic liner resonant frequency will be tuned to noise generated by internal turbomachinery, such as the blade passing frequency of the turbine. All these concepts trade favorably with cost vs return. In addition, the lack of an afterburner removes the large noise penalty associated with its usage. Thrust vectoring also promises to provide noise reduction benefits.

13 Fuel Cost Analysis

Through use of publicly available data from the Federal Aviation Administration’s (FAA) Aerospace Forecasts for 2014-2034 [61], Figure 13.1 is generated to observe the trend in jet fuel prices from 2006 to 2034. The price of jet fuel from 2016 to 2034 are projections that account for economic such as inflation and GDP.

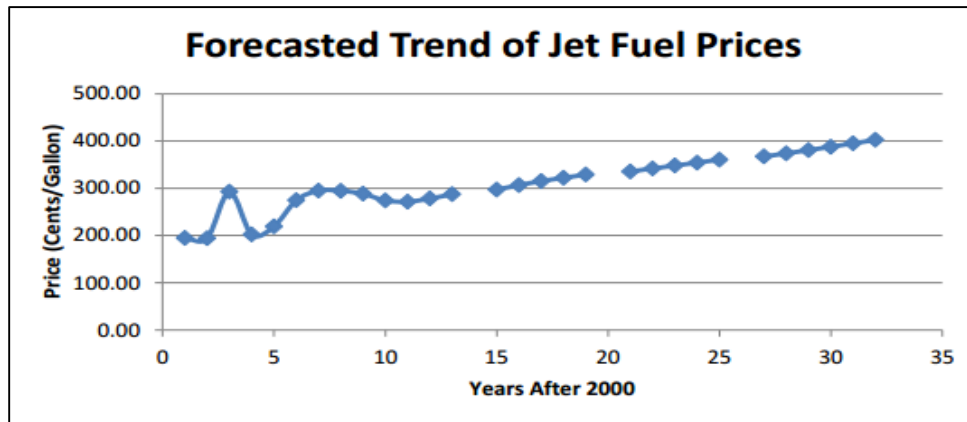


Figure 13.1: Forecasted Trend in Jet Fuel Prices [62]

We note from Figure 13.1 that jet fuel prices are going to cost approximately \$3.42 per gallon in the entry-into-service year of 2025 for the next generation trainer. Through a simple conversion from gallons to pounds (i.e. the density of jet fuel is 6.71 lb/gal), jet fuel is projected to cost \$0.51 per pound in 2025. From this projected cost of jet fuel in 2025, as well as the fuel weight calculations carried out in Section 3.1 for the combat patrol mission, a fuel cost analysis may be carried out for the baseline engine and the TF-CLAWS. Table 13.1 presents the fuel costs for a single combat patrol mission.

Table 13.1: Combat Patrol Mission Fuel Costs

Mission Parameter	Baseline Engine	TF-CLAWS	Percent Difference
Mission Fuel Weight (lb)	7016	4843	-32%
Fuel Price (\$/lb)	0.51	0.51	-
Mission Fuel Cost (\$)	3578	2422	-32%

Thus, we note that the TF-CLAWS introduces a cost savings of nearly one-third of the fuel costs associated with using the baseline engine to fly the combat patrol mission, an absolutely striking reduction. While this cost savings for a single mission is impressive, the fuel savings associated with the TF-CLAWS become even more pronounced over the entire life of the next generation trainer. Currently, the average life for a T-38A is 15,000 flight hours [63]. From the flight time durations listed in Table 3.2 and the flight time associated with traveling 1500 nmi at Mach 0.85 and 35,000 feet, a single combat patrol mission has a flight time duration of approximately four hours. Making the assumption that the next generation trainer will have the same average life as the T-38A, then the next generation trainer will fly 3716 combat patrol missions in its lifetime. Thus, Figure 13.2 presents the total fuel costs over the life of the next generation trainer using either the baseline engine or the TF-CLAWS. We note that over the life of the next generation trainer, a whopping \$4.3 million is saved in fuel costs by using the TF-CLAWS as opposed to the baseline engine. Figure 13.2 demonstrates the complete superiority of the TF-CLAWS over the baseline engine in terms of fuel efficiency.

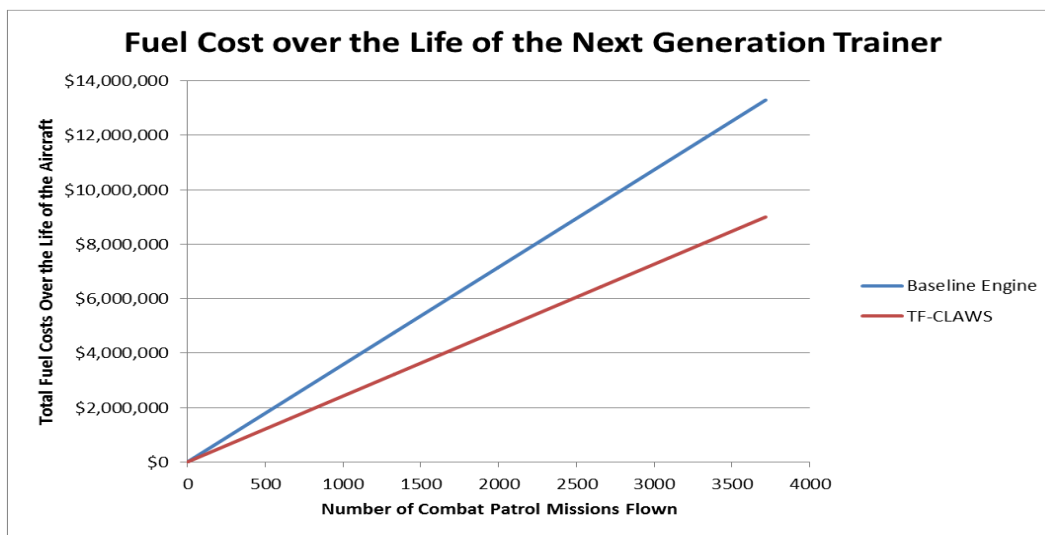


Figure 13.2: Fuel Costs over the Life of the Next Generation Trainer

14 Mission Weight Sizing for the Next Generation Trainer

In addition to the design of the TF-CLAWS engine, it is also pertinent to determine some of the preliminary sizing and performance characteristics of the next generation trainer. Specifically, it is necessary to determine a preliminary estimation of the empty and takeoff weights of the aircraft. The empty and takeoff weights are dictated by the mission profiles for the aircraft. For the purposes of the next generation trainer, a weight estimation of the combat patrol mission outlined in Section 3 will be performed. This weight estimation will be performed with an iterative process involving a Statistical Time and Market Predictive Engineering Design (STAMPED) analysis of market data on other military trainer aircraft.

14.1 STAMPED Analysis and Database for Similar Airplanes

In recent years, a new methodology for design has been developed that has the power to track any variable through time. The acronym for this methodology is STAMPED, statistical time and market predictive engineering design. A STAMPED analysis involves gathering both technical data and market share data of a particular product, and then mapping a market-weighted version of the technical data through time to project the future of the desired variable. This type of analysis is a useful technique to track the trends of military trainer properties. For mission weight estimations, two aircraft properties are of particular interest: empty-to-takeoff weight ratio (W_E/W_{TO}) and wing loading (W/S). Data on similar military trainers is then used to project the empty-to-takeoff weight ratio and wing loading of the next generation trainer as it enters service in 2025. Table 14.1 contains the database of all the aircraft included in the STAMPED analysis, as well as the projection for the next generation trainer in 2025.

Table 14.1: Database of Similar Aircraft to the Next Generation Trainer

Aircraft	First Flight	Country	W_E (lbf)	W_{TO} (lbf)	W_E/W_{TO}	W/S (ft ²)
Aero L-139 Albatross	1968	Czech Republic	7617	10632	0.716	52.6
Soko G-4 Super Galeb	1978	Serbia	7165	13955	0.513	66.4
FMA IA 63 Pampa	1984	Argentina	6525	11464	0.569	68.2
Kawasaki T-4	1985	Japan	8536	16534	0.516	73.1
Aero L-159 Alca	1997	Czech Republic	9590	17637	0.544	87.1
Hongdu L-15	2006	China	9921	18960	0.523	69.2
Next Generation Trainer Projection	2025	United States	-	-	0.48	91.3

14.2 Determination of Mission Weights

For the next generation trainer, it is necessary to determine the empty and takeoff weights corresponding to the combat patrol mission. To determine the mission weights, a modern approach may be summarized with the following procedure: [64]

- 1) Determine the sum of the payload weight and the weight of the crew;
- 2) Guess a likely value for the takeoff weight;
- 3) Determine the weight of the fuel;
- 4) Calculate a tentative operating empty weight by subtracting the fuel weight, payload weight, and crew weight from the guessed takeoff weight;
- 5) Calculate a tentative empty weight by subtracting the trapped fuel and oil weight from the tentative operating empty weight;
- 6) Calculate the empty weight by multiplying the guessed takeoff weight by the empty-to-takeoff weights ratio determined by STAMPED analysis in Section 14.1;
- 7) Compare the tentative empty weight to the calculated empty weight, and then iterate about the guessed takeoff weight to bring the empty weight to within 0.5% of the tentative empty weight.

Through utilization of the weight estimation approach outlined above, as well as the assumption of a crew of two 200 lb pilots and a payload weight of 150 lb between them [65], the mission weights of the next generation trainer are calculated and are then presented in Table 14.2.

Table 14.2: Combat Patrol Mission Weights for the Next Generation Trainer

Aircraft	Empty Weight (lbf)	Takeoff Weight (lbf)
Next Generation Trainer	5040	10486

15 Performance Constraint Analysis

The second aspect of the preliminary sizing of any aircraft is a performance constraint analysis. It is critical to determine the characteristics of an aircraft in all operations. Thus, it is useful to develop constraining equations that relate wing loading to thrust-to-weight ratio. This then sizes an aircraft for all modes of operation. The constraining equations are developed from the following performance constraints: takeoff distance constraints, landing distance constraints, climb constraints, and dash speed constraints.

15.1 Drag Polar Estimation

For nearly all of the performance constraints, the drag polar for every flight configuration must be known to proceed. There are a total of five main flight configurations for the next generation trainer, including the clean configuration (cruise), takeoff with landing gear up or down, and landing with landing gear up or down. Using the previously estimated takeoff weight, the drag polar for each of the five main flight configurations of the next generation trainer can be determined using the techniques outlined in “Airplane Design, Part I: Preliminary Sizing of Airplanes” [6]. The drag polar for every flight configuration of the next generation trainer can be seen in Table 15.1.

Table 15.1: Drag Polar Estimations for the Next Generation Trainer

Flight Configuration	Drag Polar
Low Speed, Clean	$C_D = 0.0171 + 0.1029C_L^2$
Takeoff, Gear Down	$C_D = 0.0521 + 0.1095C_L^2$
Landing, Gear Down	$C_D = 0.1021 + 0.1171C_L^2$
Takeoff, Gear Up	$C_D = 0.0321 + 0.1095C_L^2$
Landing, Gear Up	$C_D = 0.0821 + 0.1171C_L^2$

15.2 Takeoff Distance Constraints

Another one of the most important performance constraints to consider is takeoff distance. The takeoff criterion used for the next generation trainer was selected to be a minimum runway length of 6,000 ft, per the specifications in Ref. 65. Thus, the following, rearranged form of Equation 3.9 in Ref. 6 can be utilized to describe the takeoff performance constraint of the next generation trainer: [6]

$$\left(\frac{T}{W}\right)_{TO} = \frac{4(4+\lambda)}{3(5+\lambda)} + \left[\frac{\left(\frac{0.0447(W/S)_{TO}}{s_{TOG}\rho}\right) + 0.72C_{D_o}}{C_{L_{max,TO}}} + \mu_g \right] \quad (15.1)$$

In this equation, λ is the bypass ratio of the engine at takeoff, $C_{L_{max,TO}}$ is the maximum lift coefficient at takeoff (selected from Ref. 6, Table 3.1, military trainer aircraft), μ_g is the ground friction coefficient (value selected to be 0.03 from Ref. 6, pg. 103), s_{TOG} is the ground run takeoff distance (runway length of 6,000 ft), ρ is the density at sea level on a +27°F standard day, and C_{D_o} is the parasite drag coefficient for the takeoff, gears down flight configuration [6].

15.3 Landing Distance Constraints

Another one of the most important performance constraints to consider is landing distance. The landing criterion used for the next generation trainer was selected to be a minimum runway length of 6,000 ft, per the specifications in Ref. 65. The landing distance performance constraint is a single value that the wing loading cannot exceed. This landing constraint can be formulated from a form of Equation 3.1 in Ref. 6, and is as follows: [6]

$$\frac{W}{S} = \frac{\frac{1}{2}\rho V_{SL}^2 C_{L_{max,L}}}{\left(\frac{W_L}{W_{TO}}\right)} \quad (15.2)$$

In this equation, ρ is the density at sea level on a +27°F standard day, V_{SL} is the stall speed during landing, $C_{L_{max,L}}$ is the maximum lift coefficient during landing (selected from Table 3.1 of Ref. 6), and W_L/W_{TO} is the ratio of landing weight to takeoff weight (selected as 0.99 from Table 3.3 of Ref. 6) [6].

15.4 Climb Constraints

Another one of the most important performance constraints to consider is climb. Specifically, the next generation trainer is sized for climb by FAR 25.121 (OEI), which is a balked landing climb with one engine inoperative. For FAR 25.121 (OEI), the flaps of the next generation trainer are in the approach position, which is halfway between takeoff flaps with the landing gear down and landing flaps with the landing gear down.

Furthermore, for FAR 25.121 (OEI), the climb gradient (CGR) is constrained as 0.021 [6]. With this information, the next generation trainer climb constraint from FAR 25.121 (OEI) can be described using Equation 3.31a from Ref. 6 as follows: [6]

$$\frac{T}{W} = \frac{N}{N-1} \left(\frac{1}{L/D} + \text{CGR} \right) \quad (15.3)$$

In this equation, N is the number of engines on the aircraft, L/D is the lift-to-drag ratio in the approach position, and CGR is the climb gradient [6].

15.5 Dash Speed Constraints

Another one of the most important performance constraints to consider is dash speed. Per the performance specifications in the RFP [1], the next generation trainer has a defined dash speed of Mach 1.3. The dash speed constraint is defined in Ref. 6 as follows: [6]

$$\frac{T}{W} = \frac{\bar{q}C_{D_{0,cr}}}{(W/S)} + \frac{(W/S)}{\bar{q}\pi eAR} \quad (15.4)$$

In this equation, \bar{q} is the flight dynamic pressure, e is the Oswald efficiency factor for the clean configuration, AR is the aspect ratio, and $C_{D_{0,cr}}$ is the parasite drag coefficient for the dash flight condition [6].

15.6 Determination of Takeoff Wing Loading and Takeoff Thrust-to-Weight

With the performance constraint analysis for all flight conditions performed, then the highest possible wing loading and lowest possible thrust-to-weight ratio that aircraft can safely achieve are selected from the constraint diagram presented in Figure 15.1. From the constraint diagram, the next generation trainer has a takeoff thrust-to-weight ratio of 1.06 and a wing loading of 61.7 lbf/ft².

Next Generation Trainer Constraint Diagram

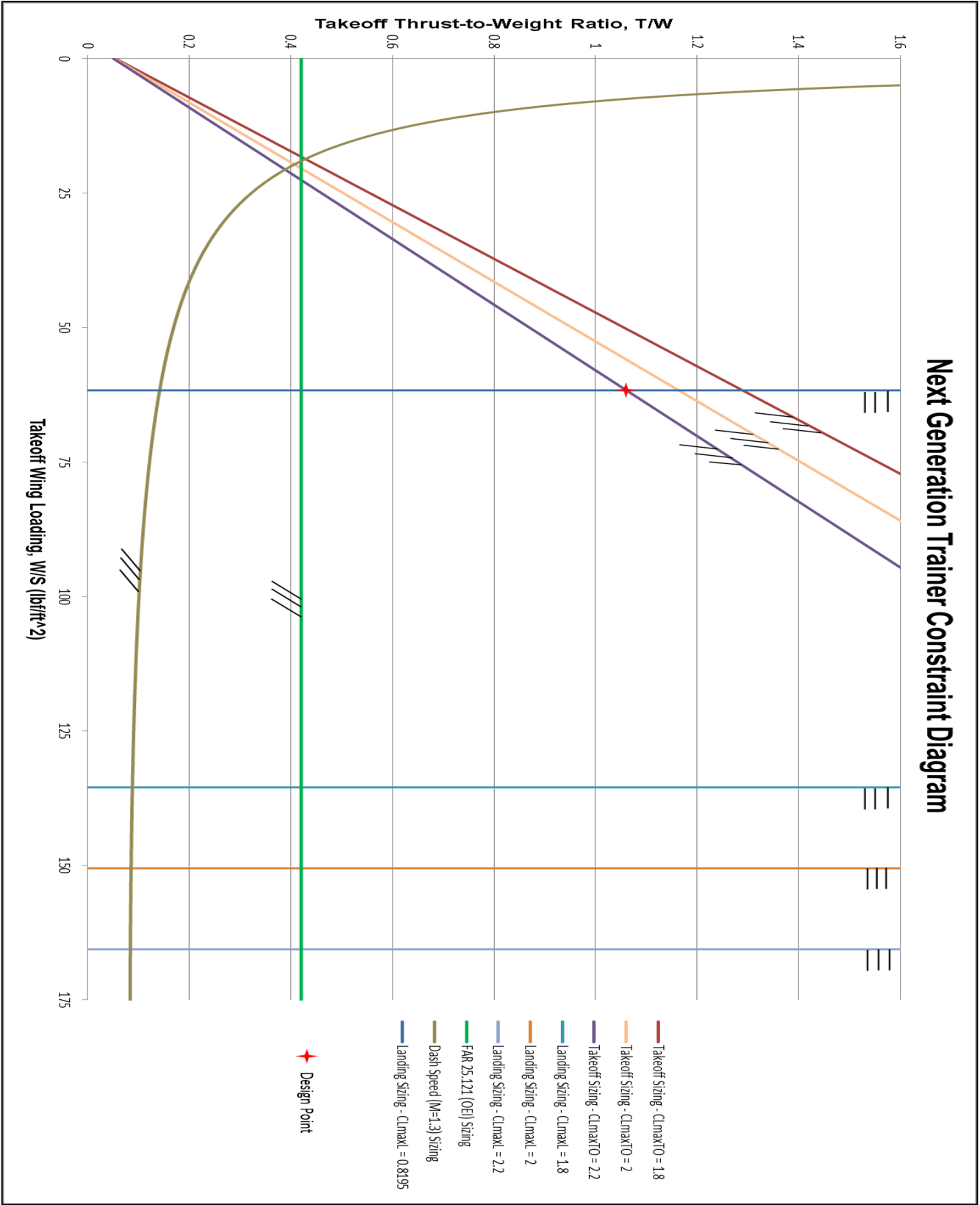


Figure 15.1: Aircraft Constraint Diagram for the Next Generation Trainer



16 TF-CLAWS Engine Integration on the Next Generation Trainer

With the TF-CLAWS designed and the preliminary design characteristics of the next generation trainer determined, then we may present the next generation trainer equipped with two TF-CLAWS engines. The following figures present the integration of the TF-CLAWS on the next generation trainer.



Figure 16.1: Front and Rear View of the TF-CLAWS on the Next Generation Trainer



Figure 16.2: Side View of the TF-CLAWS on the Next Generation Trainer

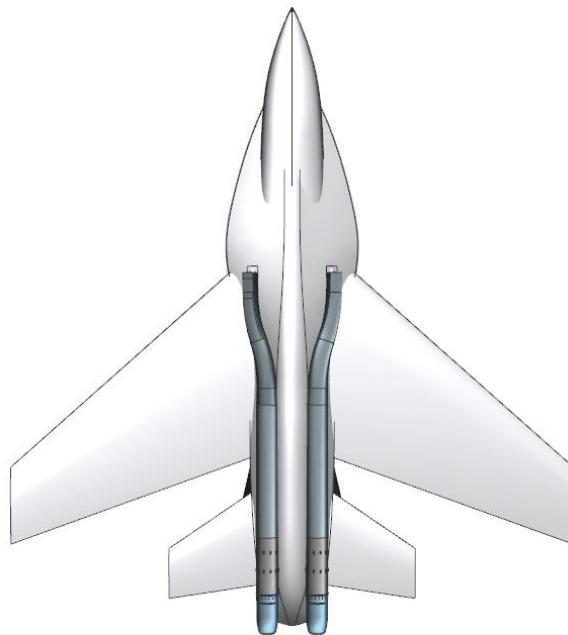


Figure 16.3: Bottom View of the TF-CLAWS on the Next Generation Trainer

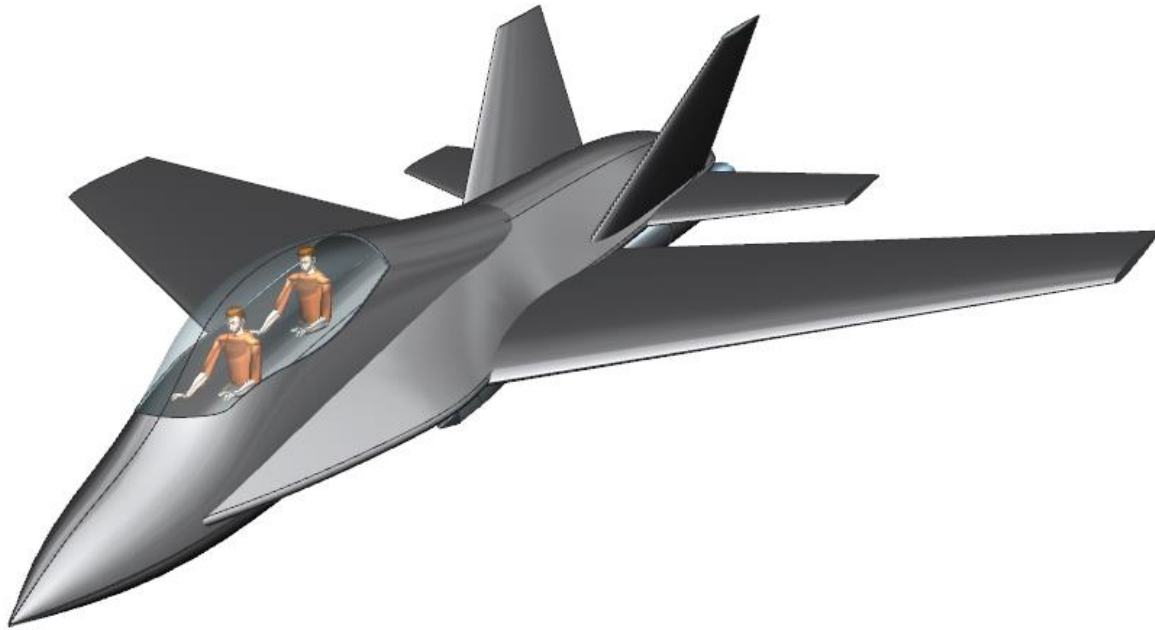


Figure 16.4: Isometric View of the TF-CLAWS on the Next Generation Trainer

17 Maintainability, Accessibility, and Serviceability

To best describe the maintainability, accessibility, and serviceability aspects of the TF-CLAWS and the next generation trainer, it is pertinent to compare with the F-22. To maintain DoD standards for engine sustainability the TF CLAWS will follow the same model as the F-22 as laid out by Lockheed Martin. For engine maintenance, the Pratt & Whitney F119 engines on the F-22 are designed to allow standard flight line maintenance using just six common tools available at commercial hardware stores [66]. Additionally, Lockheed Martin makes usage of an “Integrated Maintenance Information System (IMIS),” a system that enables a maintenance crews to work off a centralized network that consolidates maintenance and repair data worldwide [66]. Maintainers can simply plug their laptop computer into the aircraft, log completed maintenance, and plug their computer back into the system to update the global database instantaneously [66]. This ensures proper and complete maintenance records are kept, no matter where the F-22 is deployed to on the globe [66].

18 Recommendations

Future growth models of the TF-CLAWS low bypass, mixed flow turbofan engine will employ several advanced materials and technologies. One of the more interesting potential additions to the TF-CLAWS is an ejector nozzle, which would provide an incremental increase to thrust output. Another technology which might have a significant impact on future iterations of the TF-CLAWS is that of 3D-printing. As the maximum engine diameter is fixed at 22", several interior components of the TF-CLAWS are quite small and are candidates to be manufactured using the technique of 3D-printing. This could introduce cost savings in the manufacture of components like compressor or turbine blades. Yet another potential future modification to the TF-CLAWS is the usage of an aft fan as discussed previously. As engine noise restrictions continue to grow moving forward, the usage of an aft fan would increase the length of the inlet duct, allowing for more efficient sound absorption using liners. All things considered, the TF-CLAWS is an outstanding engine which will offer extreme fuel efficiency and exceptional performance on the next generation trainer, and the design will only improve moving forward with the advances of gas turbine technology.

19 References

1. Anon, "Candidate Engines for a Next Generation Trainer," *AIAA Foundation Undergraduate Team Engine Design Competition*, 23 October 2015.
2. Briganti, Giovanni, "F-35 Reality Check Ten Years On – Part 1: 'Fifth-Generation' and Other Myths," *Defense-Aerospace.com*, [[http://www.defense-aerospace.com/article-view/feature/135080/f_35-reality-check-10-years-on-\(part-1\).html](http://www.defense-aerospace.com/article-view/feature/135080/f_35-reality-check-10-years-on-(part-1).html)], Briganti et Associés, 19 Bld du Parc, 92200 Neuilly Sur Seine, France, 9 May 2012.
3. Farokhi, S., "A Candidate 2-Spool Mixed-Flow Turbofan Engine with Ejector Nozzle," *AE 524*, University of Kansas, Lawrence, KS 66045, pp. 1-3, 2016.
4. Kurzke, Joachim, "GasTurb 12: A Design & Off-Design Performance Program for Gas Turbine," [<http://www.gasturb.de>], GasTurb GmbH, Templergraben 55, 52062 Aachen, Germany, 2012.
5. Anon, "GE Successfully Tests World's First Rotating Ceramic Matrix Composite Material for Next-Gen Combat Engine," *GE Aviation*, Cincinnati, Ohio, 2015.
6. Roskam, Jan. "Preliminary Sizing of Airplanes." *Airplane Design*, Vol. I, DARcorporation, Lawrence, KS 66049.
7. Ran, H., Mavis, D., "Preliminary Design of a 2D Supersonic Inlet to Maximize Total pressure Recovery", AIAA 5th Aviation, Technology, Integration, and Operations Conference, September 2005, Arlington, VA, AIAA 2005-7357.
8. Farokhi, S., "Aircraft Propulsion." 2nd Edition, John Wiley & Sons Ltd, West Sussex, United Kingdom, 2014. Print.
9. Anon, "FAST HISTORY: LOCKHEED'S DIVERTERLESS SUPERSONIC INLET TESTBED F-16," Aviationintel Web Site, [<http://aviationintel.com>], Spring 2016.
10. Jeffrey W., Brent N., "Tactical Aircraft Aerodynamic Integration" *Encyclopedia of Aerospace Engineering*, 2010.
11. Anon, "MATLAB (Matrix Laboratory)," MathWorks Headquarters, 1 Apple Hill Drive, Natick, MA 01760-2098, United States, April 2016.
12. Farokhi, S., "TF-CLAWS Inlet Design Features," *AE524 Course Document*, University of Kansas, Lawrence, KS, pp. 1-3, April 2016.
13. G. Marsh, "Reinforced Plastics," *Materials Today*, 06 November 2012. [Online]. Available: <http://www.materialstoday.com/composite-applications/features/aero-engines-lose-weight-thanks-to-composites/>. [Accessed 15 April 2016].
14. Adkins, R. C., Matharu D. S., and Yost, J. O., "The Hybrid Diffuser", *Journal of Engineering and Power*, Vol. 103, pp. 229-36, 1981.
15. Sturgess., G. J., Shouse, T. D., Zelina, J., and Roquemore, W. M., "Emissions Reduction Technologies for Military Gas Turbine Engines", *AIAA/ICAS International Air and Space Symposium and Exposition: The Next 100 Years*, 14-17 July 2003, Dayton, Ohio, AIAA 2003-2622.



16. Haselbach, F., and Parker, R., “Hot End Technology for Advanced, Low Emission Large Civil Aircraft Engines”, 28th International Congress of the Aeronautical Sciences, 23-28 September 2012, Brisbane, Australia.
17. Moriai, H., Nakae, T., Miyake, Y., Inada, M., “Research and Development of a Combustor for an Environmentally Compatible Small Aero Engine”, Technical Review Vol. 45 No. 4, Mitsubishi Heavy Industries, Ltd., December 2008.
18. Hossaini, M. K., “Chapter 6: Review of the New Combustion Technologies in Modern Gas Turbines”, Progress in Gas Turbine Performance, InTech Online Publishing, June 2013.
19. Lieuwen, T. C., and Yang, V., Gas Turbine Emissions, Cambridge University Press, New York, 2013.
20. McKinney, R. G., Sepulveda, D., Sowa, W., and Cheung, A. K., “The Pratt & Whitney TALON X Low Emissions Combustor: Revolutionary Results with Evolutionary Technology”, 45th AIAA Aerospace Sciences Meeting and Exhibit, 8-11 January 2007, Reno, Nevada, AIAA 2007-386.
21. Anon, “HAYNES 188 ALLOY”, Haynes International. Website. [<http://www.haynesintl.com/pdf/h3001.pdf>. Accessed 04/20/2016]. April 2016.
22. Schilke, P. W., “Advanced Gas Turbine Materials and Coatings”, GER-3569G, General Electric Company, Aug 2004.
23. Lefebvre H. A. and Ballal R. D., Gas Turbine Combustion, 2nd ed., CRC Press, Florida, 2010.
24. Milberg, E., “GE Begins Ground Testing for World’s Largest Aircraft Engine”, Composite Manufacturing Magazine. Website. [<http://compositesmanufacturingmagazine.com/2016/04/ground-tests-begin-for-ge9x-engine/>. Accessed 04/20/2016].
25. Mattingly, J. D., Heiser, W. H. and Pratt D. T., Aircraft Engine Design, Reston, Virginia AIAA, 2002.
26. Samuelson, S., “Rich burn, quick-mix, lean burn (RQL) combustor”, The Gas Turbine Handbook, US Department of Energy, Office of Fossil Energy, National Energy Technology Laboratory, DOE/NETL2006-1230, pp.227-233, 2006.
27. Anon., “The Jet Engine”, Rolls-Royce plc, 2005.
28. Haynes International. *Hastelloy X Alloy*. Kokomo, Indiana.
29. Schmid and Kalpakjian. *Manufacturing Processes for Engineering Materials, 5th Ed.* University of Notre Dame.
30. Anon, “GE Advances Ceramics Matrix Composites Use,” Aviation Week and Space Technology. Aviation Week Network-Penton. 2016
31. Nageswara Rao Muktinutalapati (2011). Materials for Gas Turbines – An Overview, Advances in Gas Turbine Technology, Dr. Ernesto Benini. VIT University. India.
32. N. Takeshi, O. Takeshi, I. Kuneyuki, S. Ken-ichi, I. Masato. *Development of CMC Turbine Parts for Aero Engines*. IHI Engineering Review. Vol. 47. No. 1. 2014.



33. Zinkle, S.J, Snead, L.L. *Thermophysical and Mechanical Properties of SiC/SiC Composites*. Oak Ridge National Laboratory. 1998.
34. Kerrebrock, Jack L. *Aircraft Engines and Gas Turbines*. 2nd edition. MIT Press, 1992.
35. Tsui, Y.Y., and Wu, P.W., “Effects of Lobe Geometry on the Mixing Flow in Multilobe Mixers,” *Numerical Heat Transfer, Part A*, 2001, pp. 61-77.
36. Gamble, E., Terrell, D., and Defrancesco, R., “Nozzle Selection and Design Criteria,” *40th AIAA/ASME/SAE/ASEE Joint Propulsion Conference and Exhibit*, Nov. 2004.
37. Cadirci, S., “RF Stealth (Or Low Observable) and Counter- RF Stealth Technologies: Implications of Counter- RF Stealth Solutions for Turkish Air Force,” thesis, 2009.
38. Terrier, D., and Lu, F., “Aerodynamically Controlled Expansion Nozzle for STOVL Aircraft,” *41st Aerospace Sciences Meeting and Exhibit*, Jun. 2003.
39. Pratt and Whitney, General Electric Aircraft Engines, “Critical Propulsion Components Volume 3: Exhaust Nozzle,” NASA CR-2005-213584-VOL3, May 2005.
40. Hamstra, J. W., and McCallum, B. N., “Tactical Aircraft Aerodynamic Integration,” *Encyclopedia of Aerospace Engineering*, 2010.
41. Hunter, C., Presz, W., and Reynolds, G., “Thrust augmentation with mixer/ejector systems,” *40th AIAA Aerospace Sciences Meeting & Exhibit*, 2002.
42. Hendricks, E., and Seidel, J., “A Multidisciplinary Approach to Mixer-Ejector Analysis and Design,” *48th AIAA/ASME/SAE/ASEE Joint Propulsion Conference & Exhibit*, 2012.
43. Hoffman, D. A., “Experimental investigation of turbojet thrust augmentation using an ejector,” Thesis, 2007.
44. Debonis, J., “Full Navier-Stokes analysis of a two-dimensional mixer/ejector nozzle for noise suppression,” *28th Joint Propulsion Conference and Exhibit*, June 1992.
45. Briskin, T.A., Howell, P.N., Ewing, A.C., “J85 Rejuvenation Through Technology Insertion,” ADP010433, October 2000.
46. Halbig, M., Jaskowiak, M., Kiser, J., and Zhu, D., “Evaluation of Ceramic Matrix Composite Technology for Aircraft Turbine Engine Applications,” *51st AIAA Aerospace Sciences Meeting including the New Horizons Forum and Aerospace Exposition*, May 2013.
47. Kiser, J. D., Bansal, N. P., Szelagowski, J., Sokhey, J. (J., Heffernan, T., Clegg, J., Pierluissi, A., Riedell, J., Wyen, T., Atmur, S., and Ursic, J., “Oxide/Oxide Ceramic Matrix Composite (CMC) Exhaust Mixer Development in the NASA Environmentally Responsible Aviation (ERA) Project,” *Volume 6: Ceramics; Controls, Diagnostics and Instrumentation; Education; Manufacturing Materials and Metallurgy; Honors and Awards*, 2015.



48. “GE Unveils CMC Production Ramp-Up Plan,” *GE Unveils Ceramic Matrix Composites Production Ramp-Up Plan* Available: <http://aviationweek.com/optimizing-engines-through-lifecycle/ge-unveils-cmc-production-ramp-plan>.
49. Wijerathne, Chaminda. *Gas Turbine Engine Starters*. Sri Lanka Air Force. Aeronautics Guide. 2013. Web.
50. Clark J. Daniel, Jensen J. Mark, Montague T. Gerald. *An Overview of Magnetic Bearing Technology for Gas Turbine Engines*. University of Toledo. U.S. Army Research Laboratory. 2004.
51. Nishikawa, Takashi. Hayashi, Nao. Hayakawa, Akiko. *Technical Trend of Aircraft Bearings*. NTN Kuwana Works. NTN Technical Review No. 82. 2014.
52. Cha, J, Choi., D, Jung, K, Lee, S. and Hunter, B, “Advanced Emergency Power System Using Thermal Battery for Future Aircraft”, 4th International Energy Conversion Engineering Conference and Exhibit (IECEC), 26-29 June 2006, San Diego, California, AIAA 2006-4161.
53. Anon, “Iran Air Avionic Training SCIENCE IS USELESS UNLESS SHARE IT,” Part66online Web Site, [http://part66online.com/index.php?mod=view_qa&id=329], Spring 2016.
54. Kelley, K., “F/A-18 Program Explores the use of exhaust nozzle chevrons to reduce engine noise,” *Currents*, 2015.
55. Anon, “Report on Jet Engine Noise Reduction,” *Naval Research Advisory Committee*, Department of the U.S. Navy, 1400 Defense Pentagon, Arlington, VA 20301, April 2009.
56. Farokhi, S., “Noise in a Nutshell,” *AE 524*, University of Kansas, Lawrence, KS 66045, pp. 1-16, 2016.
57. Abdullah, et al, “3D Numerical Studies on Jets Acoustic Characteristics of Chevron Nozzles for Aerospace Applications,” *World Academy of Science, Engineering, and Technology*, International Journal of Mechanical, Aerospace, Industrial, Mechatronic, and Manufacturing Engineering, Vol:8, No:9, 2014.
58. Bridges, J., Brown, C., “An Analysis of Model Scale Data Transformation to Full Scale Flight Using Chevron Nozzles,” *NASA Glenn Research Center*, Cleveland, Ohio, December 2003.
59. Gorji-Bandpy, M., and Azimi, M., “Technologies for jet noise reduction in turbofan engines,” *Aviation*, vol. 16, 2012, pp. 25–32.
60. Horinouchi, S., “Noise Reduction By Thrust Vectoring For Supersonic Business Jet,” 26th *International Congress of the Aeronautical Services (ICAS)*, Japan Aerospace Exploration Agency, Tokyo, Japan, 2008.
61. Anon, “Fact Sheet- FAA Forecast-Fiscal Years 2014-34,” Federal Aviation Administration, March 13, 2014.
62. Mullick, et al, “CASA-25: Candidate Variable Bypass Turbofan Engine for a Supersonic Business Jet,” *The University of Kansas Department of Aerospace Engineering*, April 2014.
63. Anon, “T-38 Trainer Becoming Too Costly and Dangerous to Keep Flying,” [<http://www.freerepublic.com/focus/f-news/2771923/posts>], *Lexington Institute*, 31 August 2011.



-
64. Barrett, Ron. "Modern: Statistical Time and Market Predictive Engineering Design (STAMPED) Weight Estimation Method." *AE 521 Lecture – 8/27/2015*, University of Kansas, Lawrence, KS 66045, pp. 54-81.
 65. Anon, "Advanced Pilot Training Aircraft," *AIAA Foundation Undergraduate Individual Aircraft Competition*, October 2013.
 66. Lockheed Martin, "Sustainment," Lockheed Martin, 2016. [Online]. Available: <http://www.lockheedmartin.com/m/us/products/f22/f-22-sustainment.html>. [Accessed 15 April 2016].

